CERTIFICATION OF DISSERTATION

I certify that the ideas, experimental work, results, analyses, software and conclusions reported in this dissertation are entirely my own effort, except where otherwise acknowledged. I also certify that the work is original and has not been previously submitted for any other award, except where otherwise acknowledged.

[redacted]

Signature of Candidate

04/02/2022

Date

ENDORSEMENT

[redacted]

Signature of Supervisor

03/02/2022

Date

[redacted]

Signature of Associate Supervisor/s

Date

A century since outburst: A detailed light curve and evolution analysis of Nova Aquilae 1918

John Myles – [redacted]

Semester 2, 2021

Abstract

Nova Aquilae 1918 (V603 Aql) was the brightest classical nova observed since the invention of the telescope. As such, it has received much attention, resulting in an extensive research collection. The research presented in this thesis concentrates on time series analysis of both historical observations from the AAVSO repository and a collection of photometric observations requested for this work, producing and analysing both published and newly obtained photometric light curves. This analysis is completed using PERANSO 3.0 software. In total over 50,000 individual observations were collected by 21 professional and amateur astronomers forming the full 2021 Campaign. Sub-sets of these data are analysed to determine the past and present state of the V603 Aql photometric superhumps and any other prominent periods. Previous measurements of these phenomena show both positive and negative superhump periods drift by around $0.004\ days$ on a timescale of a few months. The aim here is to confirm this drift and possibly narrow the range, also confirming the current phase (positive or negative) of the prominent photometric period. The theory of classical novae to dwarf novae evolution has gathered increasing evidence over the last decade, therefore an analysis and comparison of the V603 Aql parameters with those of evolving systems is also undertaken.

Over the full May – July Campaign, orchestrated through the AAVSO, the system was found to have a mean photometric period of $P_{NSH} = 0.135203(6) days$, associated with the negative superhump. A month-by-month analysis revealed a change of the photometric period between June and July 2021. In June the prominent photometric period was $P_{PSH} = 0.146846(203)\ days$, associated with the positive superhump. In July the prominent period had changed to $P_{NSH} = 0.135417(196)\ days$, approximately 2% shorter than the orbital

period. This change of phase coincides with an increased system brightness of $\approx 0.1\,mag$, occurring at approximately $JD = 2459390$. The positive superhump period drift was re-analysed using historical data, and the 2021 Campaign, and was found to drift on a timescale of $\approx 25\,days$ within the period range of 0.144 - $0.147\,days$ as determined previously by Patterson et al. (1997) during their 1990 - 1994 campaigns. An analysis of the system brightness from 1950 to 2021 shows the system continues to fade, suggesting decreasing mass transfer secondary star and the orbiting accretion disk. These results fit the expected evolutionary path for classical nova systems as proposed by the hibernation model of cataclysmic variable evolution, which models the transition of old nova stars to dwarf novae.

Keywords: Cataclysmic Variables, Classical Novae, Nova Aquilae 1918, V603 Aql.

Acknowledgements

Firstly, I would like to send out some Thank You's. To Dr Joanna Turner for your help with the honours program, Dr Duncan Wright and Professor Miroslav Filipovic for your feedback and support as well as Dr Carolyn Brown for her confidence in me and attempts in scheduling observations. Thank you to my supervisors Dr Graeme White and Dr Brad Carter for your guidance and support. For supplying me with an overwhelming amount of data I would like to thank Fraser Lewis at the Las Cumbras Observatory and Elizabeth Waagen at the AAVSO. My eternal gratitude goes to all the observers spread across the globe who contributed to the 2021 Campaign. Their passion and dedication for variable star observing is truly inspiring. Lastly but most certainly not leastly, I would like to thank my family for their support and interest throughout the project, and my gratitude and love to my partner Vanessa who endured the highs and lows with me and has over the past 5 years read (and improved) most of the stuff I have written.

At times this project has been extremely difficult and stressful, though I wouldn't change a thing. As a relatively unskilled researcher this adversity has forced me to evolve and, as my supervisor Graeme hoped, I believe I have become 'a more well-rounded scientist'. I have explored and included topics well outside of the initial scope of the project, applied for telescope time on instruments scattered across three continents, learned a new programming language while writing scripts to perform data analysis and create plots, developed scientific communication skills that will serve me well into the future and established relationships with astronomers and astrophysicists across the globe. Plenty more than I ever expected.

I hope whoever reads this enjoys it. My introduction of concepts may be considered lengthy, but it was my hope that no matter who read it, astronomer, scientist or armchair

enthusiast, they might get something from it. It has been said that only your parents and your examiners will ever read your thesis anyway, so why am I even worried? In the words of my good friend Graeme White, ‘Let’s bloody get on with it shall we’.

Table of Contents

List of figures

Acronyms

AU	: Astronomical Unit
CN	: Classical Nova
CV	: Cataclysmic Variable
d	: Day (Unit of time)
DN	: Dwarf nova
LS	: Lomb-Scargle
LY	: Light Year
m	: Minute (Unit of time)
$M_\odot$	: Solar Mass
PC	: Parsec
$R_\odot$	: Solar Radius
s	: Second (Unit of time)
SH	: Superhump
SU UMa	: SU Ursa Majoris (Dwarf novae)
WD	: White Dwarf
yr	: Year (Unit of time)

Definitions

Angular Separation – The apparent distance between two objects from the view of the observer.

Apparent magnitude (brightness) – The brightness of an astronomical object as seen from Earth.

Chandrasekhar limit – The maximum stable mass of a white dwarf star. This limit is currently accepted as 1.4 $M_{\odot}$ or 2.765 x 10^{30} kg.

Inverse square law (light) - Describes the intensity of light from a source at different distances. The intensity of light is inversely proportional to the square of the distance between the source and the detector, $I \propto \frac{1}{d^2}$.

Lagrange points – positions in space where gravitational forces (attraction and repulsion) of a two-body system are enhanced.

Main sequence – A star in its stable state, producing energy by the fusion of hydrogen into helium within their core. The way in which a star evolves off the main sequence is largely reliant upon their birth mass.

Modern magnitude scale – A logarithmic scale for measuring the visible brightness of an object. The scale uses both negative and positive integers with smaller numbers denoting brighter objects. There is a $\sqrt[5]{100}$ or ≈ 2.51 steps between magnitudes. As an example, the brightest star in the night sky is Sirius A at -1.46 mag. The Sun is -26.74 mag.

Red dwarf – A low mass, cool star with a typical radius of $\approx 0.1 - 0.5_{\odot}$. These stars appear red due to low surface temperatures and have long main sequence lifetimes.

Red giant – A star in an intermediate stage of evolution. These stars are transitioning from the main sequence as their hydrogen reserves are exhausted. They have a large volume, low mass and low temperature, contributing to their reddish appearance.

Roche lobe – The region where orbiting material is gravitationally bound to the star. In a binary system this lobe may be drawn into a tear-drop shape where mass transfer can occur. The point of mass transfer will be at Lagrange point 1.

Superhump – A photometric modulation seen in close binary star system light curves. They appear with a period a few percent shorter (negative) or longer (positive) than the orbital period of the system.

Supernova – These events occur as a star comes to the end of its life. In massive stars, runaway nuclear fusion and the collapse of the stellar core leads to the destruction of the progenitor with a peak luminosity close to that of its entire host galaxy. A Type IA supernova occurs when a white dwarf star gains too much mass in a short period, exceeding the Chandrasekhar limit.

SU Ursae Majoris – A sub-class of the U Geminorium (U Gem) dwarf nova.

White Dwarf – A small and very dense star commonly the size of a planet with a mass of $\approx 1 - 1.4\ M_{\odot}$. These stars have exhausted their nuclear fuel and lost their outer layers to space.

1 Introduction

Ever-improving telescopic observations of our sky have revealed endless wonders. The development of scientific study seeks to investigate these wonders in an effort to understand the universe in a fundamental way. One discovery that has proved exceedingly important in our quest for understanding is that many of the stars we see are in fact stellar systems, living in pairs or groups and frequently interacting. As many of these stars interact, we often observe a periodic change in the brightness of the object from our point of view. These stars, among others, are known as 'Variable Stars'. This work discusses one such object, Nova Aquilae 1918 (hereafter V603 Aql), a binary stellar system in the constellation Aquila.

The V603 Aql system has received much attention historically, with an almost constant record of observations available. Analysis of the light curves of these objects tells us much about the state of the system and how it is evolving. The research presented here aims to identify and describe the range of periodic brightness fluctuations that have been discovered in the V603 Aql system. Primarily it aims to calculate by observation the photometric period of this system in order to determine any change from previously reported values. A change in period suggests the relation between the stars in the system is evolving. Further, confirmation of previously reported oscillations and an extension of the long-term system light curve may also be achieved. The introduction section provides a background into the type of system in which V603 Aql exists; a cataclysmic variable in a binary star system, providing a familiarisation of the field. Chapter 2 reviews the history of V603 Aql and explores the literature available on this object. Chapters 3, 4 and 5 discuss

the methods, observations and results from this work. A summary of the findings from the observations conducted for this project is provided in Chapter 6.

1.1 Variable Stars

Variable stars have long been known to astronomers. Evidence of the observations of these phenomena are found in the stories of ancient culture. The scientific study of variable stars has revealed the diversity of the category, leading to the establishment of an in-depth and sometimes confusing classification system. Broadly, variable stars are those that display a measurable change in brightness from our perspective on the Earth (Percy 2007). These brightness variations may be periodic or a once in a stellar lifetime event. Whilst all stars will exhibit brightness changes over their lifetime, many of these cases can be explained by the expected evolution of stars as they slowly expel their fuel or by the frequency of dark sunspots. Classified variable stars fall into many categories. Their classification is a complex process, dictated by a large range of properties. Some categories of variable stars are better understood than others and the field is constantly evolving. As technology improves, historic observations are often revisited, and stars may be reclassified as new science brings meaning to old understanding.

Variable stars fall into two main groups, intrinsic and extrinsic. This is a broad primary classification where intrinsic variability describes those stars or star systems where the variability stems from processes within the star or system itself. This may be due to mechanisms related to a single star or an interaction between stars in a system. The mode of variability in extrinsic variables occurs by completely external factors, such as rotations or eclipses (Percy 2007). These groups are further broken into six classes. Intrinsic variables have classes such as pulsating, eruptive, cataclysmic and x-ray. Extrinsic variables are classed as rotating or eclipsing variables. Each of these classes are then broken into a large number of

types, considering the finer details of the star's variability (Astronomical Society of South Australia N.D.). A classification diagram for these variables is given below in Figure 1.1.

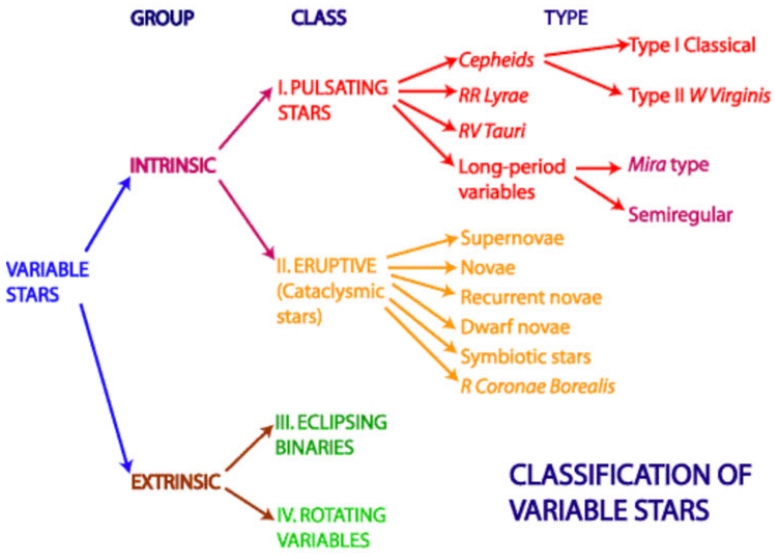

Figure 1.1: *A classification diagram of variable stars. Source: (CSIRO N.D.).*

The variable star zoo is complex. This project concentrates on a particular type of variable, known as a cataclysmic variable. This type of variable canonically exists in binary systems. Further explanation of this variable type is provided in the following section. All other variable types are given no further treatment here.

1.2 Binary Star Systems

Many of the stars we see in the night sky are in fact multiple star systems, consisting of two or more gravitationally bound companions. The most abundant of these are the binary systems, in which two stars orbit each other around a common centre of mass. In these pairs, the brighter star is referred to as the primary star and assigned the letter A, while the dimmer companion is classed as the secondary star or star B (Heintz 2012).

Binary star systems are broadly classified either by the way in which they are observed or by their orbital mechanics. Binaries classified by observation can be visual binaries which are those containing stars with a wide enough angular separation ($\approx> 1\ arcsecond$). These

stars can be resolved using a telescope, whereas spectroscopic binaries must be determined by studying the wavelengths of the emitted light (Doppler effect), as they orbit too closely to be visually separated (Heintz 2012). Stars classified by their orbit are either wide orbit binary stars – evolving separately and having little influence on the evolution of their companions – or close orbit binary stars, which commonly interact, altering their normal evolutionary path over the course of their lives (Hilditch 2001). Some mechanisms by which these interactions cause variability in a star system are discussed throughout Chapter 2.

1.3 Cataclysmic variables

Within the cataclysmic variable (CV) star group there are four main types: supernovae, classical novae, dwarf novae, and recurrent novae. These variable types are binary star systems in which a late main sequence or red dwarf star transfers its mass to its more massive white dwarf (WD) companion (Smith 2006). Supernovae differ from this description as they are not required to be in a binary system. Instead, supernovae can occur due to the internal processes of massive stars, although a sub-group of supernovae do live in binaries. These are known as Type IA supernovae. Their outbursts occur when a WD star gains too much mass in a short period and exceeds its Chandrasekhar limit (Mazzali et al. 2007). The resulting supernova destroys the progenitor WD, ending the stellar relationship in a powerful and dramatic fashion.

Classical novae (CN) have been recorded as ‘new’ or ‘guest’ stars for thousands of years as they erupt and fade, though it is only in the last century that these outbursts have been distinguished from supernovae. The discovery by Walker (1954) that classical novae occur in short period, binary star systems sparked speculation that many or all CN may be binary. Later work presented in papers by Robert Kraft (Kraft et al. 1962; Kraft 1964) supported this hypothesis and included observations of V603 Aql, providing further evidence

of the binary nature of these phenomena. It is now commonly accepted that all CN occur in binary systems consisting of a WD and a low mass, late main sequence star orbiting each other on short periods (Warner 2003).

Much of the research around these objects has concentrated on accurately determining their periods. As these systems evolve, period changes do occur, so a reliable calculation of a CV system's period says much about where the system is in its evolution. The known periods of these objects can be roughly split into two groups: those with periods in the range of $3 - 16$ hours and those in the range of $1.3 - 2$ hours (Knigge 2011). In the interval between $\approx 2 - 3$ hours, comparatively few CVs are found. This has come to be known as the orbital period gap (Zorotovic & Schreiber 2019). The expected evolutionary path of common CV objects is discussed further in the following section.

1.4 Evolution of CV binaries

As CV binaries live in close stellar relationships, the way in which the individual stars evolve is strongly influenced by their partner. Where the evolution of a single star off the main sequence can be easily predicted, close binary stars take a very different path. There exists a myriad of mechanisms and states that affect this process, dependent upon the conditions under which the partnership was born. We concentrate here on a specific binary type, those comprising of an approximately solar mass WD ($M \approx 1 - 1.4_{\odot}$) and a late main sequence red dwarf companion with an orbital period above the period gap ($P \approx 3.5hrs$). This binary configuration makes up a majority of the CV population (Knigge 2011) and represents the V603 Aql system well. As with the evolution of single stars, individual stars in a binary system are still bound by the factors of natural stellar evolution. More massive stars age more quickly and as a consequence, stars of the same age with different masses will evolve at different rates (Kalomeni et al. 2016).

Binary systems with widely separated main sequence stars may follow a complex evolutionary path bringing them into a much closer relationship. As the more massive star (Star 1) evolves off the main sequence it loses its outer layers and mass transfer begins between the two stars. This results in angular momentum loss, decreasing distance between the two companions. As the stars continue to spiral towards each other their period decreases, eventually becoming a contact binary system, sharing a common gaseous envelope. Once the evolution of Star 1 is complete the core of the star is left behind as a dense, remnant WD. As the second star (Star 2) evolves into a late main sequence star, it begins to overflow its Roche lobe, again initiating a transfer of mass between the two now close orbit, short period stars (Carroll & Ostlie 2007).

In the case of classical, dwarf and recurrent novae, the WD gravitationally accretes matter from its companion through Lagrange point 1 of the binary system, forming an accretion disk around the WD (Hack & La Dous 1993). An illustration of this process can be seen in Figure 1.2. Canonically, CV's show stable mass transfer on long time scales. In order to maintain the stable mass transfer, the system must persistently shrink, allowing the Roche lobe of the secondary star to remain in touch and thus continue transferring mass. For this process to continue occurring, continual angular momentum loss is required, decreasing the distance between the stars and reducing their period from month or years to a number of days (Knigge 2011).

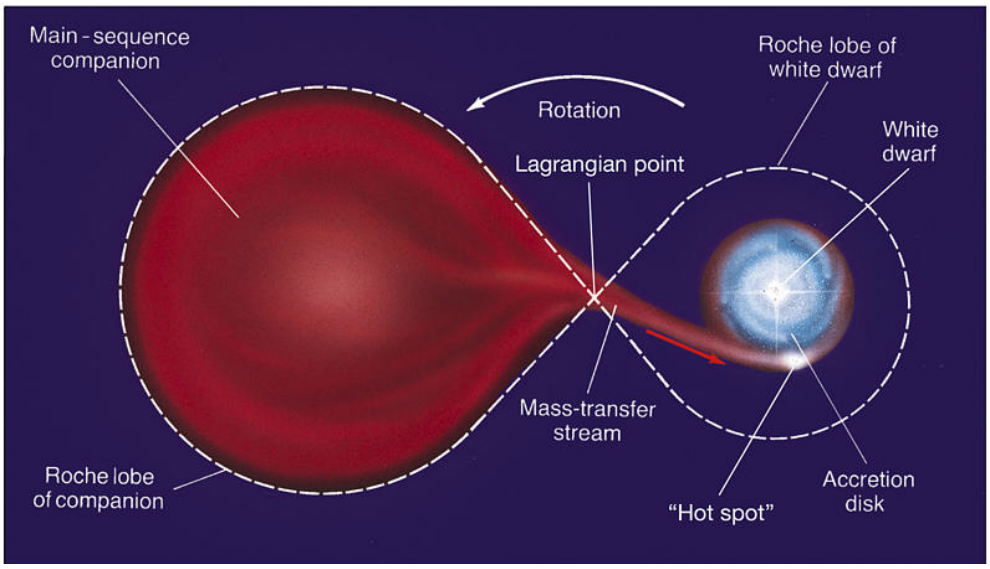

Figure 1.2: *A simple model of a CV binary star system. Source: (Coto 2016).*

Classical novae occur when material accreted on to the WD's disk undergoes runaway thermonuclear fusion. This outburst can increase the brightness of the star by 6 to 19 magnitudes before fading to its quiescent (pre-nova) brightness (Warner 2003). CN have only ever been observed to occur once for a particular system, though some theories suggest that some CN binaries may repeat the occurrence on intervals from 10,000 to 100,000 years (Truran & Livio 1986). The speed with which the system returns to its pre-nova brightness classifies the event as either a fast or slow nova, where the time taken for the system to fade by three magnitudes (t_3) below maximum brightness is measured. Fast novae fade in less than one hundred days $(t_3 < 100^d)$ and slow novae longer than one hundred days $(t_3 > 100^d)$ (Krautter 2008). After an outburst, an expanding shell of nebulosity remains, fading relatively quickly over a few decades (Hack & La Dous 1993).

1.5 Project Goals and Research Significance

The light curves of variable stars reveal much about the state of the system. Long term observations provide information on the evolution of the system over time, including change in orbital period, brightness fluctuations and the development of phenomena associated with the variable type. Classical novae binary systems are short period systems, typically exhibiting

brightness fluctuations influenced by mass transfer rates between the stars and instability in the WD accretion disk. This research aims to provide a detailed light curve analysis of Nova Aquilae 1918 in order to calculate the photometric (superhump) period and identify any short period fluctuations. An estimated mass transfer rate will also be calculated using the observed parameters of the binary pair. It is hoped the research conducted here will contribute to the knowledge around how CN evolve after outburst. Examining the phase of accretion disk phenomena such as superhumps (See section 2.3) provides direct insight into the current state of the disk and the orbital mechanics at play. The evolution of CVs is primarily determined by the mass transfer rate between the stars. Changes in these rates manifest as brightness fluctuations in the system light curves. As V603 is now over a century past outburst, continued observations of brightness fluctuations and overall system brightness as well as light curve analyses may provide a clue to its likely evolutionary path. There is mounting evidence old novae like V603 Aql evolve to DN or follow a cyclic evolution between the two types. As V603 Aql demonstrates many of the phenomena seen in DN stars it is a prime candidate to watch and see as the system ages. Indeed, V603 Aql may close the gap on the timeframe around which these stars make their transitions.

This chapter has provided a comprehensive introduction into CV classification, formation and evolution. The following section provides a description of the V603 CV system and the associated phenomena discovered over the history of its observation.

2 Nova Aquilae 1918 (V603 Aql)

2.1 Discovery and early observations

First observed on June 8th of 1918, V603 Aql appeared as a 'new star' in the constellation of the Eagle, Aquila (White & Platz 2018). According to observers of the time,

the star appeared reddish-yellow and was brighter than the brightest star in Aquila, Altair (Fowler 1918). The nova event produced a peak brightness of approximately $-1\ mag$, before fading to its quiescent magnitude of $11.47 \pm 0.03\ mag$ (Johnson et al. 2013). Pre-nova observations recorded on photographic plates at Harvard University showed the star to be a slightly irregular variable (Campbell & Shapley 1923). Subsequent work by Campbell and Shapley (1923) shows this variability continued after the outburst. Figure 2.1 is a plot of Harvard's photographic data spanning from just prior to the 1918 outburst until 6 months after the nova. The nova continues to fade, returning to below its quiescent brightness by about 1938 (Johnson et al. 2013).

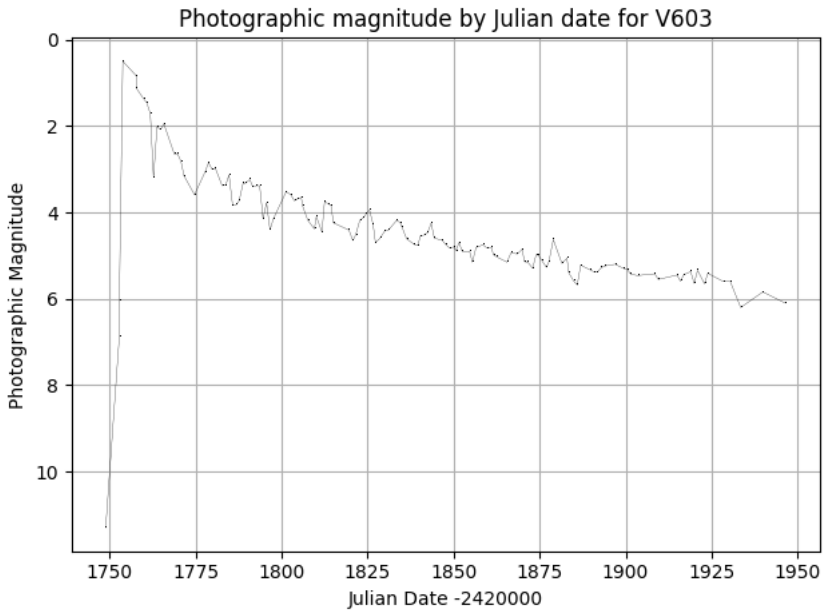

Figure 2.1: *A plot of photographic magnitude by Julian date for V603 Aql. These observations span the six months after outburst, to December 1918. The data for this plot was sourced from the AAVSO (Campbell & Shapley 1923).*

Observations of the nova have continued consistently, the AAVSO database has a repository of observations spanning over 100 years, from July 1918 to the current day. As technology has improved, a deeper knowledge of this object has led to new discoveries within this system. Early observations by Barnard (1919) were concerned with the formation and expansion of a planetary disk around the then young nova, though some 'peculiarities', as the contribution states, were seen when recording the brightness of the star. Since then, there have been many studies of V603 Aql to determine the mechanisms behind this historic outburst and the characteristics of the star's variability. A study of old novae by Walker (1956) focused on detecting short period light variations associated with this type of star. Walker (1954) had previously discovered that Nova DQ Herculis 1934 was a short period binary star system. This led some to posit that many old novae may exist in binary systems. Further studies conducted by Kraft (1964) confirmed the close binary relationship of many CN, including V603 Aql. The close stellar relationships in these systems provide a mechanism for the continued variability we see today.

2.2 Determination of period

The way in which binary star periods are calculated depends upon the orientation of the stars and how they appear to us from Earth. Eclipsing binaries for example are star systems where, from our point of view, pass in front of and behind each other. Depending on the angle of inclination (i) we may see a full or partial eclipse. Systems with an inclination of $i \approx 90^{\circ}$ will undergo total eclipses. At smaller angles, we see only a partial or grazing eclipses and at smaller angles still, we see no eclipse as the stars do not overlap at all (Morris 1999). Stellar eclipses produce a noticeable 'dip' in the star's light curve. An example of this effect is shown in Figure 2.2. The magnitude of this brightness reduction is related to the configuration

of the stars (detached, semi-detached) and the inclination at which we observe them. The eclipse with the greatest decrease in brightness is known as the primary eclipse and the lesser of the two, the secondary (Wood 1971). By plotting an extensive light curve, the period can then be calculated simply by measuring the time between consecutive primary or secondary eclipses.

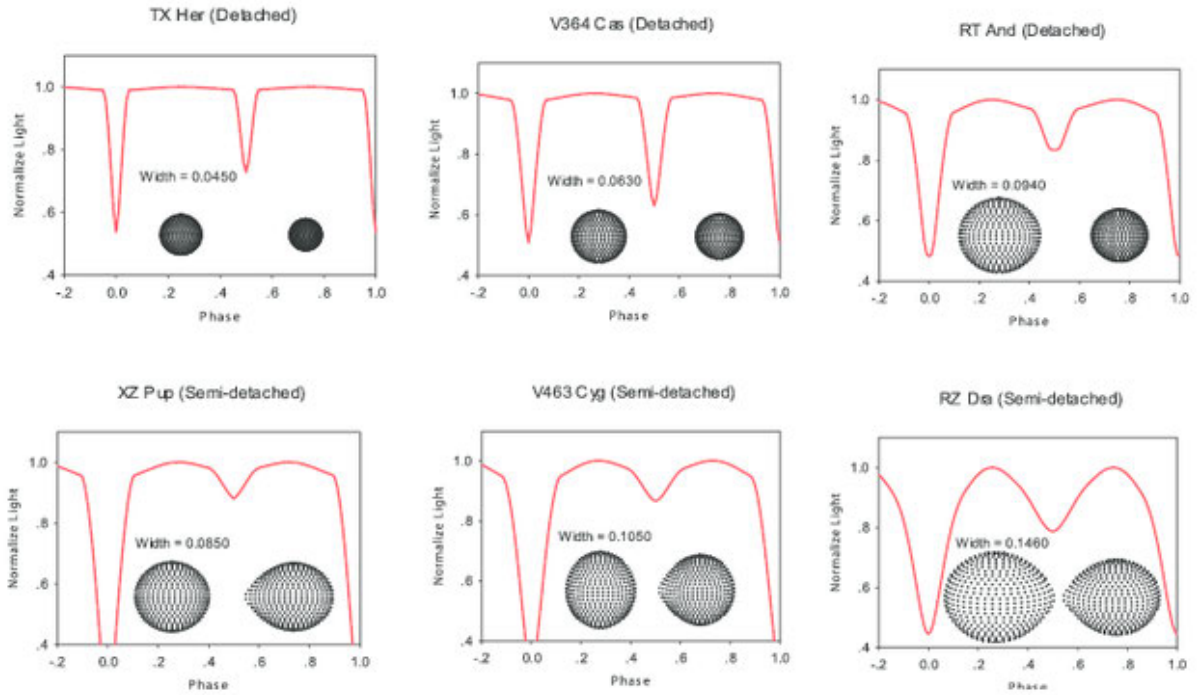

Figure 2.2: *Example stellar binary configurations and associated eclipse light curves. Source: (Kang 2010).*

A more in-depth process is required to calculate the periods of binary stars that do not eclipse and cannot be visually separated by telescopes. The radial velocity method is a common way in which this can be done. This method measures the Doppler shift in the wavelengths of light emitted from a star in order to calculate the speed at which it orbits the centre of mass of the system (Carroll & Ostlie 2007). As a star moves towards or away from an observer the emission/absorption lines will be shifted towards the blue or red part of the spectrum. Figure 2.3 illustrates this effect. By measuring the observed shift (λ_{obs}) against the known wavelength (λ_{rest}) for a particular line, a radial velocity (v_r) can be calculated using Eqn 1.

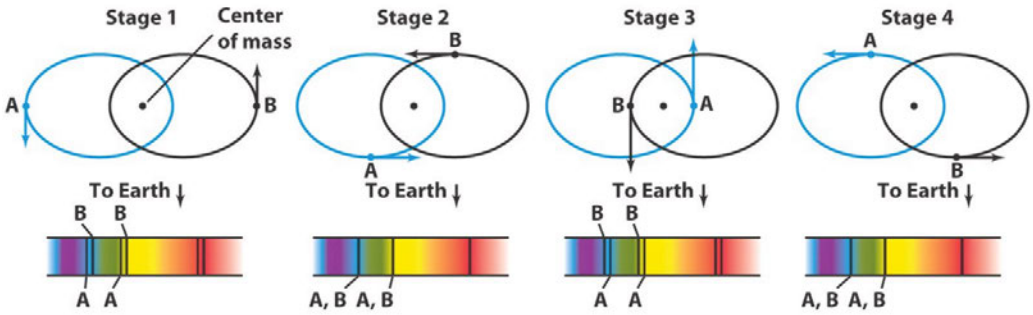

Figure 2.3: *Absorption line shifts as a binary star system orbits a common centre of mass. Source: (Caltech 2004).*

$$\frac{\Delta\lambda}{\lambda_0} = \frac{v_r}{c}$$

$$v_r = \frac{\Delta\lambda}{\lambda_0} \cdot c$$

$$v_r = \frac{(\lambda_{obs} - \lambda_{rest})}{\lambda_{rest}} \cdot c \qquad (1)$$

In order to find a true velocity for these stars, the inclination of the system must also be accounted for. The spectroscopic radial velocity of the observed star is related to the true velocity (v) by Eqn 2.

$$v = v_r \sin i \qquad (2)$$

Once sufficient points have been calculated, a velocity curve is plotted and then the orbital period is determined from the periodicity in this plot. Figure 2.4 below is the corresponding velocity curve for the stars previously shown in Figure 2.3. The calculated velocities are plotted against time. A period can then be determined by finding the time between comparable stages along the curve, shown as Stage 4 in Figure 2.4. Further, the peak radial velocity measurement (K) is at the point of Stage 3 in this graphic, calculated at $K \approx$ 50km/s.

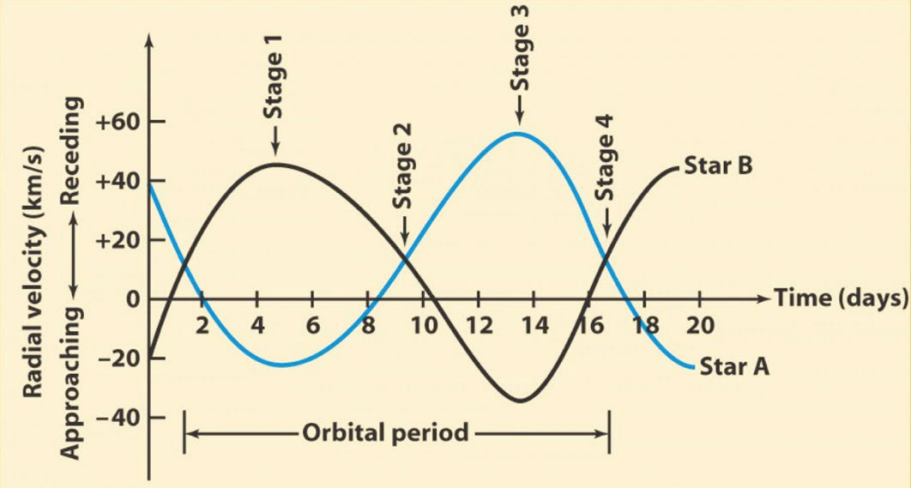

Figure 2.4: *Velocity curve for a binary star system. Source: (Caltech 2004).*

Also displayed in this graph is the speed with which the system is moving away from Earth. Note the velocities are skewed above $y = 0$ ranging between approximately -20 to +50 km/s. This indicates the system is moving away from the Earth at approximately 15 km/s. This method also allows for the calculation of the estimated mass ratio of the stars in the system, as well as their orbital eccentricity (Karttunen et al. 2016). The radial velocity method is widely applied in present studies for the detection of extra-solar planets.

2.2.1 V603 Spectroscopic Orbital period

The initial orbital period determination was performed by Kraft (1964) using radial velocity calculations from spectroscopic observations. Analysis of the $H\delta$ and $H\gamma$ emission lines led Kraft (1964) to determine a period of 3h 19.5m, $\sim 0.13854\, d$. Since this initial calculation, the orbital period of V603 Aql has been only slightly refined. Ultraviolet (UV) spectroscopic observations from the International Ultraviolet Explorer (IUE) satellite were studied in papers by Rahe et al. (1980) and Drechsel et al. (1981) confirming Kraft's spectroscopic period and radial velocity measurement of $K = 38\, km\, s^{-1}$. The low K value suggests that the system must have a low inclination $(15^{\circ} - 20^{\circ})$ relative to observations from Earth. Further, no secondary minima were found, therefore no eclipse of the system stars would be expected.

The orbital period was refined slightly by Drechsel et al. (1983) through combining the data collected by Kraft (1964) with new X-ray observations obtained from the Einstein observatory. They calculated the period as 3h 18.9m ($\approx 0.1381545d$); only a small reduction on the previously accepted measurement. A spectroscopic study of V603 Aql by Arenas et al. (2000) aimed to confirm or refine previously determined stellar parameters. In this work, they use $H\beta$ velocities from 1990 data to confirm the orbital period ($P_{Orb} = 0^d.1385 \pm 0^d.0002$). Of particular importance is a calculation of the mass ratio of the system and individual stellar masses for the primary and secondary stars. The mass of the WD primary star is calculated at $M_1 = 1.2 \pm 0.2M_\odot$ and the secondary at $M_2 = 0.29 \pm 0.04M_\odot$. This yields a mass ratio for the system of $q = 0.24 \pm 0.05$. They also worked to refine the inclination of the system finding $i = 13^\circ \pm 2^\circ$. This parameter was calculated using the binary mass ratio (q), the orbital period (P_{Orb}) and the peak radial velocity measurement (K_1) to form the binary mass function of the stars. An upper limit of $i{\sim}65^\circ$ can be applied to the system as the stars do not eclipse from our point of view. For the full derivation and method used here see Arenas et al. (2000) section 4.2. More recently, Peters and Thorstensen (2006) obtained a slightly refined orbital period value using the $He\ \mathrm{I}\ \lambda 6678$ emission line, yielding an orbital period of $0.138201(1)d$. This is the currently accepted orbital period of the V603 Aql binary star system.

2.2.2 V603 Photometric Period

Photometric observations of the system revealed a repeating 'hump like' structure in the light curve, with a period reported by Haefner and Metz (1985) as $3^h28^m35^s$ ($0.144854d$); approximately 5% longer than the known orbital period. An explanation for this phenomena posited by Patterson and Richman (1991) was the possibility of 'permanent' positive superhumps, similar to the superhumps seen in SU Ursa Majoris (SU UMa) type DN.

2.3 Superhumps

2.3.1 Superhumps. What are they?

First discovered in SU UMa type DN, superhumps are periodic brightness increases observed in the stellar system's light curve (Arenas et al. 2000). Superhumps occur with periods slightly longer (positive superhumps) or shorter (negative superhumps) than that of the orbital period of the star system. Superhumps are thought to arise as a beat period of the accretion disk motion and the orbital period, though a rigorous explanation for their formation is still needed (Stefanov 2021). Canonically, SU UMa type DN stars display well-defined positive superhumps after a superoutburst event (Warner 1976; Patterson 1979; Vogt 1982). The currently accepted model for the formation of superhumps is the eccentric precessing disc model (Vogt 1982; Whitehurst 1988; Osaki 1989), where tidal stresses from the secondary star influence the accretion disc around the white dwarf (Lubow 1991). Figure 2.5 below shows a simulation of this occurrence computed by Wood et al. (2011). The line around the disk represents the Roche lobe of the WD and the points at where this line crosses or breaks is the mass transfer point, Lagrange point 1. In these systems, the outer disc expands to a resonance radius of approximately 3:1. At this resonance the interaction between the secondary and the accretion disk leads to a growth in eccentricity in the disk (Osaki 1989; Goodchild & Ogilvie 2006). Figure 2.5 also shows the accretion disk is at its greatest eccentricity in frames 1 and 6 of the simulation. This coincides with the brightness increases in the accompanying light curve.

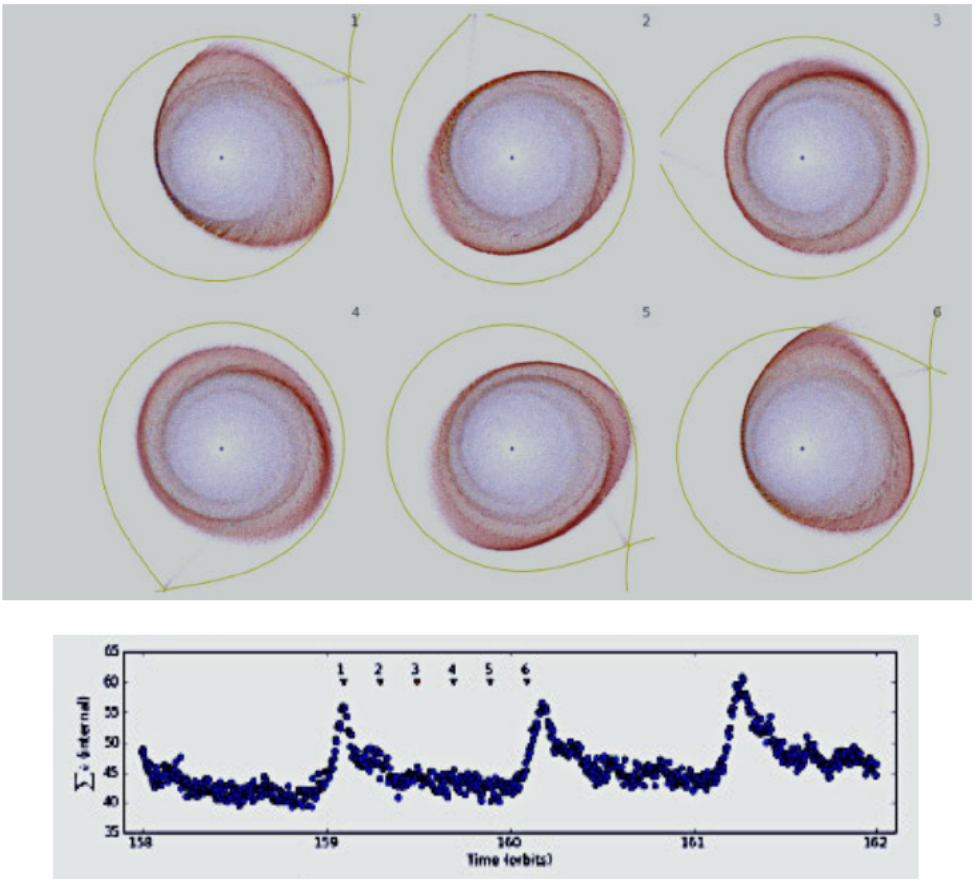

Figure 2.5: *A WD accretion disk simulation with light curve. Source: (Wood et al. 2011).*

Positive superhumps occur in systems with low mass ratios ($q \leq 0.33$) and high mass transfer rates. The mass ratio of these systems is given by Eqn 3.

$$\left(q = \frac{M_2}{M_1}\right) \tag{3}$$

where M_1 is the mass of the primary star (commonly the white dwarf), M_2 is the mass of the secondary star and q is the mass ratio of the two stars. The slightly longer period of positive superhumps (P_{SH}) is caused by apsidal precession of the elliptic accretion disk in systems where the accretion disk is tilted relative to the orbital plane (Thomas & Wood 2015). The period of this precession (P_{Prec}) is related to the orbital and superhump period by Eqn 4.

$$\frac{1}{P_{Prec}} = \frac{1}{P_{Orb}} - \frac{1}{P_{SH}} \tag{4}$$

Negative superhumps (N_{SH}), with periods slightly shorter than the orbital period are observed when the warped disk is tilted and in retrograde precession (Bruch & Cook 2018). Wood and Burke (2007) offer a deeper explanation resulting from a hydrodynamical disk simulation study where they demonstrate that negative superhump light modulations are produced as the hot spot migrates towards the primary star across a tilted accretion disk. These theories were developed primarily to explain superhumps in SU UMa DN. However, the same mechanisms can be applied to other CV types, providing these systems maintain the conditions for superhump formation (Patterson & Richman 1991). The constraints are that the disk material is viscous enough to maintain a large radius and that the mass ratio of the system is low $(q \leq 0.33)$, as given by Eqn 3. Positive and negative superhumps have been observed in CN systems decades after outburst, demonstrating that the frequent superoutbursts of DNs are not necessary for the formation of superhumps. In a study by Patterson and Richman (1991), this type of CN were labelled 'permanent superhump' systems. Since this time, many have been confirmed. Studies of the V603 Aql system have found a mass ratio of $q = 0.24 \pm 0.05$ and an orbital period of $3hr\ 19.5m\ (0.1385d)$ (Arenas et al. 2000), making V603 Aql a good candidate for superhump formation.

2.3.2 V603 Aql Superhumps

The photometric hump $(0.144854d)$ reported by Haefner and Metz (1985) was studied further in a 15-night photometry program by Patterson and Richman (1991). This '3.5-hour modulation' was confirmed and potential mechanisms for this periodicity were

discussed, including the resemblance to superhumps observed in SU UMa type DN. In this work, they claim the period to be increasing by an average rate of $\sim 5 \sec yr^{-1}$ in the decade between 1980 and 1990. During this time, calculations consistently produced a photometric period in the range of $0.1449 - 0.1466\, days$, with follow up studies revealing that this period drifts on a time scale of months (Patterson et al. 1993) and changes phase from positive to negative on time scales of years (Andronov et al. 2005).

Observations of the system from 1992-1994 revealed that the dominant positive superhump period ($\sim 0.146d$) had weakened and a stronger negative superhump period of $\sim 0.1338 - 0.1345d$ was now present. This period is shorter than the determined spectroscopic orbital period (Patterson et al. 1997). At the time, a model for how the disk simultaneously maintains both positive and negative superhumps had not been developed, though Patterson et al. (1997) suggested that as for SU UMa type DN stars the V603 Aql disk is both eccentric and tilted. The mechanisms behind superhump formation and evolution remains an active area of research. Smak (2008) asks, what conditions cause a coplanar disk to tilt or return from tilted? Though fundamental, these questions remain unanswered.

A determination of the current superhump period gives a wholistic understanding to the state of the system including active disk mechanisms and current mass transfer rates. Positive and negative superhumps are commonly seen in SU UMa type DN stars. As such, there is compiling evidence that CN such as V603 Aql may transition to DN systems (See section 2.5) a few hundred years after outburst as their mass transfer rates decrease (Mróz et al. 2016; Shara et al. 2017; Hillman et al. 2020). Therefore, regular campaign observations and the calculation of superhump periods is an important part of understanding CV system evolution. V603 is now over 100 years past outburst.

2.4 Brightness fluctuations and quasi-periodic oscillations

As the brightest observed classical nova in modern times, V603 Aql has gained much attention and as such, has a long observation history. During the decades of studies into this object, many periodic brightness fluctuations and oscillations have been found in the system's light curve. Some of these observations have proved to be important to the knowledge around the object while others have been discarded. This section summarises the more prominent of the observed brightness fluctuations.

2.4.1 Flickering and flaring

Flickering is a well-known phenomenon associated with semi-detached binary systems, including the CV types, classical, dwarf and recurrent novae, as well as nova-like variables. Flickering appears as short-term photometric variations in the system light curves, commonly occurring on time scales ranging from seconds to tens of minutes, with brightness variations of approximately $0.01 - 1$ magnitude (Bruch 1992). Many authors report the observation of flickering from V603 Aql (e.g. Haefner & Metz 1985; Bruch 1991; Patterson & Richman 1991; Bruch 1992; Suleimanov et al. 2004; Johnson et al. 2013) though few attempt to provide an explanation of the mechanisms behind it. Figure 2.6 shows a series of observations of V603 Aql using the Fine Error Sensor (FES) aboard the IUE satellite. This light curve displays short term flickering and a larger flare on rise to maximum.

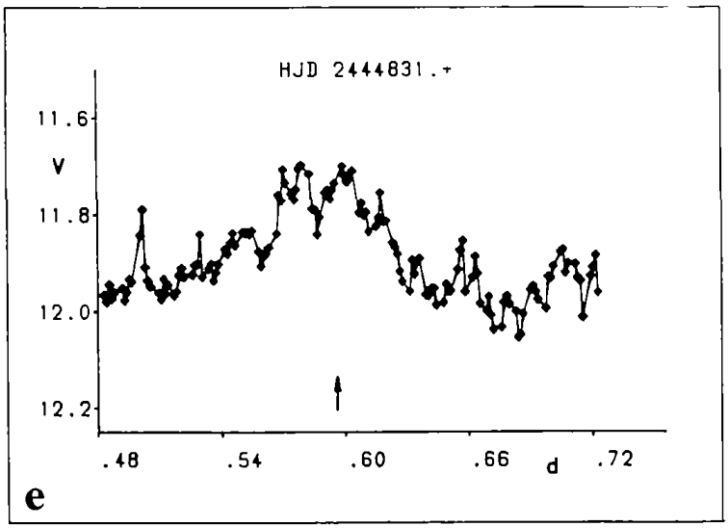

Figure 2.6: *A light curve of V603 Aql showing short term brightness variations (flickering) and short period flares on rise to maximum brightness indicated by the arrow. Source: (Haefner & Metz 1985).*

Unstable mass transfer between the secondary and primary stars is now widely accepted as the cause of these variations. Recent modelling and observations attempt to provide a more thorough explanation on how non-uniform mass transfer rates affect the mechanics of accretion disks (e.g. Scaringi et al. 2012; Scaringi 2014; Dobrotka et al. 2015). The model proposed here suggests high frequency flickering is produced as the greater and more viscous lumps of transferred matter migrate through the accretion disk toward the primary star. In a study of 107 CV light curves, Bruch (2021) reports an average flickering amplitude for V603 Aql in the V band of 0.058 ± 0.025 mag.

2.4.2 V603 Aql as an intermediate polar

Oscillations of $61.4\ min$ were reported by Udalski and Schwarzenberg-Czerny (1989) in optical and x-ray observations. The authors claim these oscillations as the rotational period of the white dwarf. For this reason, the authors argue that the system should be classified as an intermediate polar (IP) system. These systems, also known as DQ Herculis stars, typically have orbital periods between 1.5 and 10 hours, with a magnetic WD rotating on periods of $\approx 0.5m - 2hr$ (Patterson 1994). Light curves of V603 obtained in 1979 and 1983 were analysed by Bruch (1991) and failed to detect the $61\ min$ modulation. Further observations

made over 3 months in 1990, analysed by Patterson and Richman (1991) also failed to reproduce this period. Perhaps the final blow for this oscillation came when the same data studied by Udalski and Schwarzenberg-Czerny (1989) were further analysed by Eracleous et al. (1991), noting they do not find any peak of significance at this period. Although these results could not be reproduced, the intermediate polar argument continued. V603 Aql displays variability in its x-ray light curve, another feature of IP binaries. As such, the IP suggestions continued (Kang et al. 2006). In more recent studies the arguments against V603 Aql as an IP have been strong (e.g. Borczyk et al. 2003; Baskill et al. 2005). Indeed, the NASA Intermediate Polar database currently lists V603 Aql's IP status as 'doubtful' (NASA 2014).

2.4.3 Long period modulations

Cataclysmic variables also display variability over long time scales. Before the mechanisms for these fluctuations are fully investigated, their true periodicity needs to be determined. As V603 Aql is a popular object, a long history of observations is available. Bruch and Cook (2018) analysed data gathered over a 22-night period in 1991, finding a statistically significant variation with a period of 5.85 days. Their combined light curve is presented in Figure 2.7 with nightly average magnitudes (blue dots) and a least square sine fit (red curve) fixed at the 5.85-day modulation. The large amount of data considered here adds to the confidence and accuracy of the claim as a truly cyclic modulation.

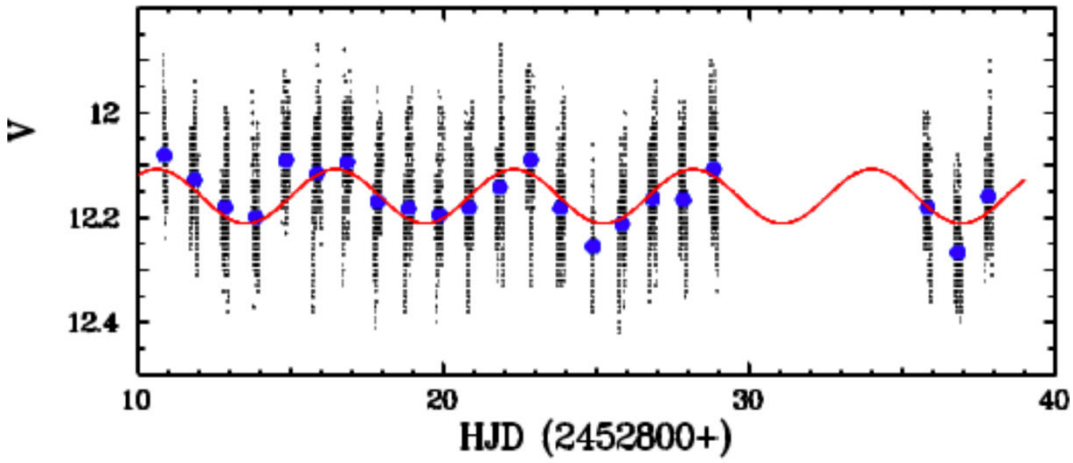

Figure 2.7: *Combined light curve for V603 Aql showing nightly individual observations (black dots), average magnitudes (blue dots) and a least squares sine fit (red line) for a 5.85-day modulation. Source: (Bruch & Cook 2018).*

Studies of four CVs with long observation histories, including V603 Aql, were undertaken by Richman et al. (1994) with the aim of determining any truly periodic long-term variations. Figure 2.8 below is the combined light curve consisting of observations made between 1965 and 1991. The curve shows a slow 'wiggle' of approximately 0.2 magnitude on the timescale of 15-20 years. The authors claim they could not fully evaluate whether the variability is a true long-term cycle or if it is an inconsistent change until another 50 years of observations could be examined. Since this time, consistent observations of V603 Aql have continued. The availability of this more expansive dataset may now help shed more light on this subject.

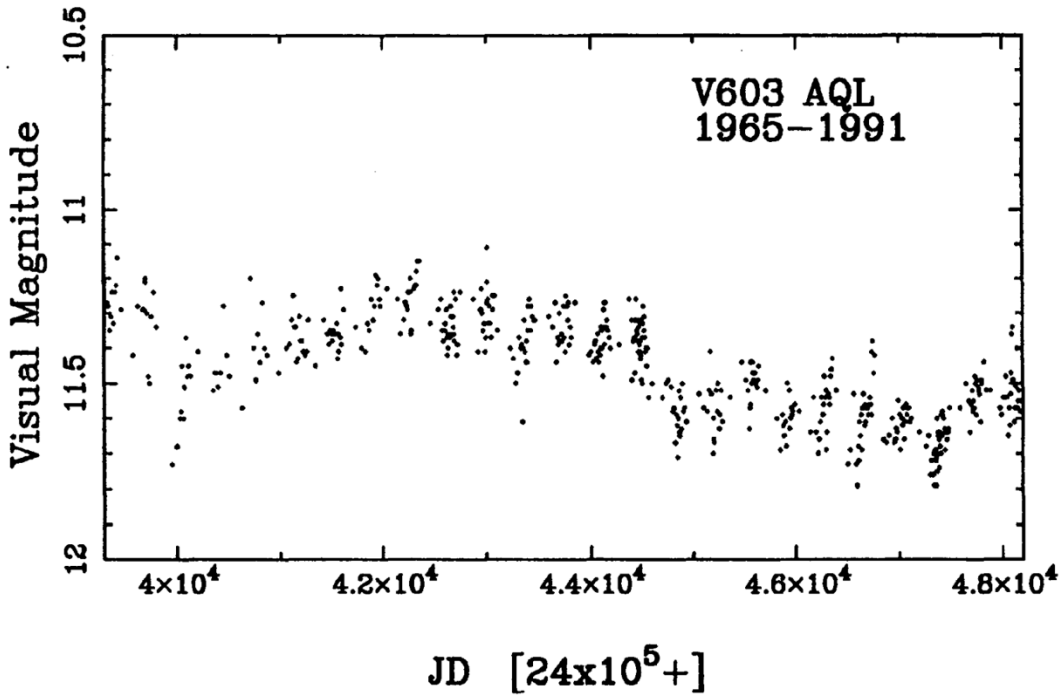

Figure 2.8: *Visual magnitude light curve for V603 Aql produced from data collected between 1965 and 1991. A brightness fluctuation of approximately 0.2 mag over 15 – 20 years is apparent here. Source: (Richman et al. 1994).*

Classical novae present a large range of periodic and quasi-periodic fluctuations, many of which are poorly understood and, as such, remain active areas of research and simulation modelling.

2.5 Cataclysmic binary system evolution

2.5.1 Mass transfer rates

The behaviour and evolution of CV systems after outburst is an active and widely researched topic in the CV field. The evolution and overall lifetime of cataclysmic binary systems is largely determined by the rate of mass transfer between the donor star and the WD. Throughout the life of CV systems mass transfer rates change as the stars age and system parameters vary. In the case of classical novae, pre and post-nova transfer rates are typically high in the century before and after nova events (Collazzi et al. 2009). These increased rates are considered stable for CN systems, in the order of $\dot{M} \gtrsim 10^{-8} M_{\odot} yr^{-1}$. The hibernation model (Prialnik & Shara 1986; Shara et al. 1986; Shara et al. 2018) suggests that nova

outbursts greatly affect these rates. High post-nova rates are explained by the irradiation and expanding of the donor star by the now hot white dwarf. The model predicts that a few centuries after outburst the white dwarf cools and the secondary star loses touch with its Roche lobe. This greatly reduces or stops mass transfer. The system enters a hibernation phase lasting hundreds or thousands of years before gravitational radiation brings the stars closer where accretion rates can increase once more. Eventually, the increased accretion of material leads to another nova outburst (Shara et al. 1986). The brightness of CV systems is primarily due to accretion luminosity in the disk (Pagnotta 2015), therefore mass transfer rates can be calculated as a function of the apparent visual magnitude of the system.

Table 2.1: V603 Aql system parameters

P_{orb}	M_{wd}	M_2	$Distance\ (d)$	m_v	A_v
$3.32hrs$[1]	~$1.2M_\odot$[2]	~$0.29M_\odot$[2]	$314(pc)$[3]	~11.8[4]	0.5[5]

References: [1]Peters and Thorstensen (2006): [2]Arenas et al. (2000); [3]Schaefer (2018); [4]This work; [5]Warner (2003).

Using Eqn 5 (Retter & Leibowitz 1998) and the parameters in Table 2.1 we can calculate the current mass transfer for V603 Aql:

$$\dot{M}_{17} = 10^{\frac{m_v - A_v - 0.69}{-2.5}} \cdot \frac{d^2}{M_1^{\frac{4}{3}}} \tag{5}$$

$$\dot{M} \approx 4.41 \times 10^{17} g/s$$

In solar masses this equates to $\dot{M} \approx 6.95 \times 10^{-9} M_\odot yr^{-1}$, less than what would be expected in a stable, post-nova CN system. Using Eqn 6 from Retter and Leibowitz (1998) and again the parameters in Table 2.1 a critical magnitude can be calculated. This is the magnitude at which the corresponding mass transfer rate falls to the point where CN to DN evolution is thought to take place.

$$m_{crit} = 2.16 - 4.25 \log P_{orb} - 3.33 \log M_1 + 5 \log d + A_v \tag{6}$$

This equation yields a critical apparent visual magnitude of $m_v \approx 12.7$. V603 Aql is currently observed at $m_v \approx 11.8$ and fading. Since the system returned to its pre-nova brightness in 1938 V603 Aql has continued to fade at a rate of 0.44 ± 0.04 magnitude per century (Johnson et al. 2013).

2.5.2 CN to DN evolution

Since the proposal of the hibernation model many studies have focused on cataclysmic binary mass transfer rates and what this means for their long-term evolution. One theory to come from this research is that these systems experience cyclic transitions from CN to DN as nova outbursts slow or halt donor transfer rates (Prialnik & Shara 1986; Shara et al. 1986). Eventually gravitational radiation brings the stars closer where higher mass transfer can begin once more (Pagnotta 2015).

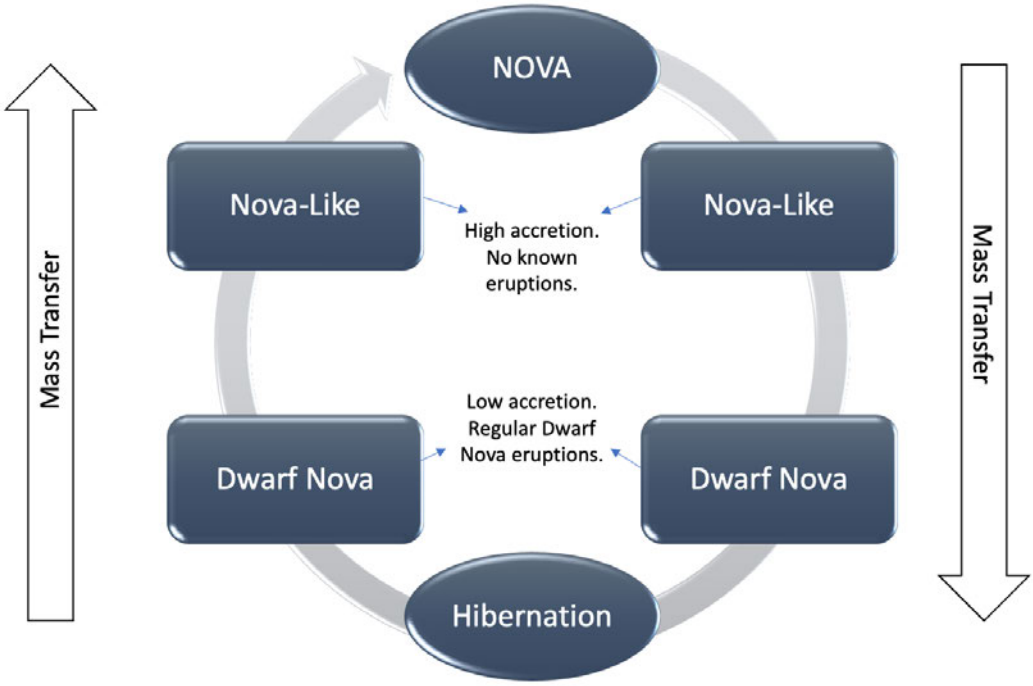

***Figure 2.9**: The hibernation model suggests CV's follow a cyclic evolution between novae as mass accretion rates vary. Figure reproduced from (Pagnotta 2015).*

Mass transfer rates of DN systems are unstable and typically 10 – 100 times less than that of CN stars. Some theories suggest mass transfer reduces quickly after a nova eruption

where CN to DN transition can take place as early as a few hundred years after outburst (Shara et al. 2016). Further considerations for the hibernation model are offered by Patterson (1984). In this work the author highlights the quantity of CN we see does not adequately account for the observed nova rate. It may be that old novae are masquerading as DN whilst in hibernation. Also, that as the accumulation of material on to the white dwarf continues, DN stars must in time go nova. An observational record of CN before and after outburst is now available and the interrogation of this data has provided evidence for a CN/DN evolutionary path. Nova shells discovered around DN stars show that in at least some cases this transition is known take place (Hillman et al. 2020). Indeed, it may be that this transition is typical for old CN stars. Some of the known examples of DN with observable nova shells are the prototypical Z Camelopardis (Shara et al. 2007; Shara, Mizusawa, Zurek, et al. 2012), AT Cancri (Shara, Mizusawa, Wehinger, et al. 2012; Shara et al. 2016) and BK Lyncis (Patterson et al. 2013). A study of pre and post nova observations by Mróz et al. (2016) revealed that the star V1213 Cen (Nova Centauri 2009) exhibited DN outbursts in the years preceding its nova outburst in 2009. Nova Centauri 2009 may be an example of the other end of the cycle, where hibernating DN stars awaken with new nova explosions.

2.6 Current project and future directions

As a prominent example of a classical nova with a rich history of observation, V603 Aql provides an opportunity for sustained research into the evolution of these objects and their behaviour post outburst. An analysis of the light curve from V603 Aql gives detail on the physical characteristics of the binary system. In this research the aim of the observations and analysis is to assess as many of the system parameters as possible in an attempt to gather information on the largescale evolution of the system. The system exhibits many similar characteristics to those of DN systems and may indeed evolve along this path. It is hoped that

the research presented here will reveal if the phenomena exhibited by V603 Aql has evolved and highlight the key characteristics that systems undertaking CN to DN evolution possess.

Key to understanding this will be confirmation of the photometric period of the system, as well as confirmed observation of current, sustained superhumps and the state (positive, negative or both) of these, providing direct insight into the disk mechanisms at play. A continuation of the work of Johnson et al. (2013) will also be conducted to determine whether V603 Aql continues to fade at the same rate and what this means for mass transfer and system evolution. The superhump period can be determined photometrically using equipment widely available. In order to determine the orbital and photometric periods, the desirable observation run is for 5 consecutive nights of 5 – 6 hours continued observation per night. However, confirmation of the 5.85-day modulation reported by Bruch and Cook (2018) may be possible if data can be gathered over an extended period of time. This oscillation has not been reported in any historical data other than the set used in their study.

An analysis of historical observations will be undertaken in an effort to refine the timescale of superhump period drift and phase change. The positive superhump period is reported to drift on a timescale of months and change from positive to negative on an unknown timescale as the influence of the secondary star on the WD accretion disk varies.

Future studies should continue to closely monitor these post-nova objects in an effort to confirm CV evolutionary path. Mass transfer is closely linked to the long-term evolution of CVs. Using historical data and researching how the magnitude of the system has changed since outburst can be used to determine how the mass transfer rate and system evolution of the binary is developing. Future research should concentrate on further closing the gap on the timeframe of CN to DN system transitions. Surveys of DN systems in search of nova shells

may also aid in this endeavour, increasing the catalogue of stars known make CN to DN transitions. It may be that this transition is in fact the normal case for this type of CV.

3 Methods

3.1 Historical data selection

The historical data selected for analysis was sourced from the American Association of Variable Star Observers (AAVSO) database (The American Association of Variable Star Observers 2021). The AAVSO data repository contains an almost constant set of observations for V603 Aql since it's eruption in 1918 through to the present day. The observational data here has been captured by dedicated observers predominantly in V, CV and Visual bands, then processed and made freely available for download and analysis.

Many of the data here have been collected as one or a few observations per night. This provides a long history of the magnitude of the V603 Aql system - some 81,000 observations are accessible - but much of the data is unsuitable for the determination of periods, such as orbital or superhump periods associated with close binary systems. The data sets targeted for period analysis were to span at least five hours per night, over three or more consecutive nights, and be of high cadence ($< 1min$ per integration is desirable). Typically, these sets were captured by a single observer in a concentrated observation campaign.

The AAVSO assigns each observer an observer code of 3 or 4 letters, attaching this designation to any data submitted. The total available data was separated into data frames categorised by this observer code, then plotted to assess the cadence and length of each observation run. This process was automated using a script written in Python. An example of the output of this script is presented below in Figures 3.1 – 3.3. Campaign or sub-set data for one observer is referred to by observer code in the methods and results section. Available observer information is provided in Appendix A, Table 2.

Table 3.1 is an example of the data frames produced by this method, showing the first 5 and last 5 observations in the set. The first column gives the selected row numbers from the

complete data set. Columns 2, 3 and 4 provide the Julian date, magnitude and the filter used for the observations respectively. Columns 5 and 6 show the observer code and their affiliation or observatory name.

	JD	Magnitude	Filter	Observer	Affiliation
49076	2456449.636	11.932	V	HMB	VVS
49077	2456449.638	11.908	V	HMB	VVS
49078	2456449.639	11.919	V	HMB	VVS
49079	2456449.640	11.988	V	HMB	VVS
49080	2456449.641	12.019	V	HMB	VVS
...	...	...	...	...	...
51100	2456488.758	12.009	V	HMB	VVS
51101	2456488.760	12.010	V	HMB	VVS
51102	2456488.763	11.916	V	HMB	VVS
51103	2456488.765	11.976	V	HMB	VVS
51104	2456488.768	11.967	V	HMB	VVS

***Figure 3.1**: Example data frame and observer information for observer 'HMB'.*

Figure 3.2 displays the combined light curve of the selected data for AAVSO observer 'HMB'. This data set was captured over 40 nights, centred on June 2013. The nightly observation sets (vertical lines), typically of $3 - 4\ hours$, have a mean magnitude variability approximately between 12 and 11.7 mag. These variations are discussed further in the following sections.

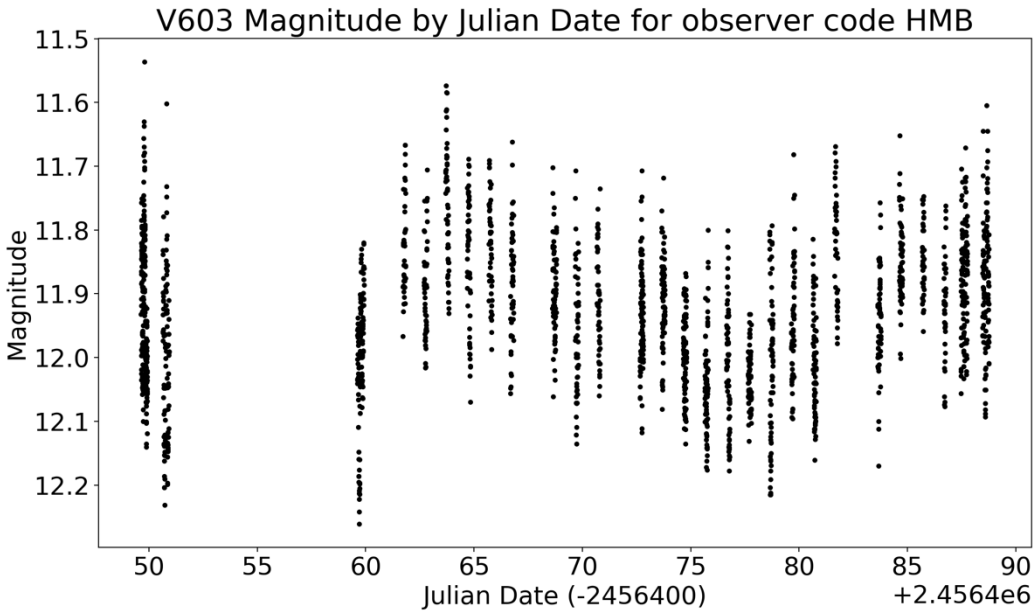

***Figure 3.2**: Plotted data for 'HMB' from the AAVSO database.*

Campaign observation sets spanning many nights were split into shorter sub-sets, Figure 3.3, usually of 5 consecutive nights. As nightly observation sets typically averaged 4 hours, it was not possible to analyse the 3.32-hour photometric period from a single night's data. Using a combined light curve ensures sufficient cycles are captured during period analysis. By reducing campaign data sets to a 5-night series any change in the superhump period on weekly timescales can be assessed.

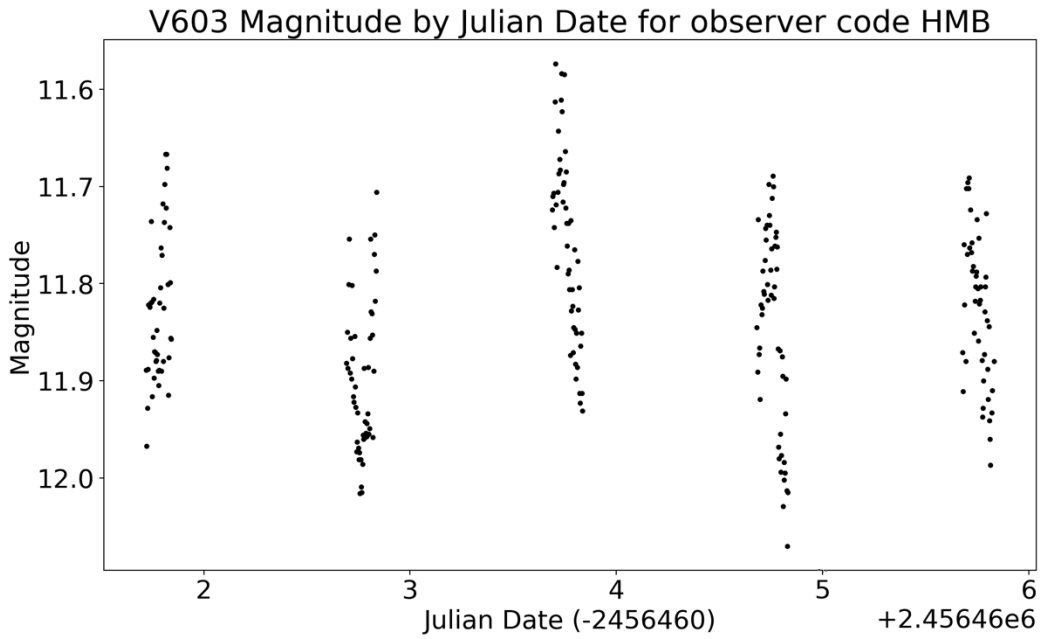

Figure 3.3: *A 5-night sub-set of 'HMB' data for Julian dates 2456460 – 2456466.*

The selected data frames are then written out to .csv files for time series analysis as described in Section 3.3. A table of the historical observation campaigns used in this analysis is available in Appendix A, Table 3.

3.2 Observational data collection and processing

3.2.1 Photometric data collection

Photometric data sets were collected from a range of observers and equipment. A summary of the collected data and associated information is available in Table 1 – Table 3 in Appendix A. The bulk of the new data was collected during an observation campaign granted by the AAVSO.

3.2.2 The AAVSO campaign

The requested AAVSO campaign ran through May, June and July 2021 forming the most comprehensive, high cadence observation set known for V603 Aql. The campaign data comprises 48,387 individual observations, over 77 almost consecutive nights, collected by 17

professional and amateur astronomers spanning the globe. The data from the AAVSO campaign were downloaded from the AAVSO photometry database in .csv file format with calculated magnitudes.

The data collected by the AAVSO observers, and any other new data collected for this study will hereafter collectively be referred to as the 2021 Campaign, where AAVSO data only is utilised the data set will be referred to as the AAVSO 2021 Campaign.

3.2.3 Data preparation and processing

Comparatively few erroneous observations were found in the data sets. Before the observations are accepted by the AAVSO they are processed through their data pipeline and checked for homogeneity. As the source of any error in these observations is unknown none of the repository data has been rejected. The files downloaded from the AAVSO for Lomb-Scargle analysis needed a small amount of pre-processing before they could be read by the script. Column names and zero or null values were corrected before this analysis.

3.3 Data analysis

The collected and refined data sets were examined for significant periods by time series analysis using the PERANSO 3.0 software developed by Paunzen and Vanmunster (2016) and checked by a Lomb-Scargle period finder written in Python using the module Astropy (Robitaille et al. 2013; Günther et al. 2018).

3.3.1 Time series analysis

PERANSO can be programmed to automatically ingest data from external databases, such as the AAVSO, or accept a prepared .csv file. Typically astronomical data is unequally spaced in time, caused by such affects as charge coupled device (CCD) download times, start and stop times of observations (sampling rates) and weather interruptions (Vityazev 1997). In this case an analysis method to compensate for these factors must be adopted. Here a

method known as CLEANest, developed by Foster (1995), is used as it compensates well for unequally spaced data while also dampening period aliases. Alias periods appear as multiples of significant periods and may appear significant if not correctly identified. Further to this the CLEANest method is able to detect multi-periodic signals, seen commonly in CN observations including V603 Aql (Bruch 1991; Patterson et al. 1997).

3.3.2 Pre-whitening data

Multi night astronomical data are prone to 'false' signals generated as a function of observational conditions such as cadence and sampling rates. These signals and their alias signals may appear significant in the computed power spectra. Unwanted signals such as these can be removed from the analysis output using a method known as 'pre-whitening' (Paunzen & Vanmunster 2016). This method is built-in to the PERANSO software. In the same way multi-periodic systems can be identified after the prominent period and its alias periods have been removed.

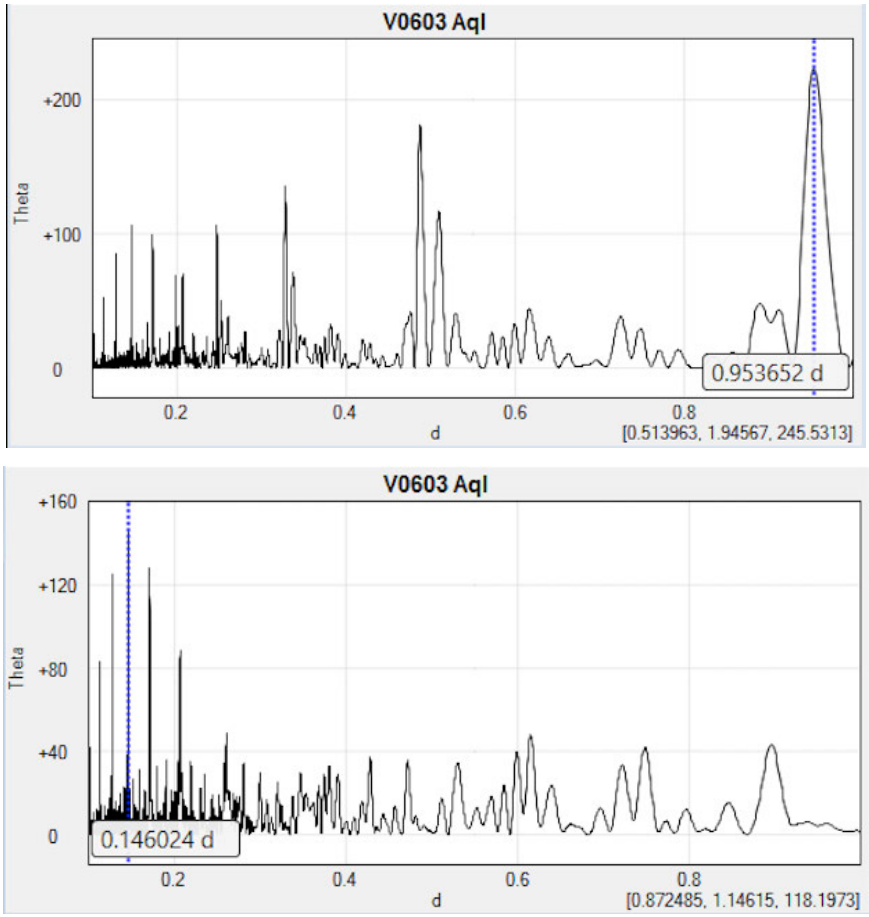

Figure 3.4a and 3.4b: *Period analysis for V603 Aql before (Top) and after (Bottom) PERANSO pre-whitening.*

Figure 3.4a and 3.4b show a period analysis of V603 data with a 'one-day' period and alias periods appearing dominant. After the data is cleaned with pre-whitening the true photometric period becomes prominent. In the same way the multiperiodic nature of CV's can be analysed, and as V603 Aql is known to display positive and negative superhumps simultaneously, by removing the prominent photometric period and it's alias signals underlying periods can be discovered.

3.3.3 Lomb-Scargle Analysis

The data sets first analysed in PERANSO were then checked using a Python scripted Lomb-Scargle (LS) method (Lomb 1976; Scargle 1982). The code used in this analysis is presented in Appendix B. The LS periods are in excellent agreement with those produced by

the PERANSO/CLEANest method. The results from both analyses are available in Appendix A, Table 3.

4 Results

For each of the sub-sections in Part 4 there is a corresponding discussion in Section 5. Appendix A, Table 1 summarises the full 2021 AAVSO Campaign observation set. The data collected during this campaign were analysed in the same method as the historical data.

4.1 PERANSO outputs

The PERANSO CLEANest period analysis returns a combined light curve of all observations used in each analysis, a power spectrum by period and frequency, and a prominent period table displaying the most prominent periods by power. An example of the output from this method used for the 5-night sub-set data is presented in Figures 4.1 – 4.4. The same analysis output was produced for all suitable campaign and sub-set data.

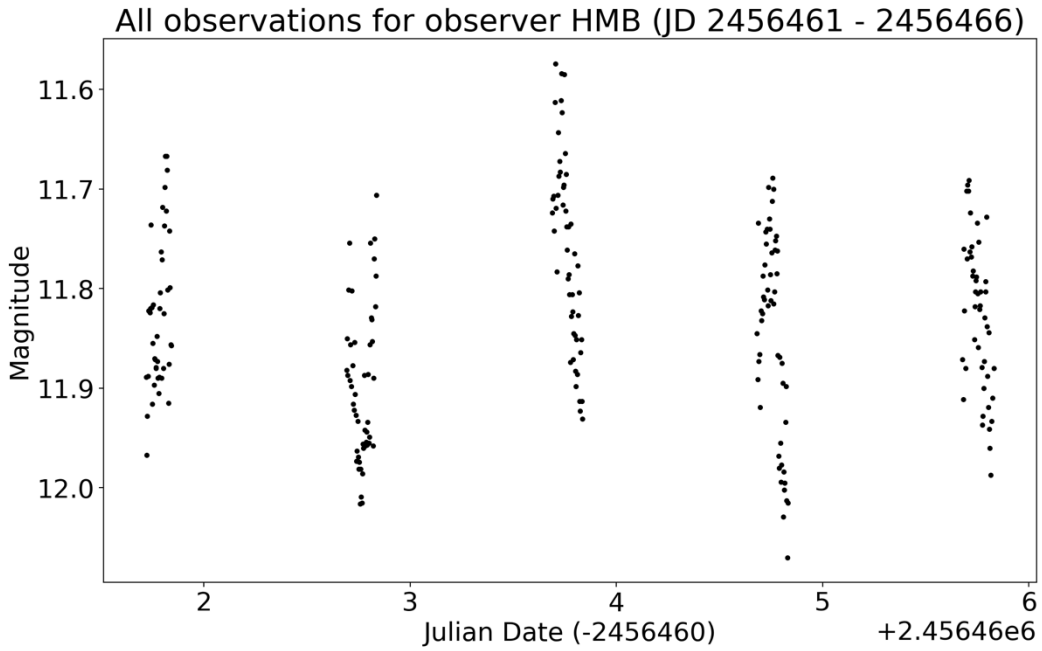

Figure 4.1: *Plot of a selected part of a larger observation run. This is a combined light curve for five nights of observations from observer 'HMB'. The observations were made in June 2013, between Julian dates 2456461 – 2456466.*

Figures 4.2 and 4.3 are the analysis outputs for this data showing the prominent periods ranked by power (Theta). The most prominent period is marked by a blue dotted line. The 'mirrored' peaks around the prominent period in Figure 4.3 is a good example of aliasing,

described in section 3.3.2. The removal of these peaks returns a new power spectrum and period table.

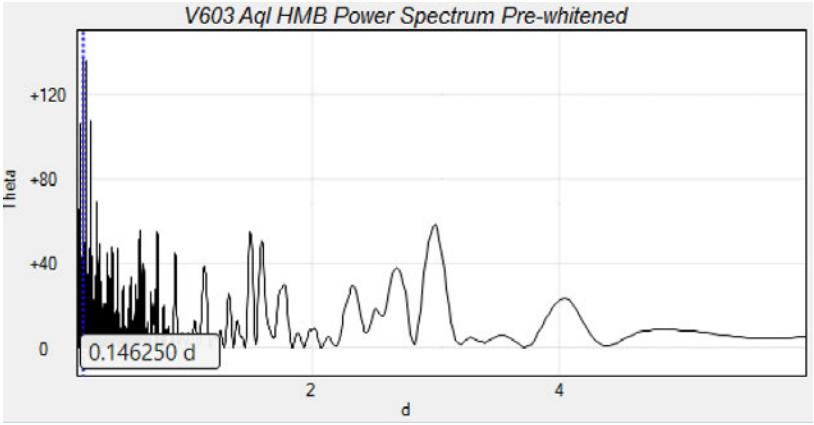

Figure 4.2: *PERANSO output. Power spectrum for prominent period.*

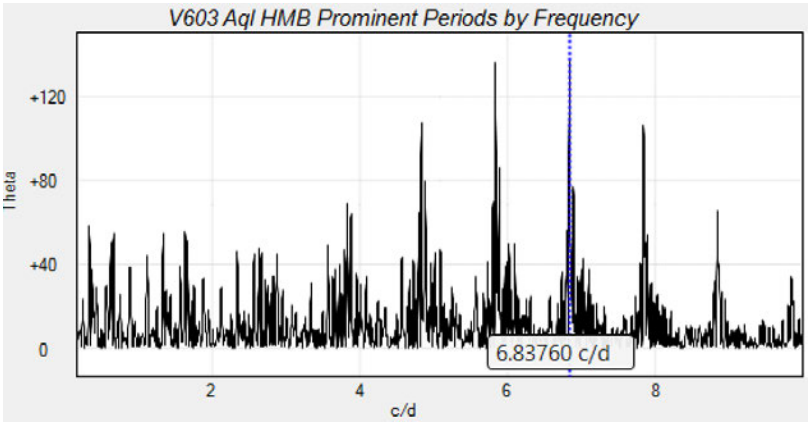

Figure 4.3: *PERANSO output. Prominent periods by frequency.*

Figure 4.4 is a period table produced from the PERANSO analysis. The power spectra above point principally at the prominent period where this table allows other periods to be explored. Column 1 gives the prominent periods in frequency (counts/day), column 2 is the time in days of this period and column 3 is the power at which the signal appears in the power spectra. This table contains all periods and their alias signals. The pre-whitening process described in Section 3 can be used to clean these signals out and search for multiple periods.

Freq (c/d)	Time (d)	Theta
6.83760	0.146250	136.72
5.83460	0.171391	136.41
4.83160	0.206971	107.60
7.84060	0.127541	105.95
5.88770	0.169846	86.48
4.88273	0.204803	79.56
6.89267	0.145082	77.22
5.80117	0.172379	69.66
3.82860	0.261192	69.24
8.84360	0.113076	65.21
4.79817	0.208413	65.02
3.87973	0.257750	63.96
0.33383	2.995507	58.11
6.80417	0.146969	56.58
1.63183	0.612808	55.38
1.33487	0.749138	55.09
0.66620	1.501051	54.65

Figure 4.4: *PERANSO output. Prominent period table for 'HMB' data.*

For each of the campaign data sets the period search range was set between 0.01 and 10 days. This large window allowed the confirmation of any multi-day periods, such as the speculated 5.85-day period. Following this analysis, the search window was refined so the photometric period could be targeted.

4.2 Photometric (Superhump) period analysis

4.2.1 The positive superhump photometric period

Figure 4.5 is a single night light curve from the 2021 Campaign. Spanning approximately 4.5 hours on the 2nd of June 2021 (JD 2459368), the superhump can be seen as a $\sim 0.3\ mag$ increase in brightness, peaking around JD 2459368.960.

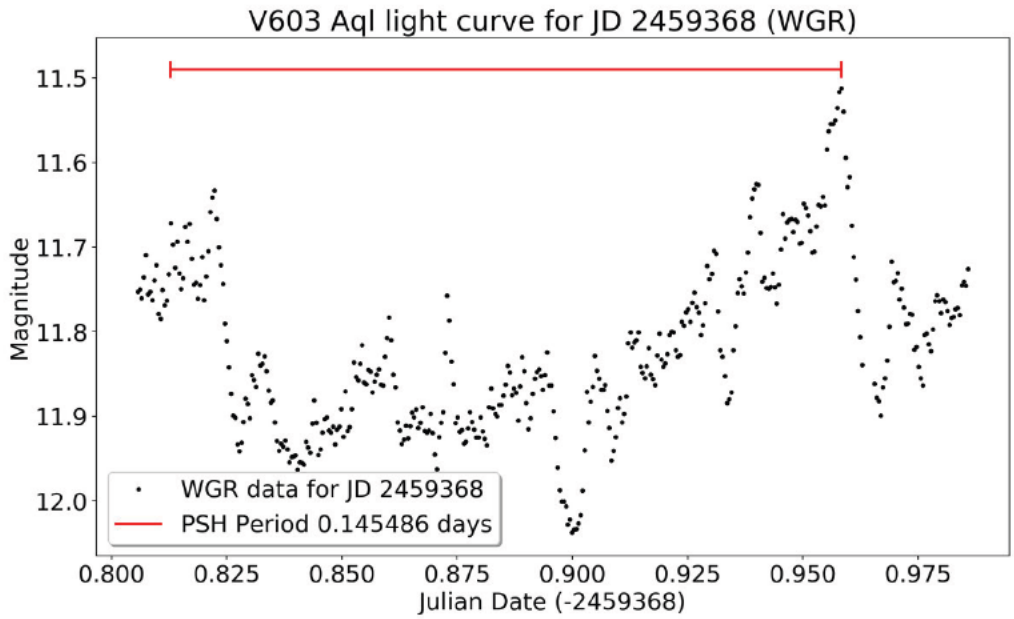

Figure 4.5: *Single night observation from the AAVSO Campaign made by observer 'WGR'. The photometric superhump is the bright peak at approximately JD = 0.960 (-2459368).*

The positive superhump photometric period was calculated for all historic campaigns and 2021 Campaign data sets. Table 4.1 contains the positive superhump periods calculated for the available campaign data sets as well as reported periods found throughout the literature where raw data was not available for re-analysis. For the 2021 Campaign an average positive superhump period of $P_{PSH} = 0.145466(87)\ days$ is found. This period is $\approx 5\%$ longer than the orbital period. The results presented here are discussed further in Section 5.

Table 4.1: Observing campaign information and positive superhump period in days.

Epoch	Campaign	Period (Reported)	Period (CLEANest)	Observer or Telescope	Reference
2444816.39	1981	0.144854 +/- 0.000008*	-	FES/IUE	(Haefner & Metz 1985)
2448067.87	1990	0.14548 +/- 0.0005	-	Lick Observatory	(Patterson & Richman 1991)
2449538.5	1994	0.14686 +/- 0.0007	-	Cerro Tololo, Sth Af. Observatory, Braeside Observatory	(Patterson et al. 1997)
2452811.78	2003	0.1453 +/- 0.0003	0.145327 +/- 0.000113	Lewis Cook – Concord Observatory (AAVSO)	(Bruch & Cook 2018)
2453908.4	2006	-	0.144792 +/- 0.000159	Bart Staels (AAVSO)	This work
2456449.64	2013	-	0.146216 +/- 0.000083	Franz-Josef Hambsch (AAVSO)	This work
2458686	2019	-	0.146331 +/- 0.001484**	Graeme White/John Pratt	This work

2459347.31	2021	-	0.145466 +/- 0.000087	AAVSO 2021 Campaign	This work

*The very small period uncertainty in the 1981 campaign ($\pm 0.000008d$) may be incorrectly reported in Haefner and Metz (1985). As pointed out by Patterson and Richman (1991) this suggests a measurement of the superhump period to within a minute.

**The large error associated with the 2019 data set is a function of a small sample size (545), where other campaigns contain upward of 2000 observations.

Figure 4.6 is a graph of the mean positive superhump photometric periods for each campaign. The blue line represents the orbital period of the system of $P_{Orb} = 0.1382\ days$ (Peters & Thorstensen 2006), where photometric periods above this line are positive superhumps, typically a few percent longer than the orbital period.

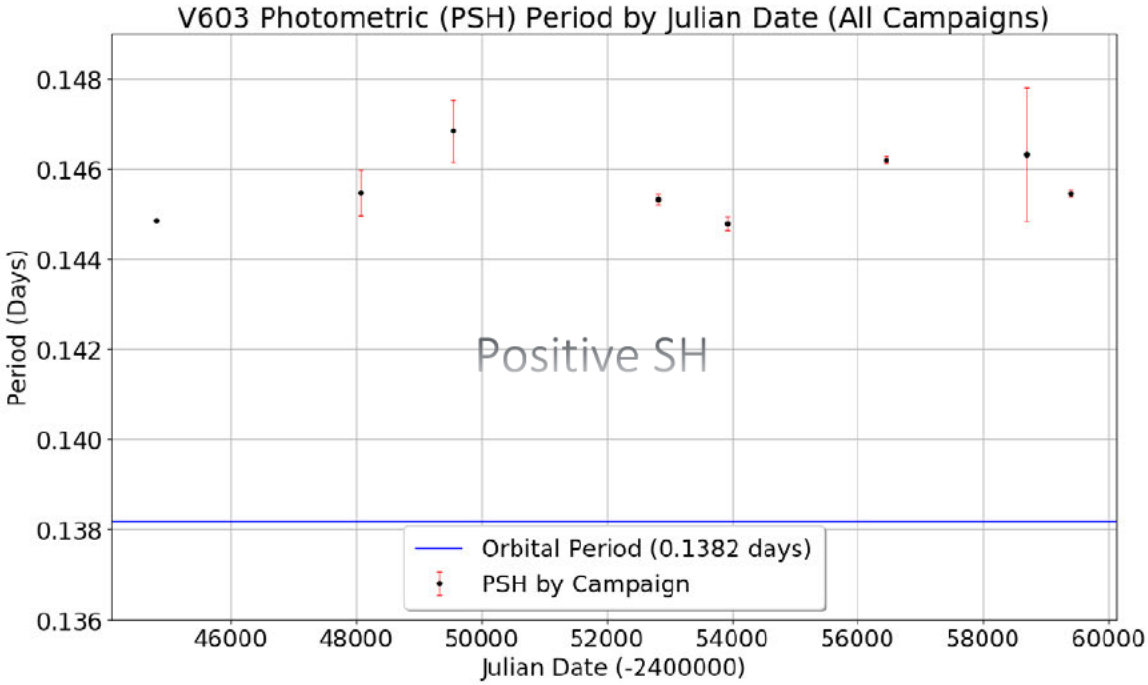

Figure 4.6: *Positive superhump period by campaign since 1985. The blue line represents the orbital of the V603 Aql system.*

The average period for these campaigns combined is, $P_{PSH} = 0.1456\ days$, 5.01% longer than P_{Orb}.

4.2.2 The positive superhump period drift

The positive superhump period drift has previously been reported by Patterson et al. (1997) as fluctuating between 0.144 and $0.147\ days$, 'wandering' on a timescale of months. The period variation calculated from the 2003, 2013 and 2021 Campaign data shows this

period fluctuating between a minimum of 0.144192 and a maximum of $0.14686\,days$, consistent with the reported fluctuations. Using 5-day sub-sets of the full campaign observations the timescale of this drift can be assessed. Figures 4.7 and 4.8 are graphs of the positive superhump period calculated from the 2003 and 2013 campaigns respectively.

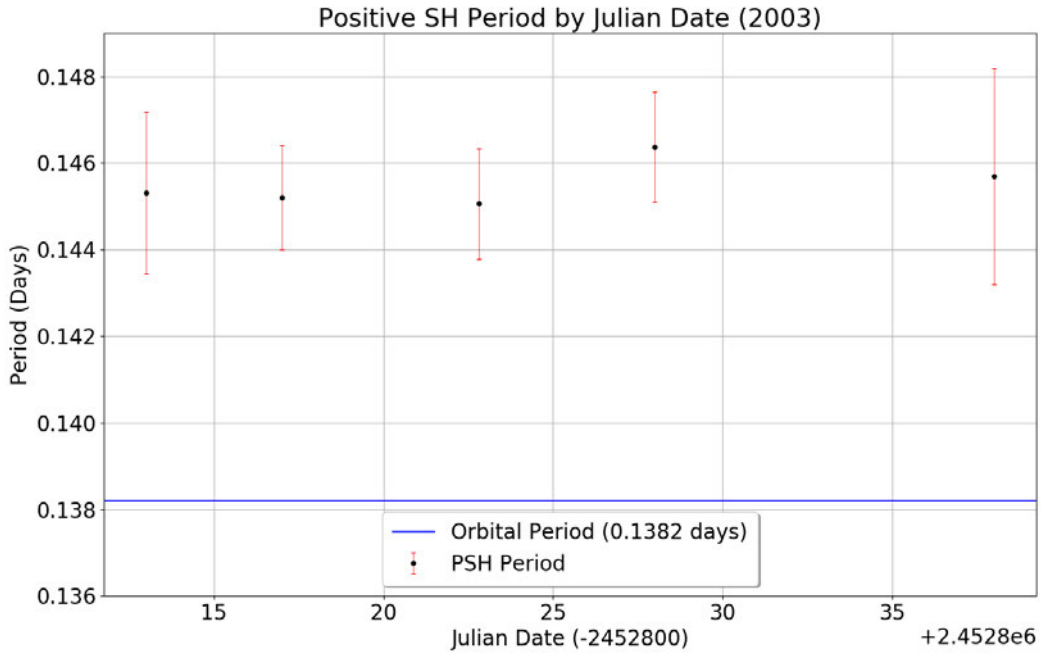

Figure 4.7: *Positive superhump period for the 2003 V603 campaign, observed by Lewis Cook (COO) (The American Association of Variable Star Observers 2021).*

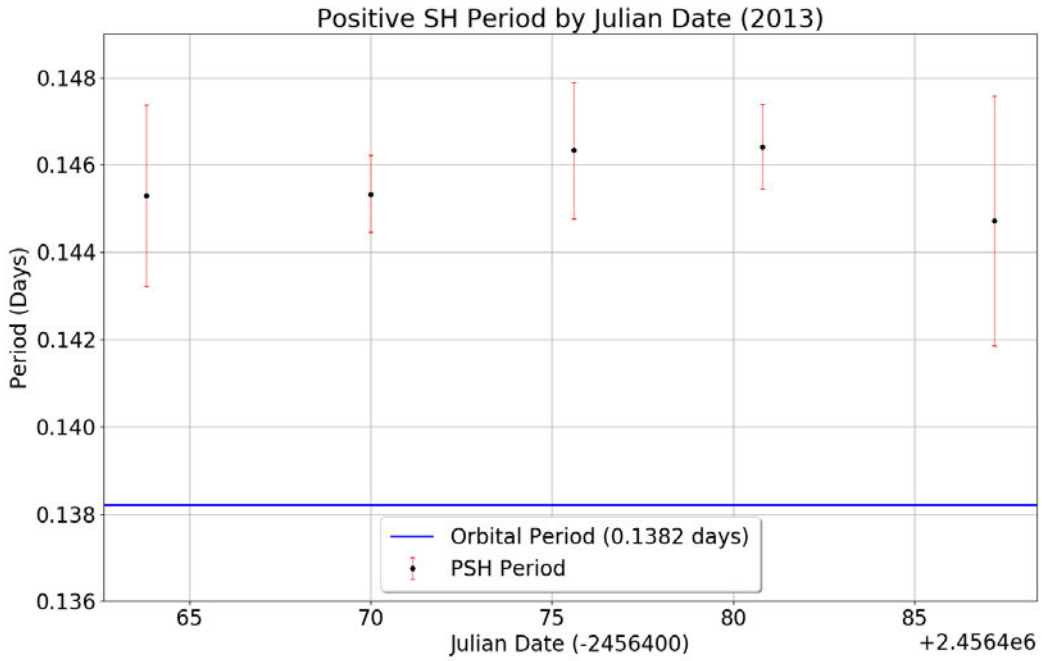

Figure 4.8: *Positive superhump period for the 2013 V603 campaign, observed by Franz-Josef Hambsch (HMB) (The American Association of Variable Star Observers 2021).*

Figure 4.9 is the 2021 Campaign data analysed by the same method. The data used here were collected by two observers affiliated with the AAVSO. Throughout June Franz-Josef Hambsch (HMB) collected nightly light curves of up to 7-hours per night, from the Remote Observatory Atacama Desert (ROAD). In July high cadence light curves were gathered at the Las Pegueras Observatory, by the owner, Teófilo Arranz (ATE). The Las Pegueras observations were made in Johnson V-band with a Meade LX200 14" telescope, reduced to F/5. The integration time was 20 seconds using an Atik 460 EX Monochrome camera (Arranz 2021, pers. comm., 15 September).

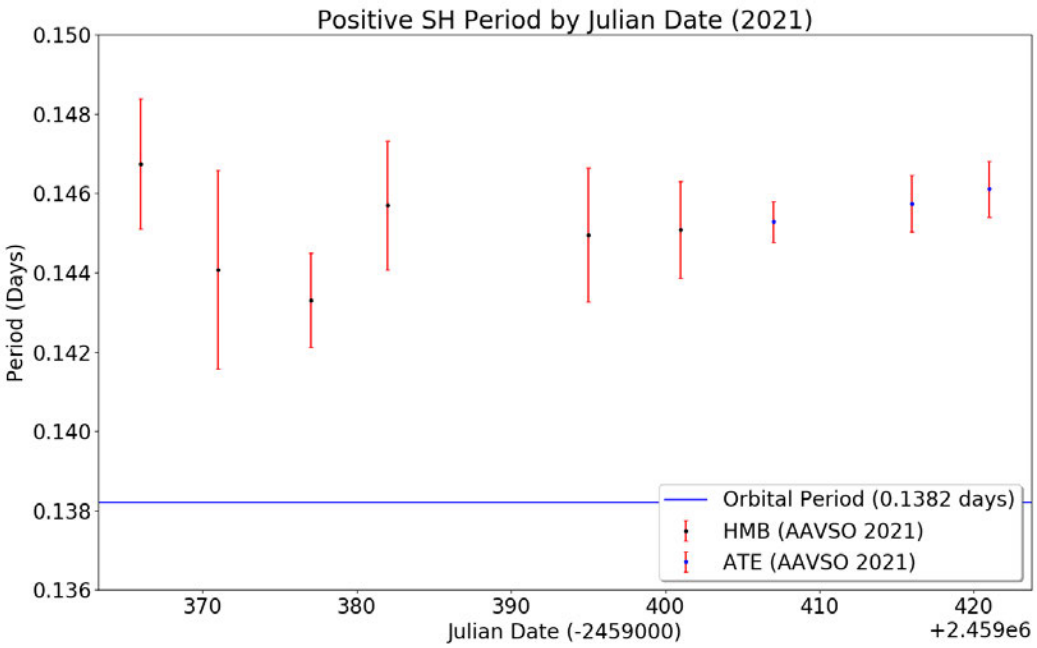

Figure 4.9: *Positive superhump period for the 2021 V603 campaign, observed by Franz-Josef Hambsch (HMB) and Teófilo Arranz (ATE) (The American Association of Variable Star Observers 2021).*

The previously discussed 'wandering' of this period was though to take place over a period of a few months. The analysis of sub-sets of the above campaigns shows that this period fluctuates weekly, within the same range previously specified (0.144 - 0.147 $days$). The steady increase in period after JD 245390 of the 2021 Campaign may be a function of the phase change from positive to negative superhump domination of the light curve. This change is discussed in the following sections.

4.2.3 Prominent period: Positives and negatives.

In the previous sections the positive superhump period has been analysed, and though typically dominant, this is not always the case. An in-depth analysis of the power spectrum for each campaign reveals in nearly all cases a signal fitting the negative superhump is also present. Table 4.2 summarises the campaign data by mean magnitude, prominent period and secondary period. Typically, the negative superhump period emerges as secondary, though at times appears as the prominent period. Indeed, the 2021 Campaign analysed as a full set

shows the system is in a negative superhump phase. A month-by-month analysis of the same data reveals a potentially new and important discovery for this system, the prominent period changes phase. In June the prominent photometric period was calculated at $P_{PSH} = 0.146846(203)\ days$, associated with the positive superhump. An identical analysis of the July data reveals the prominent period had changed to $P_{NSH} = 0.135417(196)\ days$, approximately 2% shorter than the orbital period. This change of phase coincides with an increased system brightness of $\approx 0.1\ mag$. Suleimanov et al. (2004) found the system to be $0.2 - 0.3\ mag$ brighter in the negative state.

Table 4.2: Prominent and secondary periods by campaign.

Campaign	Mean Mag (V)	Prominent Period	Secondary Period	Reference/Observer
1990	-	0.146(2)	0.132(1)	(Arenas et al. 2000)
1992	11.71	0.1345(2)	-	(Patterson et al. 1997)
1994	11.674	0.13382(5)	0.14686(7)	(Patterson et al. 1997)
2003	12.1604 (CV)*	0.145327(113)	-	(Bruch & Cook 2018)
2006	12.5259 (CV)*	0.144792(159)	0.134560(293)	This work (SBL)
2013	11.9284	0.146216(83)	0.134542(160)	This work (HMB)
2019	-	0.146273(1111)	0.136600(1070)	This work (GW/JP)
2021 (All)	11.70	0.135203(6)	0.145466(87)	This work (AAVSO)
2021 (Jun)	11.74	0.146846(203)	0.135417(196)	This work (AAVSO)
2021 (Jul)	11.64	0.134997(217)	0.144622(239)	This work (AAVSO)

*CV is the AAVSO designation for unfiltered, reduced to V magnitudes ('Clear V'). The effective wavelength captured in these observations is dependent upon the camera used and are typically reported as brighter than the corresponding Johnson-V observations. As such they are analysed for periods as stand-alone data sets, categorised by individual observer. These observations are removed from any analysis where consistent magnitudes in a selected band is essential to the result.

The occurrence of these two signals together is not uncommon in CVs possessing a permanent positive superhump. Further discussion on the V603 Aql photometric period is provided in Section 5.1.2 and Section 5.1.3.

4.3 Other reported periods

4.3.1 The 5.85-day period.

A re-analysis of the 2003 campaign shows the 5.85 day period as second most prominent period as reported by Bruch and Cook (2018), however, there is no sign of this period in all other campaign data analysed for this work, using the same methods. If the

period is indeed present in any of the power spectra produced in the analysis here and has been overlooked, it must be of very little power, much less than the significance it displays in the 2003 campaign observation set.

4.3.2 Flickers and flares.

High-cadence light curves obtained during the 2021 Campaign display short period variabilities, known as quasi-periods, characteristic of CV systems. Some of these periods are associated with flickering and flaring (previously introduced in Section 2.4.1). Quasi-periods as short as $9\ min$ are reported for V603 Aql. In order to detect these short periods a frequency search range between $1 - 200\ counts/day$ was selected. The range of frequencies searched in this analysis is broad, and as such a Generalised Lomb-Scargle (GLS) method is used here as it is far more efficient than the CLEANest method previously used in the photometric period analysis. The upper end of this range equates to $1440\ min\ (1\ day)$, while the lower end ensures periods as short as $7.2\ min$ are captured.

Figure 4.10 is a differential photometry plot of V603 Aql against comparison star 99 $(\mathrm{RA}: 18: 48: 40.87\ \mathrm{DEC}: 00: 38: 47.9\ \mathrm{Magnitude}: 9.868)$, and a power spectrum revealing the prominent periods captured during the observation session. The plot is a typical nightly light curve obtained during the 2021 Campaign by observer 'ATE', at high cadence $(\sim 20\ secs)$. The accompanying Table 4.3 describes the quasi-periods in more detail, giving the frequency of the top 10 periods by power (theta), and the period time in minutes.

The shortest period found here was $12.91\ min$. Table 4.4 summarises the most prominent quasi-periods for each of the analysed nights. A further 6 nights of identical analysis and a series of differential photometry plots are provided in Appendix C.

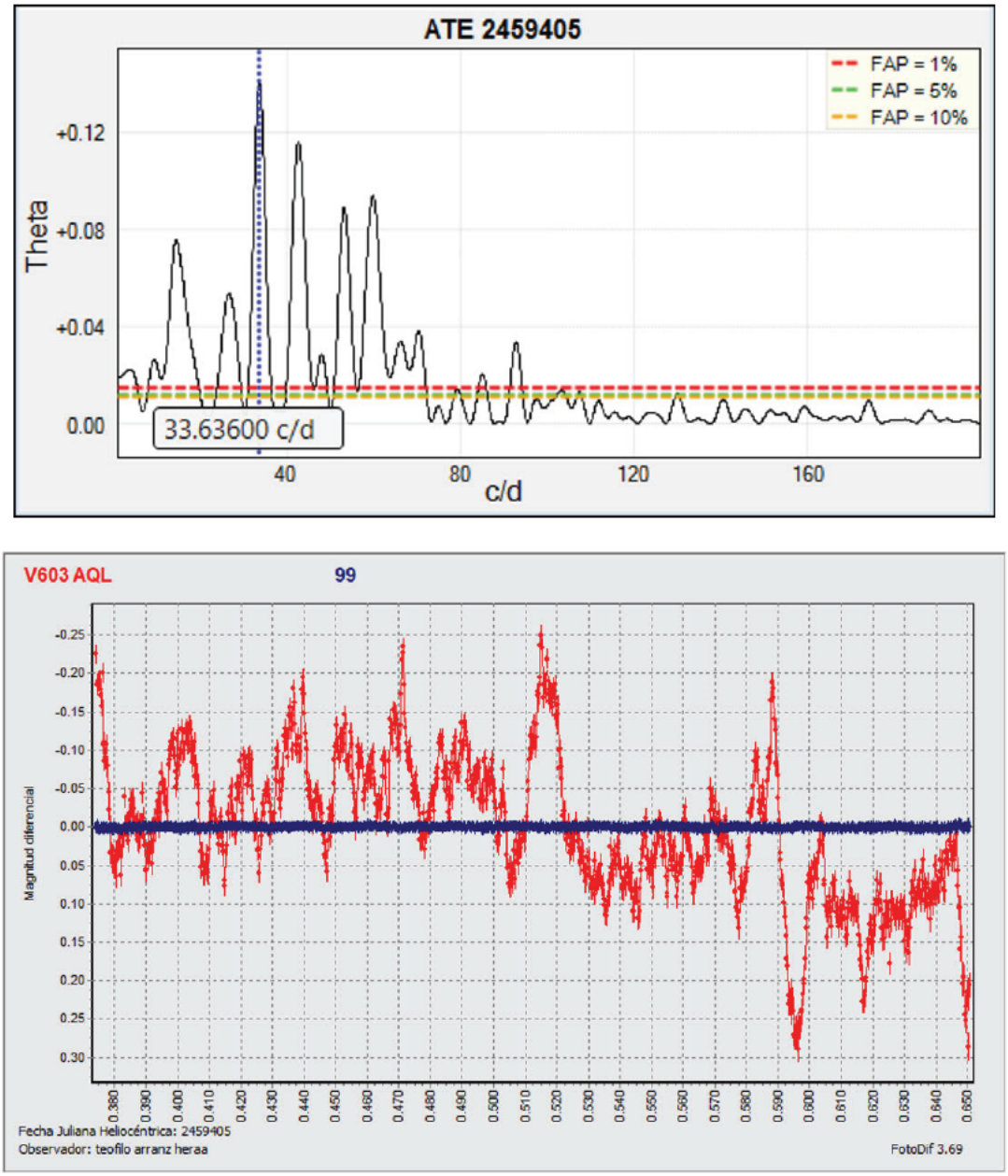

Figure 4.10: *PERANSO power spectrum and differential photometry plot of V603 and comparison star 99, for JD 2459405. The short duration variability of V603 Aql is evident here (Arranz 2021, pers. comm., 15 September).*

Table 4.3: Most prominent short duration periods by power (Theta) for JD 2459405.

No.	Frequency	Time (mins)	Theta
1	33.63600	42.81	0.14
2	42.63080	33.78	0.12
3	59.82440	24.07	0.09
4	53.17780	27.08	0.09
5	14.41260	99.91	0.08
6	26.59140	54.15	0.05
7	70.37140	20.46	0.04
8	66.19240	21.75	0.03
9	92.85840	15.51	0.03
10	48.00380	30.00	0.03

Table 4.4: Prominent short duration periods for seven separate nightly analysis. The periods listed here are from greatest to least power (Theta).

Julian Date	Identified quasi-periods (mins)
2459405	42.81, 33.78, 24.07, 27.08, 99.91, 54.15, 20.46, 21.75, 15.51, 30.00
2459406	109.93, 347.47, 76.96, 21.02, 41.92, 36.62, 24.83, 32.92, 22.70, 48.43
2459407	211.34 (P_{NSH}), 1440 ($1\ day$), 58.06, 96.19, 36.50, 23.12, 18.45, 27.79, 17.41, 13.27
2459408	405.95, 73.07, 30.66, 28.09, 41.92, 18.15, 34.03, 54.40, 132.47, 23.55
2459410	133.45, 1440 ($1\ day$), 45.85, 20.56, 293.85, 18.58, 91.57, 71.35, 56.17, 34.69
2459411	1440 ($1\ day$), 137.50, 34.36, 50.88, 20.28, 26.41, 16.50, 15.10, 30.10, 12.91
2459412	152.58, 88.43, 1440 ($1\ day$), 16.42, 22.28, 13.09, 35.85, 58.06, 24.66, 47.85

4.4 V603 Aql continues to fade

The V-Band data for V603 Aql, including the 2021 Campaign data, were converted to 'Vis' to maintain continuity. The V-Band data was converted to 'Vis' magnitudes using the conversion equation from (Stanton 1999)

$$Vis = V + 0.21 \times (B - V)$$

where $B - V$ for V603 $= -0.04$ (Johnson et al. 2013).

Figure 4.11 shows V603 Aql by magnitude since eruption in 1918 through to the 2021 Campaign. Since returning to quiescence around 1938, Johnson et al. (2013) calculate a linear fading rate of $0.44 \pm 0.04\ mag$ per century.

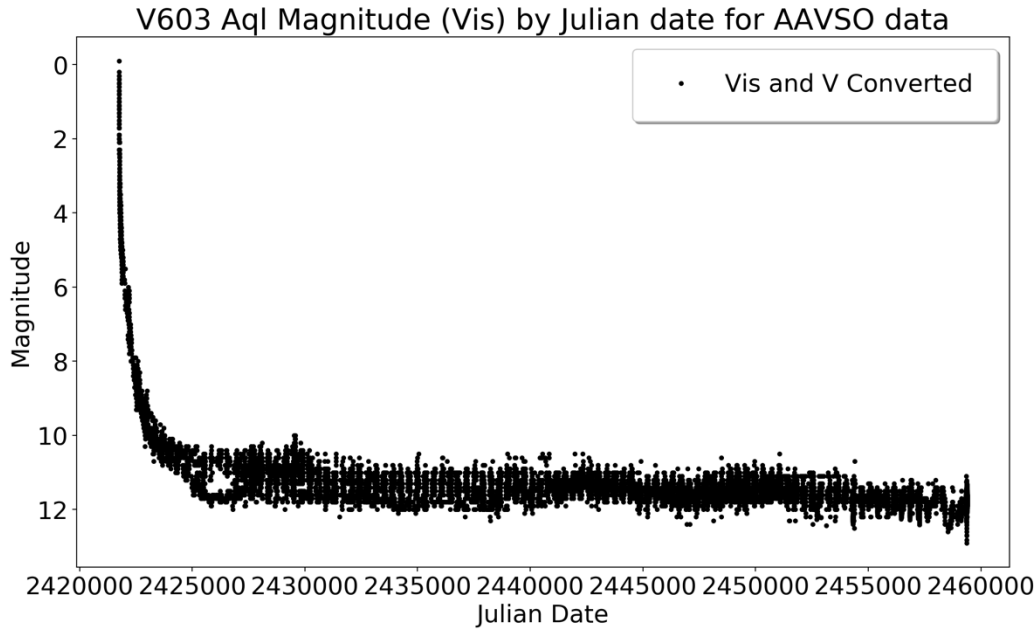

Figure 4.11: *All available Vis and V band data for V603 Aql from JD 2421753.4 to 2459383. Data from The American Association of Variable Star Observers (2021).*

Figure 4.12 is a closer inspection of the same data spanning 1950 – 2021. The dense regions are the result of intensive observation campaigns. The 2021 Campaign is at the extreme right of the graph.

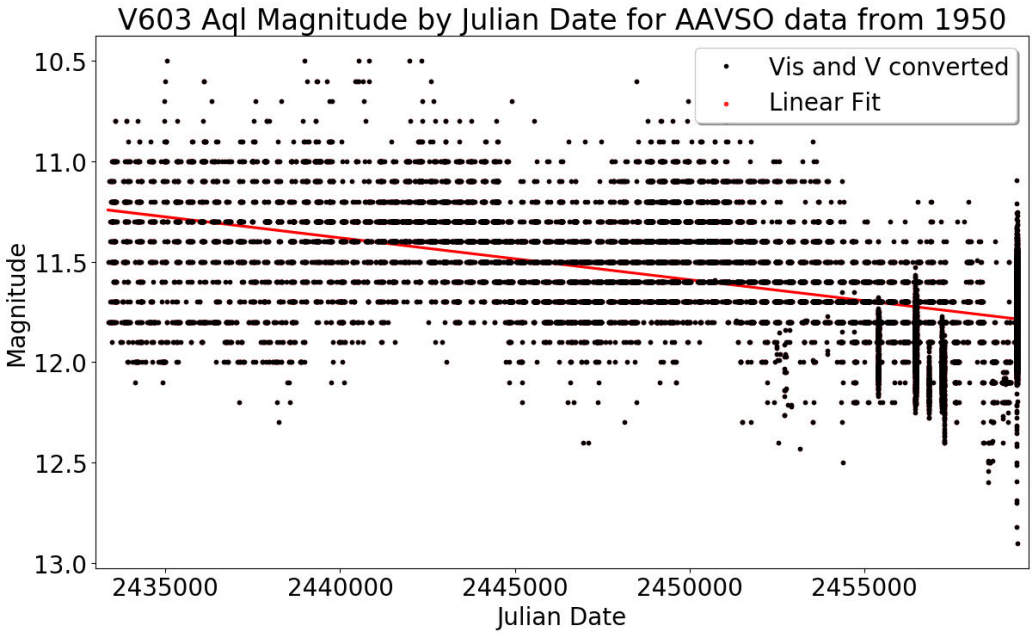

Figure 4.12: *Vis and V observations (converted to Vis) since January 1950 (JD 2433282). The 2021 AAVSO Campaign data is included here at the extreme right of the figure. This data used here is from the records of The American Association of Variable Star Observers (2021).*

In this analysis the rate of fading from the available Vis data between 1950 and 2021 is calculated at $0.62\ mag$ per century. Figure 4.13 is a graph of the data used in this analysis, binned by year.

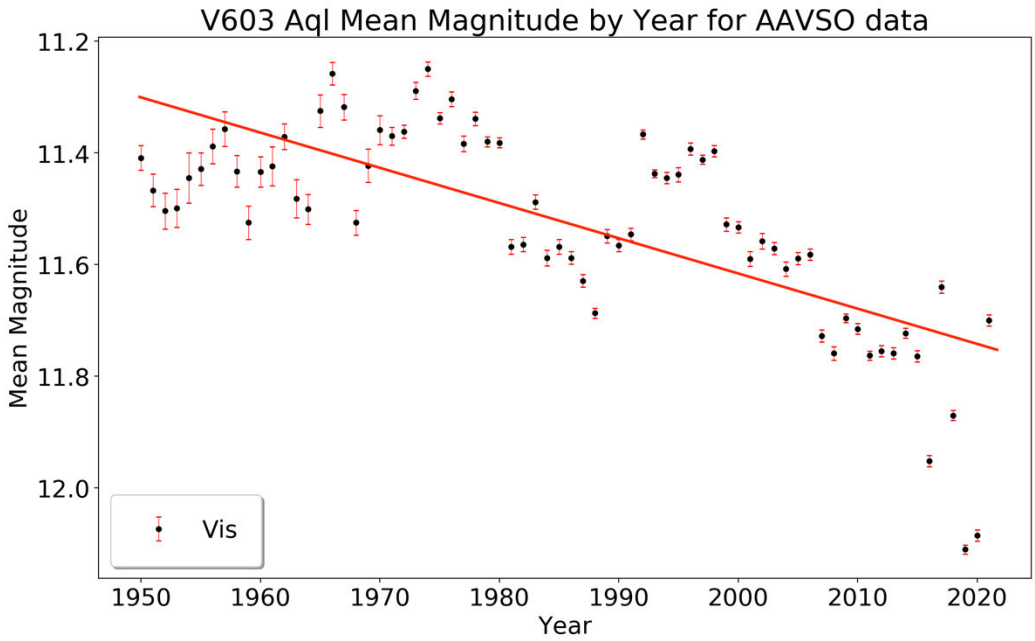

Figure 4.13: *Vis data for V603 Aql binned by year from 1950 to 2021. The rate of change in brightness is calculated at* $0.62\ mag$ *per century.*

The 2021 Vis data shows the system has a current mean brightness of $\approx 11.70\ mag$, consistent with the Johnson et al. (2013) prediction.

5 Discussion

5.1 The V603 Aql photometric period

5.1.1 An unrealised discovery?

The first observation of a superhump in the V603 light curve was reported by Haefner and Metz (1985). Although this was the first reported confirmation of the superhump it is likely that the period of this phenomena had in the past been observed and wrongly reported as the orbital period of the system. Indeed, during the analysis of reported periods for this work at least one instance of such a mistake is possible. Using the FES aboard the IUE Drechsel et al. (1981) report a photometric period of $P_{Orb} \approx 0.1377\ days$, with a change in magnitude of approximately 0.3 mag. This was reported as the orbital period of the system, comparable with the accepted orbital period of the time, spectroscopically determined by Kraft (1964) at $0.13854\ days$. The characteristics of this period determination, in particular the magnitude variation, and that it was observed photometrically leave little doubt that this was in fact an earlier observation of the V603 Aql negative superhump. A similar photometric period is present in the AAVSO 2021 Campaign data, calculated in this thesis at $P_{NSH} \approx 0.137339\ days$. From HMB data.

5.1.2 The 2021 Campaign photometric period

Some authors claim the negative superhump becomes prominent when the system is at increased brightness (See; Suleimanov et al. 2003). This claim is difficult to verify as campaign data sufficient in length and quality for period determination is intermittent, often spaced by a decade or more. Furthermore, data revealing a prominent negative superhump is rarer still (the positive superhump signal is typically prominent) and as such refining the superhump phase change on timescale or magnitude basis is problematic. An analysis of the

negative superhump phase, observed in 1992 (See Table 4.2) and discussed in Patterson et al. (1997), shows the system has a mean photometric period of $P_{NSH} = 0.1345(2)\ days$ with average brightness of $11.71\ mag$.

The analysis of the full 2021 AAVSO Campaign as a complete set indicates the system was in a negative superhump phase with an average brightness of $11.70\ mag$ with a prominent photometric period of $P_{NSH} = 0.135203(6)\ days$. Analysis of the same data month by month reveals during June 2021 the prominent photometric period was that of the positive superhump, where $P_{PSH} \approx 0.146846(203)\ days$, with a mean magnitude of $\approx 11.74\ mag$. In July the negative superhump period was again dominant, calculated at $P_{NSH} = 0.134997(217)\ days$. This change of phase in July 2021 coincided with an increased brightness of the system, measuring $\approx 0.1\ mag$, with the mean brightness of the system now measured at $\approx 11.64\ mag$. This may be the first observation of the superhump phase change within a single campaign. Previous studies have reported both positive and negative prominent periods, though these have been in separate campaigns conducted in different years.

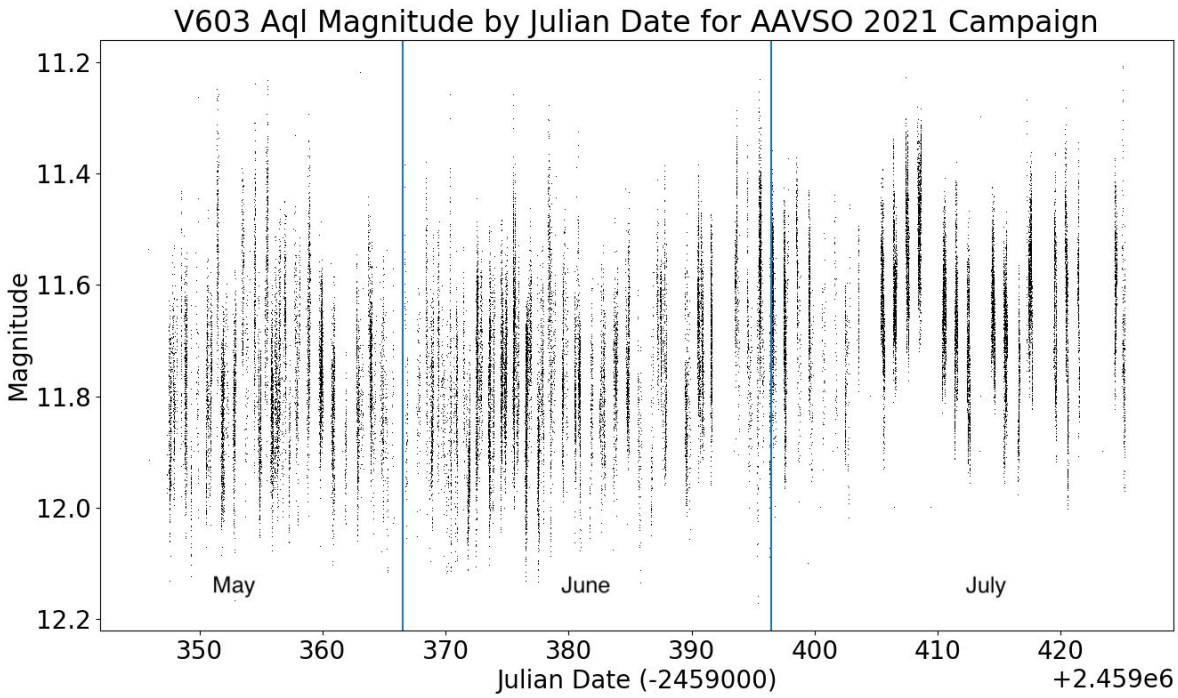

Figure 5.1: *The full AAVSO 2021 Campaign separated by month. An increase in the mean magnitude of the system is seen after JD 2459390. This increase was calculated at ≈ 0.1 mag. Data from The American Association of Variable Star Observers (2021)*

Increased brightness of a CV system suggests an increase in mass transfer, as per the magnitude/mass transfer relation (See section 2.5.1). Dwarf novae have been shown to exhibit negative superhumps on rise to superoutburst when their mass transfer rates, and consequently brightness, are increased (Smak 2008). Continued, consistent observations of V603 AQL will be required to verify the true timescale of the period shift.

5.1.3 Superhump period and magnitude relations

Both positive and negative superhump signals are commonly seen together in period analysis, either of which may be the prominent period for a given epoch. The positive and negative superhump periods have been shown to share a relationship where the longer positive superhump period coincides with a shorter negative superhump period. This relationship was discovered by Patterson et al. (1997) and described further by Suleimanov et al. (2004) as tidal effects on the disk precession act to alter these periods. Figure 5.2, adapted from Suleimanov et al. (2004) demonstrates this relationship using their data as well

as data from the original study by Patterson et al. (1997). The results from the full 2021 Campaign have been added here.

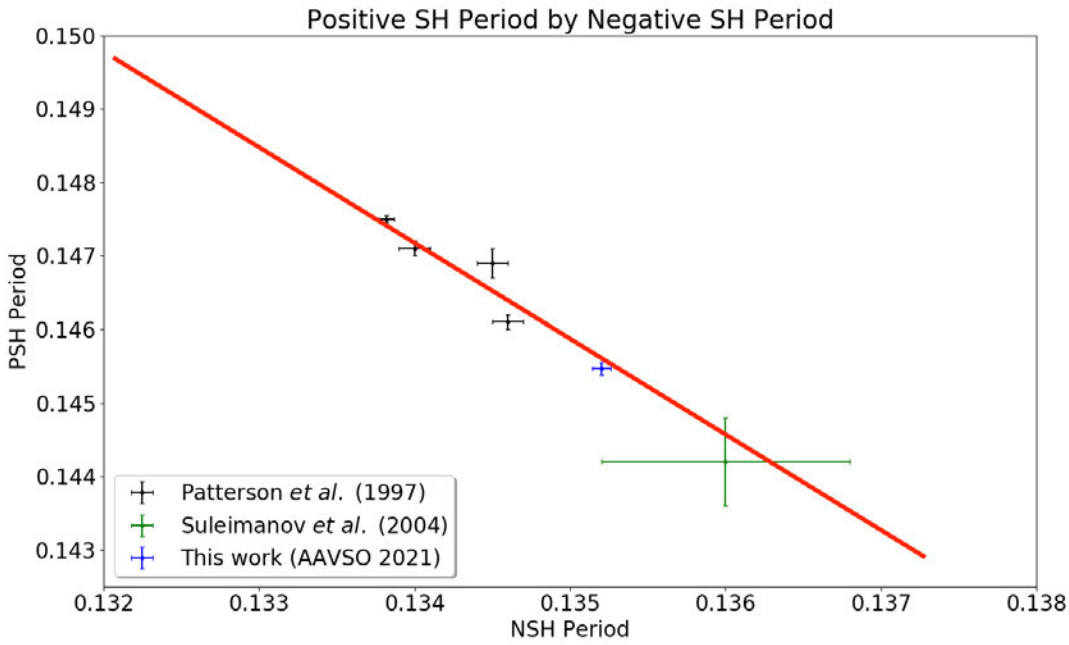

Figure 5.2: *Positive and negative superhump relation. As the positive period increases the negative decreases (Patterson et al. 1997; Suleimanov et al. 2004).*

Patterson et al. (1993) suggest a similar period-magnitude relation for the V603 Aql positive superhump, where a shorter period relates to an increase in system brightness. Figure 5.3 is an illustration of this relationship as reported by Suleimanov et al. (2004), again using their data and that from an earlier study by Patterson et al. (1993). The 2021 Campaign results are also included in this plot.

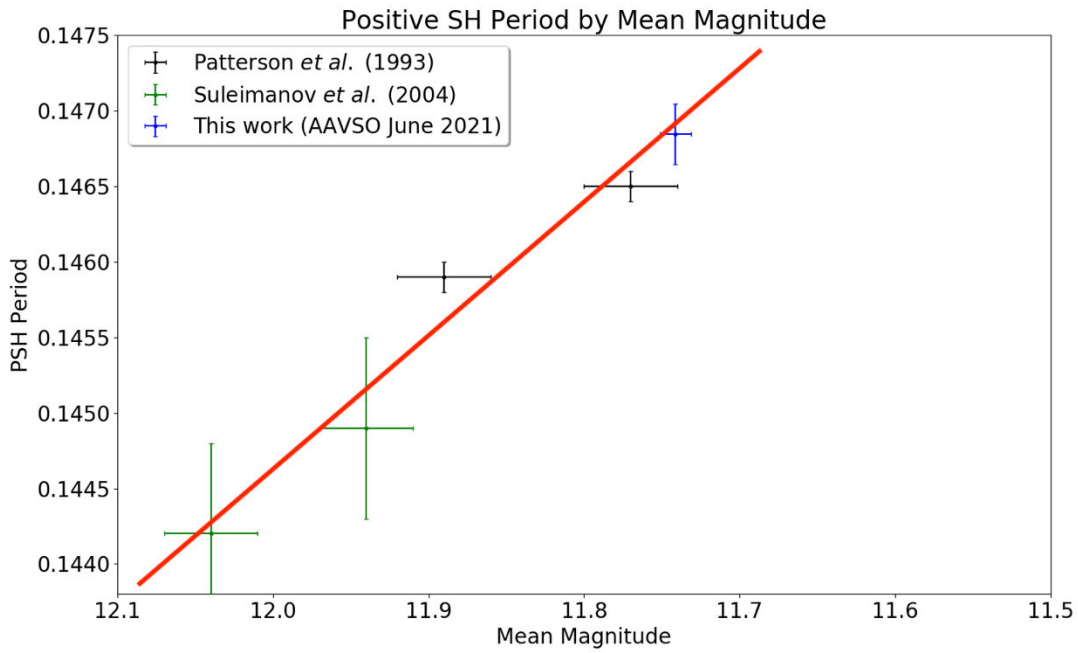

Figure 5.3: *Positive superhump period by mean magnitude for 1991/1992 and 2001/2002 observing campaigns. The 2021 Campaign results for June have been added to this plot.*

The 2021 Campaign data for June fits this relationship well. At this time the prominent photometric period was related to the positive superhump. In July the system mean magnitude is increased and the prominent period is the negative superhump signal.

As a further example of this relationship all data from one observer (HMB), over two separate observing campaigns (2013, 2021) has been analysed to assess the correlation of this theory. Figure 5.4 is a plot of the positive superhump photometric period versus mean magnitude. The blue shaded area corresponds to a 95% confidence interval for the data.

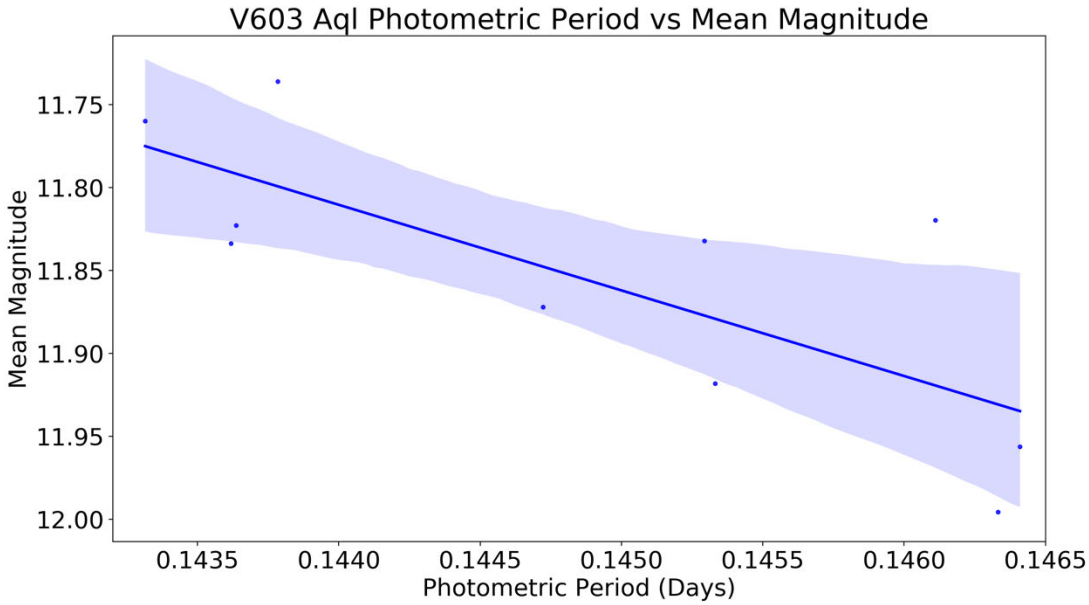

Figure 5.4: *A graph of photometric period vs mean magnitude for 'HMB' data from the 2013 and 2021 V603 Campaigns. The relation between increased system brightness and shorter periods is evident here. The shaded area is the 95% confidence interval for this data.*

These relations are not exclusive to V603 Aql, other CV's also exhibit the same features. As an example, TT Arietis (TT Ari) is a nova-like variable with characteristics and periods similar to those of V603 Aql. The TT Ari orbital period is $P_{Orb} \approx 0.1375\, days$ with superhump periods of $P_{PSH} \approx 0.1492\, days$ and $P_{NSH} \approx 0.1329\, days$ (Patterson 1999; Bruch 2019).

As a summary to these relations, as the system brightens the positive superhump period increases, the negative superhump period decreases and becomes prominent in the light curve. The length of the 2021 Campaign (77 days) has afforded the opportunity to capture this phenomenon in transition. Earlier campaigns of 20 – 30 days may have only captured the system in one of these phases. It may be that the transition from a prominent positive to negative signal occurs on a timescale of months, captured here for the first time. A sustained observation campaign spanning 6 months or more could verify this claim and any previous claims relating the aforementioned phenomena.

5.2 V603 Aql Flickers and flares

Certainly not alone in this affliction, the V603 Aql light curve resembles that of many of the stars in the CV family. Figure 5.5 shows example light curves from a few of these members, including V603 Aql.

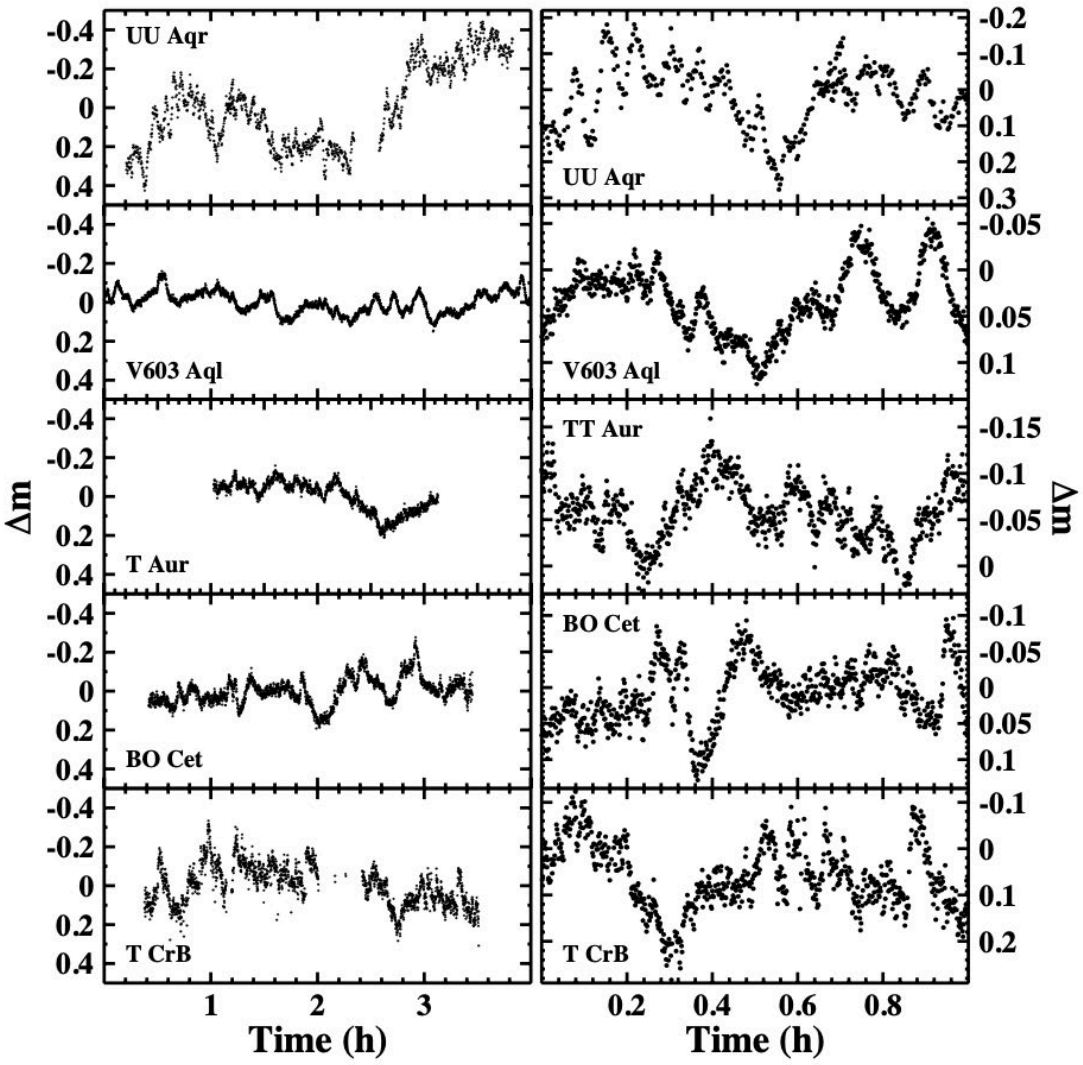

Figure 5.5: *Typical light curves of mass accreting CV stars. The left side panels are 4-hours in duration (or part thereof) and the right side is a zoomed in section at 1-hour duration (Bruch 2021).*

The variability in these light curves at first raise suspicion, as the apparent patterns within them hint at observational errors such as poor tracking. Thankfully the V603 Aql light curve is well documented in the literature and once plotted with comparison star data the true variability is revealed (See Figure 4.13 and Appendix C).

In a study of quasi-periodic oscillations (QPO's) by Suleimanov et al. (2004) they report periodic time scales of $9 - 70\,min$ across any individual night, finding periods of $19 - 25\,min$ as most prominent. The 2021 Campaign analysis reveals many similar periods, typically $10 - 60\,min$, summarised in Table 4.4. Aliasing, beat periods and the effects of observation times are not accounted for, so certainly some of the reported periods should not be included as true QPO's, though this consideration is beyond the scope of this brief analysis. Periods that immediately flag as mistaken QPO's are the $1440\,min\ (1 - day)$ and $211\,min\ (P_{NSH})$ periods.

On any night the amplitude and magnitude of these oscillations will differ. There are two arguments for the formation and maintenance of QPO's, but a combination of both is not discarded. The first claims inhomogeneities in the disk, scientifically dubbed 'blobs', they are formed in the outer and middle regions of the disk by the fluctuations in mass accretion. The periods of flickering then correspond to the Keplerian orbits of the blobs (Pavlenko & Shugarov 1999). The second scenario suggests the accretion rate is altered as the companion star is irradiated by the accretion disk at the boundary layer, near L1, creating an oscillating ionisation front (King 1989). These findings further support the hibernation model of CV evolution, suggesting irradiation of the secondary star increases mass transfer.

5.3 V603 Aql continues to fade

During outburst V603 Aql reached a maximum brightness of $\approx -1\,mag$. Classified as a fast nova, the system had fully faded to its calculated average pre-eruption magnitude of $V = 11.47 \pm 0.03\,mag$ by 1938. Since this time V603 Aql has faded at approximately $0.44\,mag$ per century (Johnson et al. 2013). Following on from this work the rate of fading was calculated from 1950 onwards, incorporating all Vis data available for 2021 from the

AAVSO database. This analysis yields a rate of fading calculated at $0.62\ mag$ per century. For the 2021 Vis data alone the system has a mean brightness of $\approx 11.70\ mag$. This current brightness is consistent with the predictions made by Johnson et al. (2013).

The following section discusses further how the fading of CV systems is related to system mechanics and their evolution.

5.4 Will V603 Aql evolve to a Dwarf Nova?

Evidence for the common evolution of CN to DN continues to mount. Whether these transitions are once in a stellar lifetime or cyclic is still a matter of debate, but for at least some systems this evolution has already been observed.

5.4.1 It has the right stuff

V603 Aql exhibits many of the same characteristics commonly associated with DN systems. Osaki (1996) claims the only parameters that distinguish the classes of CV's are the orbital period and the rate of mass transfer between the stars, also stating that the mechanism differentiating permanent superhump systems, like V603 Aql, and regular DN superhumpers is determined by the rate of mass transfer alone. The orbital period of V603 Aql is well established at $0.1382\ days\ \ (3.32\ hrs)$. As a short period, cataclysmic binary system V603 Aql certainly lives in the realm of the dwarves. The similarities between V603 Aql and SU UMa type DN stars has been discussed previously (E.g.Patterson et al. 1993), though SU UMa type DN systems typically have an orbital period below the period gap ($<$ $2\ hours$), some undeniable parallels remain. V603 Aql is a permanent positive superhump system with a negative superhump signal prominent when the system is at increased brightness. This behaviour fits the SU UMa type DN costume nicely.

The mass transfer rates in CV systems is closely linked to their brightness (See section 2.5.2) as described by the hibernation theory (Shara et al. 1986). This theory predicts that CN systems that have faded to an absolute magnitude of $M \leq 5$ are now accreting mass from their donor stars at rates typically seen in DN systems. The absolute magnitude of V603 Aql is calculated from its apparent magnitude as:

$$M = m - 5\log\frac{d}{10} \approx 4.32 \quad (7)$$

The V603 Aql mass transfer rate, calculated using the parameters in Table 2.1, is $\dot{M} \approx 6.95 \times 10^{-9} M_{\odot} yr^{-1}$. The calculated critical apparent magnitude for V603 Aql is $m \approx 12.7$ (See Section 2.5.1, Eqn 6), corresponding to an absolute magnitude of $M \approx 5.2$. This suggests that if the system continues to fade at the same rate it has historically, V603 Aql is predicted to reach critical magnitude in approximately 250 years. At this magnitude the mass transfer rate for the V603 Aql system is estimated at $\dot{M} \approx 3.02 \times 10^{-9} M_{\odot} yr^{-1}$. Fluctuations in brightness, as seen during the 2021 Campaign and the existence of a myriad of QPO's would suggest the current mass flow is unstable.

5.4.2 Who else is doing it? A roster of stars

Prototypical DN Z Camelopardis (Z Cam) and Z Cam type star AT Cancri, both display nova shells from previous nova events. Z Cam provided the first observational link of CN to DN evolution. While there is no direct record of the Z Cam nova taking place, the extent of the nova shell suggests the star erupted between 2500 and 3000 years ago. AT Cancri is considered to have made the most rapid transition yet found at 330^{+135}_{-90} years. This demonstrates that in some cases the mass accretion rate drops very rapidly in the few centuries after eruption (Shara et al. 2016).

Nova-like variable BK Lyncis, now a bona fide ER UMa type DN, took nearly 2000 years for its mass accretion rate to slow to where DN outburst occur. The star now exhibits superoutbursts on 45 day intervals, displaying a permanent positive superhump and a rapidly developing negative superhump on rise to superoutburst (Kemp et al. 2012).

V1213 Cen (Nova Centauri 2009) is an example of the cyclic theory of CV evolution. V1213 Cen erupted as a CN in May 2009, approximately 6 days after a DN outburst. Pre-eruption light curves of the system reveal outbursts similar to those of U Geminorium (U Gem) type DN, occurring every 12 – 24 days and lasting an average of 6 days (Mróz et al. 2016).

Many of the studies around CV evolution and the hibernation theory rely on historic or ancient accounts of novae where there is some speculation around the times of eruptions. We have been able to record these events directly and accurately over the last century, gathering extensive data through continued observation. Narrowing the gap of a few hundred or a few thousand years at which CN/DN transitions take place will become more precise with long, patient and frequent observing campaigns. In this regard V603 Aql is one to watch.

6 Conclusions

Presented in this thesis is an analysis of data from historical observing campaigns and new data obtained by a collaborative campaign conducted throughout May – July of 2021. The aim here was to analyse the V603 Aql photometric period as well as any other observed phenomena to determine any changes in the previously observed occurrences. Also, an evolutionary path for the V603 Aql is suggested. The analysis of the 2021 data shows the photometric periods continue to drift and the system has faded in agreement with the predictions of Johnson et al. (2013), calculated at $0.44\ mag$ per century.

The 2021 Campaign revealed V603 Aql was in a brightened state, $\approx 11.70\ mag$, with a prominent photometric period associated with the system's negative superhump phenomena measured at $P_{NSH} = 0.135203(6)\ days$. A month-by-month analysis of the 2021 data reveals a change in the photometric period in the second half of the campaign. The prominent period in June was associated with the positive superhump, measured at $P_{PSH} = 0.146846(203)\ days$. In July the prominent period had changed to $P_{NSH} = 0.135417(196)\ days$, coinciding with a brightness increase of $\approx 0.1\ mag$. Also, the system continues to fade as the mass transfer between the stars decreases and destabilises. A sustained photometric campaign of 6 months or more may reveal that the prominent photometric period change from positive to negative superhump occurs more frequently than previously thought and that the system is at increased brightness when this change occurs, analogous to SU UMa dwarf nova systems in superoutburst. Indeed, as the mass transfer to the WD accretion disk continues to decline V603 Aql may become a bona fide DN in its own right.

References

Andronov, IL, Ostrova, NI, Kim, Y-G & Burwitz, V 2005, 'Two-Color VR CCD Photometry of Old Nova V603 Aquilae', *Journal of Astronomy and Space Sciences*, vol. 22, no. 3, pp. 211-22.

Arenas, J, Catalán, M, Augusteijn, T & Retter, A 2000, 'A spectroscopic study of V603 Aquilae: stellar parameters and continuum—line variations', *Monthly Notices of the Royal Astronomical Society*, vol. 311, no. 1, pp. 135-48.

Arranz, T 2021, *V603 Aql light curves and differential photometry*, 15/09/21.

Astronomical Society of South Australia N.D., *Classifying Variable Stars*, viewed 22/06/2020, <https://www.assa.org.au/resources/variable-stars/classifying-variable-stars/>.

Baklanov, A, Andronov, I & Pavlenko, E 2003, 'Nova-like varible V603 Aquilae in 1999', *Odessa astronomical publications*, vol. 16, pp. 15-7.

Barnard, EE 1919, 'Some peculiarities of Nova Aquilae III of 1918', *The Astrophysical Journal*, vol. 49.

Baskill, DS, Wheatley, PJ & Osborne, JP 2005, 'The complete set of ASCA X-ray observations of non-magnetic cataclysmic variables', *Monthly Notices of the Royal Astronomical Society*, vol. 357, no. 2, pp. 626-44.

Borczyk, W, Schwarzenberg-Czerny, A & Szkody, P 2003, 'Variability of The Old Nova V603 Aquilae in UV and X-ray bands', *Astronomy & Astrophysics*, vol. 405, no. 2, pp. 663-76.

Bruch, A 1991, 'V603 Aquilae-The multiple periodic brightness variations of an old nova', *Acta astronomica*, vol. 41, pp. 101-8.

Bruch, A 1992, 'Flickering in cataclysmic variables-Its properties and origins', *Astronomy and Astrophysics*, vol. 266, pp. 237-65.

Bruch, A 2019, 'TT Arietis: 40 years of photometry', *Monthly Notices of the Royal Astronomical Society*.

Bruch, A 2021, 'A comparative study of the strength of flickering in cataclysmic variables', *Monthly Notices of the Royal Astronomical Society*, vol. 503, no. 1, pp. 953-71.

Bruch, A & Cook, LM 2018, 'Cyclic variations with twice the accretion disk precession period in the old nova V603 Aquilae', *New Astronomy*, vol. 63, pp. 1-5.

Kepler's Laws, Binaries and Stellar Masses 2004, Created by Caltech, <https://www.astro.caltech.edu/~george/ay20/Ay20-Lec4x.pdf>.

Campbell, L & Shapley, H 1923, 'The light curve of Nova Aquilae no. 3', *Annals of Harvard College Observatory*, vol. 81, pp. 113-78.

Carroll, B & Ostlie, D 2007, 'An Introduction to Modern Astrophysics, 2nd edn., ed', *SFP Addison-Wesley*, vol. 29, p. 32.

Collazzi, AC, Schaefer, BE, Xiao, L, Pagnotta, A, Kroll, P, Löchel, K & Henden, AA 2009, 'The behavior of novae light curves before eruption', *The Astronomical Journal*, vol. 138, no. 6, p. 1846.

Coto, RL 2016, *Very-high-energy gamma-ray observations of pulsar wind nebulae and cataclysmic variable stars with MAGIC and development of trigger systems for IACTs*, Springer.

CSIRO N.D., *Variable Stars*, viewed 22/06/2020, <https://www.atnf.csiro.au/outreach/education/senior/astrophysics/variable_types.html>.

Dobrotka, A, Mineshige, S & Ness, J-U 2015, 'Rms–flux relation and fast optical variability simulations of the nova-like system MV Lyr', *Monthly Notices of the Royal Astronomical Society*, vol. 447, no. 4, pp. 3162-9.

Drechsel, H, Rahe, J, Holm, A & Krautter, J 1981, 'Phase-dependent optical and ultraviolet observations of the old nova V 603 Aquilae/1918', *Astronomy and Astrophysics*, vol. 99, pp. 166-72.

Drechsel, H, Rahe, J, Wargau, W, Seward, F & Wang, Z 1983, 'The X-ray emission of the old Nova V603 Aquilae (1918)', *Astronomy and Astrophysics*, vol. 126, pp. 357-62.

Eracleous, M, Patterson, J & Halpern, J 1991, 'A search for periodicities in the X-ray emission from cataclysmic variables', *The Astrophysical Journal*, vol. 370, pp. 330-40.

Foster, G 1995, 'The cleanest Fourier spectrum', *The Astronomical Journal*, vol. 109, pp. 1889-902.

Fowler, A 1918, *The New Star in Aquila*, Nature Publishing Group.

Goodchild, S & Ogilvie, G 2006, 'The dynamics of eccentric accretion discs in superhump systems', *Monthly Notices of the Royal Astronomical Society*, vol. 368, no. 3, pp. 1123-31.

Günther, H, Lim, P, Crawford, S, Conseil, S, Shupe, D, Craig, M, Dencheva, N, Ginsburg, A, VanderPlas, J & Bradley, L 2018, 'THE ASTROPY PROJECT: BUILDING AN INCLUSIVE, OPEN-SCIENCE PROJECT AND STATUS OF THE V2. 0 CORE PACKAGE', *arXiv preprint arXiv:1801.02634*.

Hack, M & La Dous, C 1993, *Cataclysmic variables and related objects*, vol. 507, National Aeronautics and Space Administration, Scientific and Technical.

Haefner, R & Metz, K 1985, 'The old nova V 603 AQL-an intermediate polar?', *Astronomy and Astrophysics*, vol. 145, pp. 311-20.

Haefner, R, Pietsch, W & Metz, K 1988, 'X-Ray and optical observations of the old nova V 603 Aql', *Astronomy and Astrophysics*, vol. 200, pp. 75-8.

Heintz, WD 2012, *Double stars*, vol. 15, Springer Science & Business Media.

Hilditch, RW 2001, *An introduction to close binary stars*, Cambridge University Press.

Hillman, Y, Shara, MM, Prialnik, D & Kovetz, A 2020, 'A unified theory of cataclysmic variable evolution from feedback-dominated numerical simulations', *Nature Astronomy*, pp. 1-7.

Johnson, CB, Schaefer, BE, Kroll, P & Henden, AA 2013, 'Nova Aquilae 1918 (V603 Aql) Faded by 0.44 MAG Per Century from 1938 to 2013', *The Astrophysical Journal Letters*, vol. 780, no. 2, p. L25.

Kalomeni, B, Nelson, L, Rappaport, S, Molnar, M, Quintin, J & Yakut, K 2016, 'Evolution of Cataclysmic Variables and Related Binaries Containing a White Dwarf', *The Astrophysical Journal*, vol. 833, no. 1, p. 83.

Kang, TW, Retter, A, Liu, A & Richards, M 2006, 'Nova V4743 Sagittarii 2002: an intermediate polar candidate', *The Astronomical Journal*, vol. 132, no. 2, p. 608.

Kang, Y-W 2010, 'New light curve analysis for large numbers of eclipsing binaries I. Detached and semi-detached binaries', *Journal of Astronomy and Space Sciences*, vol. 27, no. 2, pp. 75-80.

Karttunen, H, Kröger, P, Oja, H, Poutanen, M & Donner, KJ 2016, *Fundamental astronomy*, Springer.

Kemp, J, Patterson, J, de Miguel, E, Roberts, G, Campbell, T, Hambsch, F-J, Krajci, T, Dvorak, S, Koff, RA & Morell, E 2012, 'BK Lyncis: The Oldest Old Nova? or: Archaeo-Astronomy 101', *Society for Astronomical Sciences Annual Symposium*, pp. 7-15.

King, A 1989, 'Irradiation of the companion star in cataclysmic variables', *Monthly Notices of the Royal Astronomical Society*, vol. 241, no. 3, pp. 365-74.

Knigge, C 2011, 'The Evolution of Cataclysmic Variables', *Evolution of Compact Binaries*, p. 3.

Kraft, RP 1964, 'Binary Stars among Cataclysmic Variables. III. Ten Old Novae', *The Astrophysical Journal*, vol. 139, p. 457.

Kraft, RP, Mathews, J & Greenstein, JL 1962, 'Binary Stars among Cataclysmic Variables. II. Nova WZ Sagittae: a Possible Radiator of Gravitational Waves', *The Astrophysical Journal*, vol. 136, pp. 312-5.

Krautter, J 2008, 'Classical Novae', in *The Universe in X-Rays*, Springer, pp. 169-82.

Lomb, NR 1976, 'Least-squares frequency analysis of unequally spaced data', *Astrophysics and space science*, vol. 39, no. 2, pp. 447-62.

Lubow, SH 1991, 'Simulations of tidally driven eccentric instabilities with application to superhumps', *The Astrophysical Journal*, vol. 381, pp. 268-77.

Mazzali, PA, Röpke, FK, Benetti, S & Hillebrandt, W 2007, 'A common explosion mechanism for type Ia supernovae', *science*, vol. 315, no. 5813, pp. 825-8.

Morris, SL 1999, 'The Limits of Inclination for Binary Star Partial Eclipses', *The Astrophysical Journal*, vol. 520, no. 2, p. 797.

Mróz, P, Udalski, A, Pietrukowicz, P, Szymański, MK, Soszyński, I, Wyrzykowski, Ł, Poleski, R, Kozłowski, S, Skowron, J & Ulaczyk, K 2016, 'The awakening of a classical nova from hibernation', *Nature*, vol. 537, no. 7622, pp. 649-51.

NASA, ASDo 2014, *The Intermediate Polars*, viewed 18/08/2020, <https://asd.gsfc.nasa.gov/Koji.Mukai/iphome/iphome.html>.

Osaki, Y 1989, 'A model for the superoutburst phenomenon of SU Ursae Majoris stars', *Publications of the Astronomical Society of Japan*, vol. 41, pp. 1005-33.

Osaki, Y 1996, 'Dwarf-nova outbursts', *Publications of the Astronomical Society of the Pacific*, vol. 108, no. 719, p. 39.

Pagnotta, A 2015, 'A New Review of Old Novae', *Acta Polytechnica CTU Proceedings*, vol. 2, no. 1, pp. 199-204.

Patterson, J 1979, 'Eruptions and superhumps in dwarf novae', *The Astronomical Journal*, vol. 84, pp. 804-11.

Patterson, J 1984, 'The evolution of cataclysmic and low-mass X-ray binaries', *The Astrophysical Journal Supplement Series*, vol. 54, pp. 443-93.

Patterson, J 1994, 'The DQ Herculis stars', *Publications of the Astronomical Society of the Pacific*, vol. 106, no. 697, p. 209.

Patterson, J 1999, 'Permanent Superhumps in Cataclysmic Variables', *FRONTIERS SCIENCE SERIES*, pp. 61-70.

Patterson, J & Richman, H 1991, 'Permanent superhumps in V603 Aquilae', *Publications of the Astronomical Society of the Pacific*, vol. 103, no. 666, p. 735.

Patterson, J, Thomas, G, Skillman, DR & Diaz, M 1993, 'The 1991 V603 Aquilae campaign-Superhumps and P-dots', *The Astrophysical Journal Supplement Series*, vol. 86, pp. 235-54.

Patterson, J, Kemp, J, Saad, J, Skillman, DR, Harvey, D, Fried, R, Thorstensen, JR & Ashley, R 1997, 'Superhumps in Cataclysmic Binaries. XI. V603 Aquilae Revisited', *Publications of the Astronomical Society of the Pacific*, vol. 109, no. 734, p. 468.

Patterson, J, Uthas, H, Kemp, J, de Miguel, E, Krajci, T, Foote, J, Hambsch, F-J, Campbell, T, Roberts, G & Cejudo, D 2013, 'BK Lyncis: the oldest old nova and a Bellwether for cataclysmic variable evolution', *Monthly Notices of the Royal Astronomical Society*, vol. 434, no. 3, pp. 1902-19.

Paunzen, E & Vanmunster, T 2016, 'Peranso–Light curve and period analysis software', *Astronomische Nachrichten*, vol. 337, no. 3, pp. 239-45.

Pavlenko, E & Shugarov, SY 1999, 'Photometric study of the nova-like variable MV Lyrae during an enormous outburst in 1997', *Astronomy and Astrophysics*, vol. 343, pp. 909-15.

Percy, JR 2007, *Understanding variable stars*, Cambridge University Press.

Peters, CS & Thorstensen, JR 2006, 'Spectroscopy of five old novae: New or refined orbital periods', *Publications of the Astronomical Society of the Pacific*, vol. 118, no. 843, p. 687.

Prialnik, D & Shara, MM 1986, 'Rapid accretion and hibernation in the preoutburst history of classical novae', *The Astrophysical Journal*, vol. 311, pp. 172-82.

Rahe, J, Boggess, A, Drechsel, H, Holm, A & Krautter, J 1980, 'Detection of periodic light variations in the old nova V 603 Aquilae/1918', *Astronomy and Astrophysics*, vol. 88, p. L9.

Retter, A & Leibowitz, E 1998, 'Predicting the future of superhumps in classical nova systems', *Monthly Notices of the Royal Astronomical Society*, vol. 296, no. 4, pp. L37-L41.

Richman, HR, Applegate, JH & Patterson, J 1994, 'Long-term periods in cataclysmic variables', *Publications of the Astronomical Society of the Pacific*, vol. 106, no. 704, p. 1075.

Robitaille, TP, Tollerud, EJ, Greenfield, P, Droettboom, M, Bray, E, Aldcroft, T, Davis, M, Ginsburg, A, Price-Whelan, AM & Kerzendorf, WE 2013, 'Astropy: A community Python package for astronomy', *Astronomy & Astrophysics*, vol. 558, p. A33.

Scargle, JD 1982, 'Studies in astronomical time series analysis. II-Statistical aspects of spectral analysis of unevenly spaced data', *The Astrophysical Journal*, vol. 263, pp. 835-53.

Scaringi, S 2014, 'A physical model for the flickering variability in cataclysmic variables', *Monthly Notices of the Royal Astronomical Society*, vol. 438, no. 2, pp. 1233-41.

Scaringi, S, Körding, E, Uttley, P, Groot, P, Knigge, C, Still, M & Jonker, P 2012, 'Broad-band timing properties of the accreting white dwarf MV Lyrae', *Monthly Notices of the Royal Astronomical Society*, vol. 427, no. 4, pp. 3396-405.

Schaefer, BE 2018, 'The distances to Novae as seen by Gaia', *Monthly Notices of the Royal Astronomical Society*, vol. 481, no. 3, pp. 3033-51.

Shara, MM, Livio, M, Moffat, AF & Orio, M 1986, 'Do novae hibernate during most of the millenia between eruptions? Links between dwarf and classical novae, and implications for the space densities and evolution of cataclysmic binaries', *The Astrophysical Journal*, vol. 311, pp. 163-71.

Shara, MM, Prialnik, D, Hillman, Y & Kovetz, A 2018, 'The Masses and Accretion Rates of White Dwarfs in Classical and Recurrent Novae', *The Astrophysical Journal*, vol. 860, no. 2, p. 110.

Shara, MM, Drissen, L, Martin, T, Alarie, A & Stephenson, FR 2016, 'When does an old nova become a dwarf nova? Kinematics and age of the nova shell of the dwarf nova AT Cnc', *Monthly Notices of the Royal Astronomical Society*, p. stw2753.

Shara, MM, Mizusawa, T, Zurek, D, Martin, CD, Neill, JD & Seibert, M 2012, 'The inter-eruption timescale of classical novae from expansion of the Z Camelopardalis shell', *The Astrophysical Journal*, vol. 756, no. 2, p. 107.

Shara, MM, Mizusawa, T, Wehinger, P, Zurek, D, Martin, CD, Neill, JD, Forster, K & Seibert, M 2012, 'AT Cnc: a second dwarf nova with a classical nova shell', *The Astrophysical Journal*, vol. 758, no. 2, p. 121.

Shara, MM, Martin, CD, Seibert, M, Rich, RM, Salim, S, Reitzel, D, Schiminovich, D, Deliyannis, CP, Sarrazine, AR & Kulkarni, SR 2007, 'An ancient nova shell around the dwarf nova Z Camelopardalis', *Nature*, vol. 446, no. 7132, pp. 159-62.

Shara, MM, Iłkiewicz, K, Mikołajewska, J, Pagnotta, A, Bode, M, Crause, L, Drozd, K, Faherty, J, Fuentes-Morales, I & Grindlay, J 2017, 'Proper-motion age dating of the progeny of Nova Scorpii AD 1437', *Nature*, vol. 548, no. 7669, pp. 558-60.

Smak, J 2008, 'Superoutbursts of Z Cha and their Interpretation', *Acta astronomica*, vol. 58, pp. 55-64.

Smith, RC 2006, 'Cataclysmic variables', *Contemporary Physics*, vol. 47, no. 6, pp. 363-86.

Stanton, RH 1999, 'Visual Magnitudes and the" Average Observer": The SS Cygni Field Experiment', *Journal of the American Association of Variable Star Observers (JAAVSO)*, vol. 27, pp. 97-112.

Stefanov, S 2021, 'Unveiling the multiple periodicities of the cataclysmic variable LS Cam', *arXiv preprint arXiv:2106.03568*.

Suleimanov, V, Bikmaev, I, Belyakov, C, Sakhibullin, N, Zhukov, G, Asian, Z, Kizilogly, U & Khamitov, I 2003, 'Disk precession of V603 Aql in 2001-2002', *Odessa astronomical publications*, no. 16, pp. 81-4.

Suleimanov, V, Bikmaev, I, Belyakov, K, Sakhibullin, N, Zhukov, G, Aslan, Z, Kiziloglu, U & Khamitov, I 2004, 'Disk precession and quasi-periodic brightness oscillations of V603 Aql in 2001–2002', *Astronomy Letters*, vol. 30, no. 9, pp. 615-29.

The American Association of Variable Star Observers 2021, https://www.aavso.org/>.

Thomas, DM & Wood, MA 2015, 'The Emergence of Negative Superhumps in Cataclysmic Variables: Smoothed Particle Hydrodynamics Simulations', *The Astrophysical Journal*, vol. 803, no. 2, p. 55.

Truran, J & Livio, M 1986, 'On the frequency of occurrence of oxygen-neon-magnesium white dwarfs in classical nova systems', *The Astrophysical Journal*, vol. 308, pp. 721-7.

Udalski, A & Schwarzenberg-Czerny, A 1989, 'Photometry of cataclysmic variables. IV-Nova V603 Aquilae: Discovery of a magnetic rotator', *Acta astronomica*, vol. 39, pp. 125-38.

Vityazev, V 1997, 'Time series analysis of unequally spaced data: intercomparison between estimators of the power spectrum', *Astronomical Data Analysis Software and Systems VI*, p. 166.

Vogt, N 1982, 'Z Chamaeleontis-Evidence for an eccentric disk during supermaximum', *The Astrophysical Journal*, vol. 252, pp. 653-67.

Walker, MF 1954, 'Nova DQ Herculis (1934): An eclipsing binary with very short period', *Publications of the Astronomical Society of the Pacific*, vol. 66, p. 230.

Walker, MF 1956, 'A Photometric Investigation of the Short-Period Eclipsing Binary, Nova DQ Herculis (1934)', *The Astrophysical Journal*, vol. 123, p. 68.

Warner, B 1976, 'The Structure and Evolution of Close Binary Systems, ed', *IAU Symposium 73*.

Warner, B 2003, *Cataclysmic variable stars*, vol. 28, Cambridge University Press.

White, G & Platz, D 2018, 'The man who tamed the Vulcan Star', *Australian Sky & Telescope*, vol. November/December, p. 74.

Whitehurst, R 1988, 'Numerical simulations of accretion discs–I. Superhumps: a tidal phenomenon of accretion discs', *Monthly Notices of the Royal Astronomical Society*, vol. 232, no. 1, pp. 35-51.

Wood, D 1971, 'An analytic model of eclipsing binary star systems', *The Astronomical Journal*, vol. 76, pp. 701-10.

Wood, MA & Burke, CJ 2007, 'The physical origin of negative superhumps in cataclysmic variables', *The Astrophysical Journal*, vol. 661, no. 2, p. 1042.

Wood, MA, Still, MD, Howell, SB, Cannizzo, JK & Smale, AP 2011, 'V344 Lyrae: A touchstone Su UMa cataclysmic variable in the Kepler field', *The Astrophysical Journal*, vol. 741, no. 2, p. 105.

Zorotovic, M & Schreiber, MR 2019, 'Cataclysmic variable evolution and the white dwarf mass problem: A Review', *Advances in Space Research*.

Appendix A

Table 1: Log of AAVSO 2021 Campaign observations. This campaign is described further in Section 3 of this thesis. Sub-sets of the full campaign are used for analysis throughout.

Date (UTC:2021)	Observer Code	Start→End (JD 2459000+)	Band	Duration (sec)	No. of obs.	Check Star
13/05	LTAA	347.50119 – 0.68286	TG	15,696	370	-
13/05	HMH	347.776365 – 0.975082	V	17,196	232	124
13/05	PJAD	348.10762 – 0.12918	V	1,863	31	124
14/05	HMB	348.693125 – 0.97461	V	24,320	50	123
14/05	AVKB	349.307889 – 0.335613	V	2,395	67	-
15/05	HMB	349.690313 – 0.909965	V	18,978	51	123
16/05	LTAA	350.50216 – 0.67569	TG	14,993	346	-
16/05	HMB	350.686771 – 0.911366	V	19,405	62	123
16/05	HMH	350.840509 – 0.974535	V	11,580	196	124
17/05	HMB	351.684236 – 0.911285	V	19,617	63	123
17/05	SGOR	351.73958 – 0.96137	V	19,162	427	85
17/05	HMH	351.775196 – 0.973934	V	17,171	320	124
17/05	MMEA	352.05753 – 0.33036	V	23,572	61	124
18/05	HMB	352.681354 – 0.911111	V	19,851	64	123
18/05	SGOR	352.73029 – 0.92153	V	16,523	389	136
18/05	SCRB	353.434798 – 0.567176	TG	11,437	187	122
19/05	HMB	353.678646 – 0.911539	V	20,122	58	122
20/05	HMB	354.675995 – 0.912106	V	3,867	53	123
20/05	HMH	354.764810 – 0.972599	V	17,953	334	124
20/05	WGR	354.941574 – 0.986331	V	20,400	100	136
21/05	HMH	355.762890 – 0.971279	V	18,005	313	124
21/05	HMB	355.765984 – 0.913391	V	12,736	39	123
21/05	SGOR	355.81433 – 0.95966	V	12,557	273	124
22/05	HMB	356.670521 – 0.911748	V	20,842	58	123
22/05	WGR	356.898646 – 1.009155	V	9,548	221	136
23/05	HMB	357.667882 – 0.912616	V	21,145	59	123
23/05	HMH	357.757053 – 0.969113	V	18,322	176	124
24/05	HMB	358.665104 – 0.913565	V	21,467	60	123
24/05	SGOR	358.75760 – 0.95865	V	17,370	382	124
24/05	HMH	358.822351 – 0.971077	V	12,850	102	124

25/05	HMB	359.662176 – 0.914595	V	21,809	58	123
25/05	SGOR	359.72848 – 0.95808	V	19,837	451	136
25/05	HMH	359.751010 – 0.958482	V	17,926	145	124
25/05	WGR	359.818356 – 0.998449	V	15,560	396	136
26/05	HMB	360.659329 – 0.907801	V	21,468	59	123
26/05	HMH	360.745833 – 0.965588	V	19,047	145	124
27/05	HBB	361.839652 – 0.888279	V	4,201	97	125
28/05	SGOR	362.72532 – 0.95690	V	20,008	457	124
28/05	MMEA	363.04441 – 0.30813	V	22,785	61	124
28/05	SGOR	363.68645 – 0.71257	V	2,257	60	124
28/05	HMH	363.745241 – 0.96849	V	19,289	163	124
28/05	SGOR	363.87962 – 0.944	V	5,563	119	136
28/05	WGR	363.819444 – 0.998565	V	15,476	790	136
29/05	MMEA	364.03703 – 0.34341	V	26,472	68	124
29/05	HMB	364.648900 – 0.914977	V	22,989	65	123
29/05	HMH	364.745415 – 0.966429	V	19,095	173	124
30/05	MMEA	365.02561 – 0.32451	V	25,825	66	124
31/05	HMB	365.646134 – 0.764514	V	10,228	26	123
01/06	HMB	366.643426 – 0.906574	V	22,736	78	123
02/06	HMB	367.639688 – 0.907049	V	23,100	86	123
03/06	HMB	368.636991 – 0.916273	V	24,130	91	123
03/06	WGR	368.805706 – 0.985845	V	15,564	395	136
04/06	HMB	369.634051 – 0.918704	V	24,594	85	123
04/06	MMEA	370.03212 – 0.27765	V	21,214	56	124
05/06	HMB	370.632060 – 0.920370	V	24,910	89	123
05/06	LMN	371.43109 – 0.49558	V	5,572	90	99
06/06	HMB	371.628646 – 0.920613	V	25,226	81	123
06/06	WGR	371.794954 – 0.974826	V	15,541	395	124
06/06	ATE	372.48069 – 0.62106	V	12,128	501	99
07/06	HMB	372.625972 – 0.919676	V	25,376	87	123
07/06	HMH	372.719356 – 0.964379	V	21,170	184	124
08/06	ATE	373.52960 – 0.64705	V	10,148	456	99
08/06	HMB	373.631123 – 0.929329	V	25,765	83	123
08/06	LMN	374.45093 – 0.51206	V	5,282	130	99
08/06	ATE	374.49512 – 0.62233	V	10,991	494	99

09/06	HMB	374.620486 – 0.928877	V	26,645	103	123
09/06	HMH	374.719560 – 0.965992	V	21,292	155	124
09/06	WGR	374.778958 – 0.95941	V	15,591	395	136
09/06	ATE	375.48337 – 0.65071	V	14,458	651	99
10/06	HMB	375.617465 – 0.929572	V	26,966	105	123
10/06	HMH	375.718715 – 0.958649	V	20,730	168	124
10/06	VMT	376.460174 – 0.579213	CV	10,285	443	128
10/06	ATE	376.47391 – 0.64744	V	14,993	675	99
11/06	HMB	376.614757 – 0.930602	V	27,289	107	123
11/06	HMH	376.720004 – 0.965762	V	21,231	249	124
11/06	VMT	377.459630 – 0.579097	CV	10,332	444	128
12/06	HMB	377.612106 – 0.929873	V	27,455	87	123
12/06	HMH	377.712917 – 0.965559	V	21,828	210	124
13/06	HMB	378.609086 – 0.930590	V	27,778	89	123
14/06	HMB	379.606574 – 0.930197	V	27,961	89	123
15/06	HMB	380.603866 – 0.91147	V	26,577	78	123
15/06	HMH	380.758010 – 0.945523	V	16,201	173	124
15/06	WGR	380.774803 – 0.954711	V	15,544	395	136
16/06	HMH	381.707205 – 0.955545	V	21,456	186	124
17/06	HMB	382.598643 – 0.930625	V	28,684	84	123
17/06	HMH	382.703714 – 0.956165	V	21,812	214	124
18/06	HMB	383.595984 – 0.896528	V	25,967	74	123
18/06	HMH	383.697322 – 0.952414	V	22,040	242	124
18/06	WGR	383.776632 – 0.857419	V	6,980	177	136
19/06	HMB	384.593646 – 0.891285	V	25,716	64	123
19/06	HMH	384.697507 – 0.82977	V	11,427	81	124
19/06	WGR	384.751238 – 0.931944	V	15,613	395	136
20/06	HMB	385.590984 – 0.891944	V	26,003	73	123
21/06	SGOR	386.72016 – 0.74728	V	2,343	60	124
21/06	HMB	386.823495 – 0.885648	V	5,370	20	123
22/06	SGOR	387.64638 – 0.67253	V	2,260	60	124
22/06	WGR	387.764306 – 0.945845	V	15,685	392	136
23/06	ATE	389.46596 – 0.5051	V	3,382	147	99
24/06	CDZ	389.51895 – 0.62081	V	8,801	245	124
24/06	HMB	389.580069 – 0.880845	V	25,987	76	123

24/06	ATE	390.4615 – 56836	V	9,232	425	99
25/06	CDZ	390.5162 – 0.61446	V	8,489	236	124
25/06	HMB	390.575856 – 0.878322	V	26,133	96	123
25/06	SGOR	390.68828 – 0.71447	V	2,263	60	124
25/06	WGR	390.762801 – 0.944259	V	15,678	395	136
26/06	ATE	391.51691 – 0.62427	V	9,276	429	99
28/06	ATE	393.51663 – 0.64584	V	11,164	351	99
28/06	HMB	393.567442 – 0.869282	V	26,079	96	123
29/06	HMB	394.564641 – 0.867049	V	26,128	95	123
30/06	HMB	395.562118 – 0.863981	V	26,081	96	123
30/06	ATE	396.48120 – 0.62417	V	12,352	606	99
30/06	CDZ	396.49972 – 0.62348	V	10,693	284	136
01/07	HMB	396.559097 – 0.861435	V	26,143	96	123
01/07	ATE	397.45510 – 0.62758	V	14,902	737	99
01/07	CDZ	397.49750 – 0.62448	V	10,971	306	136
02/07	HMB	397.573009 – 0.858553	V	24,671	69	123
02/07	ATE	398.49108 – 0.59247	V	8,760	262	99
03/07	HMB	398.570174 – 0.855532	V	24,655	70	123
04/07	HMB	399.567407 – 0.853056	V	24,680	70	123
05/07	HMB	400.580081 – 0.850498	V	23,364	59	123
06/07	HMB	401.577083 – 0.799468	V	19,214	49	123
06/07	ATE	402.46473 - 0.52152	V	4906	202	99
07/07	HMB	402.574433 – 0.845417	V	23,413	59	123
08/07	ATE	403.53762 – 0.56403	V	2282	105	99
09/07	ATE	405.37417 – 0.65068	V	23,890	1154	99
10/07	ATE	406.36593 – 0.63953	V	23,639	1151	99
11/07	ATE	407.37433 – 0.65213	V	24,001	1173	99
12/07	ATE	408.3605 – 0.63669	V	23,862	1129	99
14/07	ATE	410.36661 – 0.64701	V	24,226	1194	99
15/07	ATE	411.36154 – 0.59754	V	20,390	1000	99
16/07	ATE	412.36391 – 0.60249	V	20,613	1016	99
18/07	ATE	414.36089 – 0.63273	V	23,486	1161	99
19/07	ATE	415.35825 – 0.62469	V	23,020	1133	99
21/07	ATE	416.53606 – 0.63496	V	8,544	423	99
21/07	ATE	417.3609 – 0.66134	V	25,958	1277	99

23/07	ATE	419.43539 – 0.65566	V	19,031	787	99
24/07	ATE	420.35279 – 0.59862	V	21,239	996	99
25/07	ATE	421.37863 – 0.49949	V	10,442	356	99
28/07	ATE	424.35006 – 0.52024	V	14,703	691	99
29/07	PJAD	424.99366 – 1.22223	V	19,748	300	124

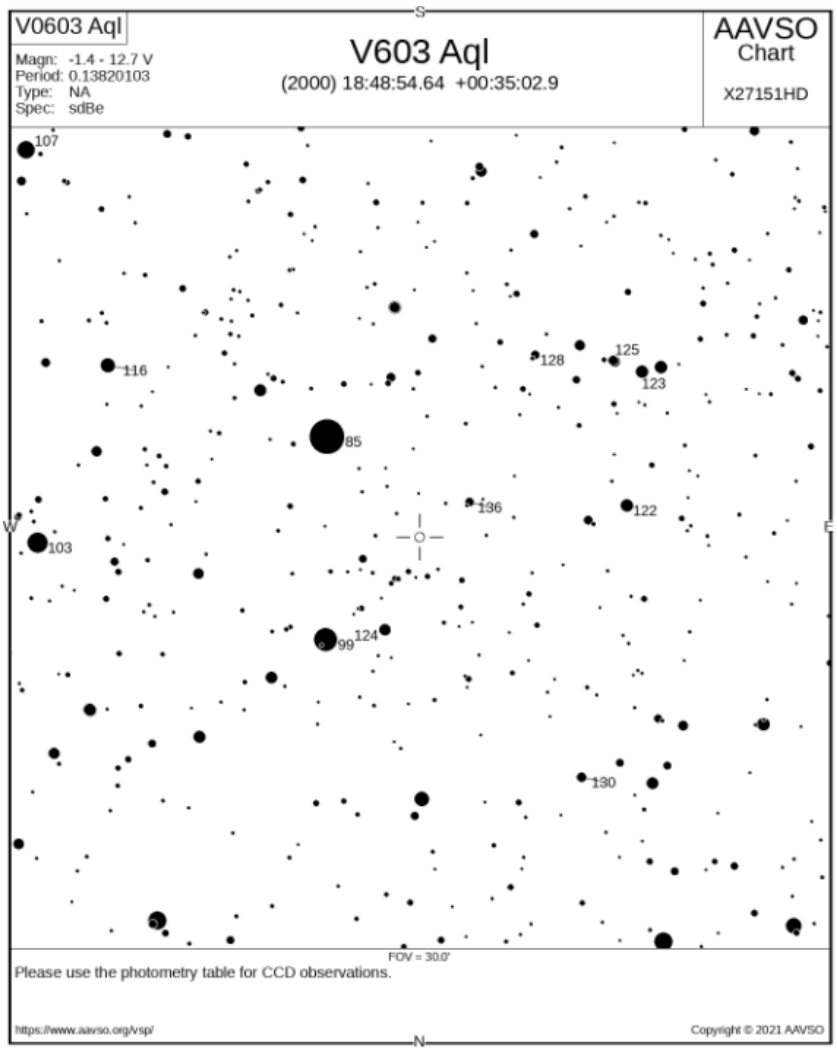

Figure A.1: AAVSO finder chart for V603 Aql with common check stars used by the observers listed in Appendix A, Table 1 (The American Association of Variable Star Observers 2021).

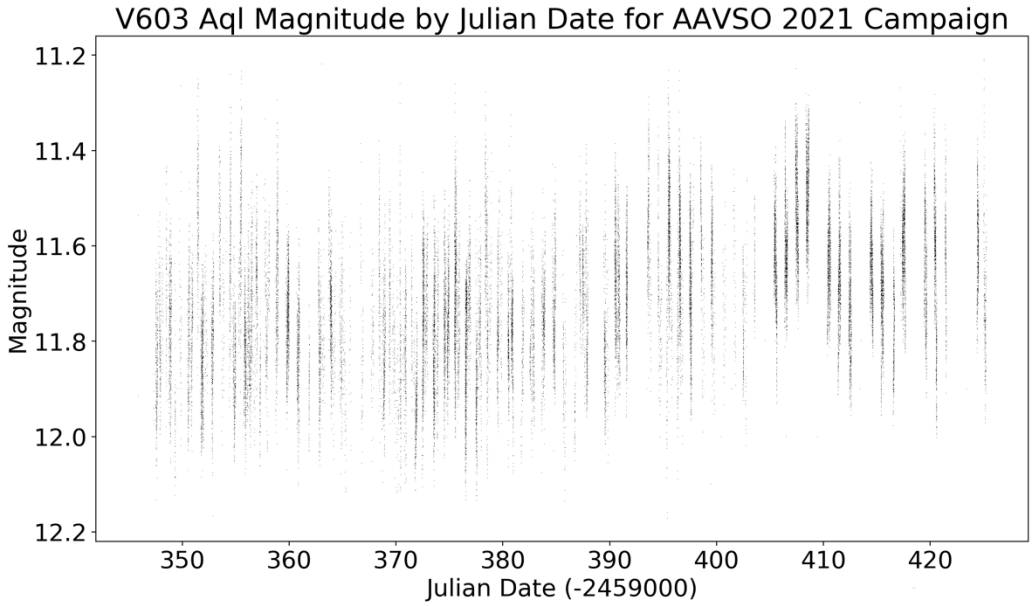

Figure A.2: Plot of the full AAVSO 2021 Campaign data provide by the observers in Appendix A, Table 1. Each point represents a single observation (The American Association of Variable Star Observers 2021).

Table 2: AAVSO Observer information

Observer Code	Name	Location	Affiliation
COO	Lewis Cook	US	AAVSO
VMT	Tonny Vanmunster	BE	AAVSO
SBL	Bart Staels	BE	-
DPP	Pierre de Ponthiere	BE	AAVSO
CTX	Timothy Crawford	US	-
LTAA	Tapio Lahtinen	FI	URSA
HMH	Michael Heald	US	AAVSO
PJAD	James Pierce	AU	AAVSO
HMB	Franz-Josef Hambsch	BE	VVS, Belgium
AVKB	Vikrant Agnihotri	IN	AAVSO
SGOR	George Sjoberg	US	-
MMEA	Mervyn Millward	AU	AAVSO
WGR	Gary Walker	US	AAVSO
HBB	Barbara Harris	US	AAVSO
LMN	Magnus Larsson	SE	SAAF
ATE	Teófilo Arranz	ES	AAVSO

Table 3: Photometric periods. Reported and calculated by CLEANest and Lomb-Scargle methods. The results in this table are discussed fully in Section 4 and 5.

Mean JD	Mean Date UTC	Prominent Period (Reported)	Prominent Period (CLEANest)	Prominent Period (Lomb-Scargle)	Observer or Telescope	Reference
2444400.5	10/06/1980	0.1377	-	-	FES/IUE Satellite	(Drechsel et al. 1981)
2444826	09/08/1981	0.144854	-	-	FES/IUE Satellite	(Haefner & Metz 1985)
2445949	05/09/1984	0.1454	-	-	FES/IUE Satellite	(Haefner et al. 1988)
2447390.5	17/08/1988	0.14567	-	-	-	(Udalski & Schwarzenberg-Czerny 1989)
2448046.5	04/06/1990	0.146	-	-	-	(Arenas et al. 2000)
2448046.5	04/06/1990	0.132	-	-	-	(Arenas et al. 2000)
2448067.9	25/08/1990	0.14548	-	-	-	(Patterson & Richman 1991)
2448779.5	06/06/1992	0.1339	-	-	-	(Patterson et al. 1997)
2448835.5	01/08/1992	0.1345	-	-	-	(Patterson et al. 1997)
2448860.5	26/08/1992	0.1346	-	-	-	(Patterson et al. 1997)
2448811.5	08/07/1994	0.13414	-	-	-	(Patterson et al. 1997)
2448811.5	08/07/1994	0.1465	-	-	-	(Patterson et al. 1997)
2451399.3	08/08/1999	0.144437	-	-	-	(Baklanov et al. 2003)
2452077.5	17/06/2001	0.1442	-	-	-	(Suleimanov et al. 2003)
2452144.5	23/08/2001	0.145	-	-	-	(Suleimanov et al. 2003)
2452471.5	16/07/2002	0.1449	-	-	-	(Suleimanov et al. 2003)
2452822.8	01/07/2003	-	0.145071	0.145304	COO	-

2452828	07/07/2003	0.1453	0.14637	0.145965	COO	(Bruch & Cook 2018)
2452833.5	12/07/2003	-	0.146101	0.146147	VMT	-
2452838	17/07/2003	-	0.145679	0.14529	COO	-
2453214	27/07/2004	0.14813	-	-	-	(Andronov et al. 2005)
2453917.9	30/06/2006	-	0.144806	0.14464	SBL	-
2453934.4	17/07/2006	-	0.144806	-	DPP	-
2453935.2	18/07/06	-	0.144768	-	SBL	-
2454313.8	31/07/2007	-	0.146139	0.146871	CTX	-
2456463.8	19/06/2013	-	0.145298	0.144931	HMB	-
2456470	26/06/2013	-	0.145336	0.145083	HMB	-
2456475.6	01/07/2013	-	0.1463311	0.146261	HMB	-
2456480.8	06/07/2013	-	0.146409	0.146339	HMB	-
2456487.2	13/07/2013	-	0.14473	0.14428	HMB	-
2458686.9	22/06/2019	-	0.146331	0.145905	GW/JP	-
2459380.5	15/06/2021	-	0.145466	-	AAVSO (2021)	-

Appendix B

A sample of the Lomb-Scargle method used for the period confirmations, as described in Section 3 of this thesis.

lomb_scargle.py > ...

```
#-------------------------------------------------------------------------------#
#Create dataframes from .csv file and analyses for prominent periods by
Lomb-Scargle method. The data is selected by conditions and the new dataframe
can be written to .csv file. Plots all selected observations, power spectrum by
frequency for the prominent periods and a phase digram.
#--------------------Written by John Myles April 2021---------------------------#
#-------------------------------------------------------------------------------#

#Import required modules
import numpy as np
import pandas as pd
import matplotlib.pyplot as plt
from astropy.timeseries import LombScargle
import julian
import datetime

#Reads in csv and selects columns to use
df = pd.read_csv('AAVSO_V603_New.csv', dtype = {'Observer': str}, usecols = [
                    'JD', 'Magnitude', 'Filter', 'Observer', 'Affiliation'])

#Sets relevant column data to numeric and fixes null values
df['JD'] = pd.to_numeric(df['JD'], errors = 'coerce')
df['Magnitude'] = pd.to_numeric(df['Magnitude'], errors='coerce')
#print(df)

#Selects observer data by conditions, returns dataframe to the terminal and
writes to csv file.
observer_data = df[df['Observer'] == 'HMB']
obs_data_short = observer_data[(observer_data['JD'] >= 2456461) & (
    observer_data['JD'] <= 2456466)]#.to_csv('SBL_2453914.csv')
print(obs_data_short)

#Calculates Mean JD from the selected data and returns to terminal
JD_mean = obs_data_short['JD'].mean()
print('Mean Julian Date is :', JD_mean)

#Converts Mean JD to UTC and returns to terminal
dt = julian.from_jd(JD_mean, fmt = 'jd')
print('UTC Time is :', dt)

#Gets the mean magnitude for the selected run and returns to terminal
mag_mean = obs_data_short['Magnitude'].mean()
print('The mean magnitude is :', mag_mean)

```

```
#----------------------------Lomb-Scargle Analysis--------------------------#

jd = obs_data_short['JD']
mag = obs_data_short['Magnitude']

lombscar = LombScargle(jd, mag)

frequency, power = lombscar.autopower(
    minimum_frequency = 1 / 10, maximum_frequency = 1 / 0.1)

#The period is the inverse of frequency
period = 1 / frequency

#Returns the 5 strongest frequencies. Period with the strongest signal will
have the greatest power.
first_period = 1 / frequency[np.argsort(power)[-1]]
second_period = 1 / frequency[np.argsort(power)[-2]]
third_period = 1 / frequency[np.argsort(power)[-3]]
fourth_period = 1 / frequency[np.argsort(power)[-4]]
fifth_period = 1 / frequency[np.argsort(power)[-5]]

print('First period: {:.6f} (days)'.format(first_period))
print('Second period: {:.6f} (days)'.format(second_period))
print('Third period: {:.6f} (days)'.format(third_period))
print('Fourth period: {:.6f} (days)'.format(fourth_period))
print('Fifth period: {:.6f} (days)'.format(fifth_period))

#--------------------------------Plots---------------------------------------#

#Plots all observations for the selected observer and date range
plot1 = plt.figure(1)
plot1.set_facecolor('xkcd:gray')
plt.plot(jd, mag, 'k.')
plt.xlabel('Julian Date')
plt.ylabel('Magnitude')
plt.title('All observations for observer HMB for JD 2456461 - 2456466')

#Plots power spectrum
plot2 = plt.figure(2)
plt.plot(frequency, power, 'k-')
plt.xlabel('Frequency')
plt.ylabel('Power')
plt.title('Power spectrum for prominent periods by frequency')

#Plots observations phased on the strongest period
plot3 = plt.figure(3)
phase = (jd / first_period) % 1
plt.plot(phase, mag, 'k.')
plt.xlabel('Phase')
plt.ylabel('Magnitude')
plt.title('Phase diagram for all observations')
plt.show()
```

Appendix C

Power spectra and differential photometry plots of V603 Aql against comparison star 99 (RA: 18: 48: 40.87 DEC: 00: 38: 47.9 Magnitude: 9.868). These raw data for the differential photometry are used in the analysis of short period flickers and flares. The plots were provided by Teófilo Arranz (AAVSO observer code ATE) by private communication. The raw data was downloaded from the AAVSO repository. The power spectra for each night from JD2459405 to JD24559412 were produced using PERANSO 3.0 software. Section 4.3.2 describes this analysis in full.

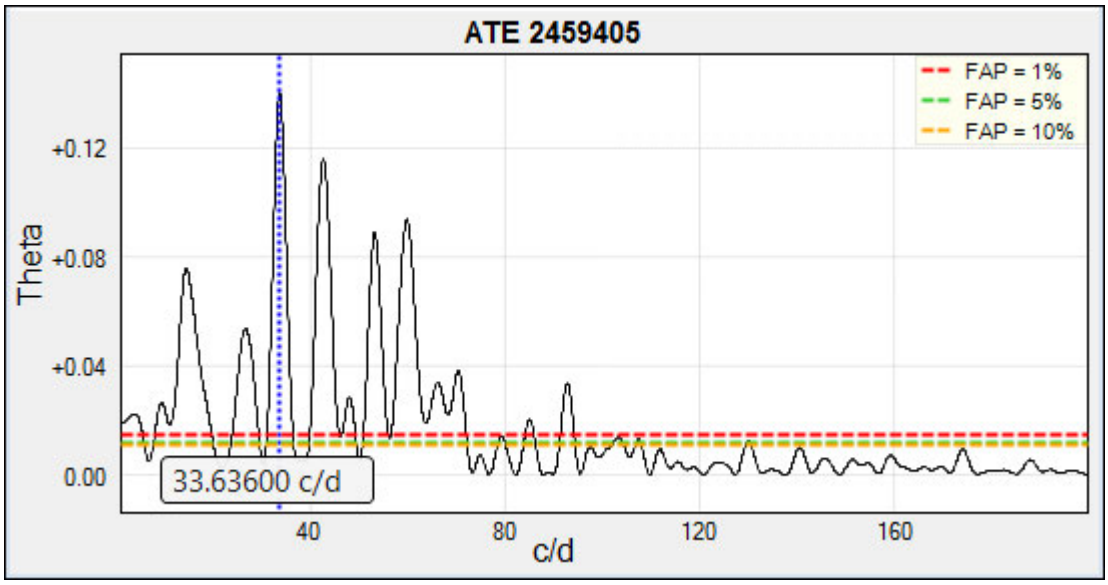

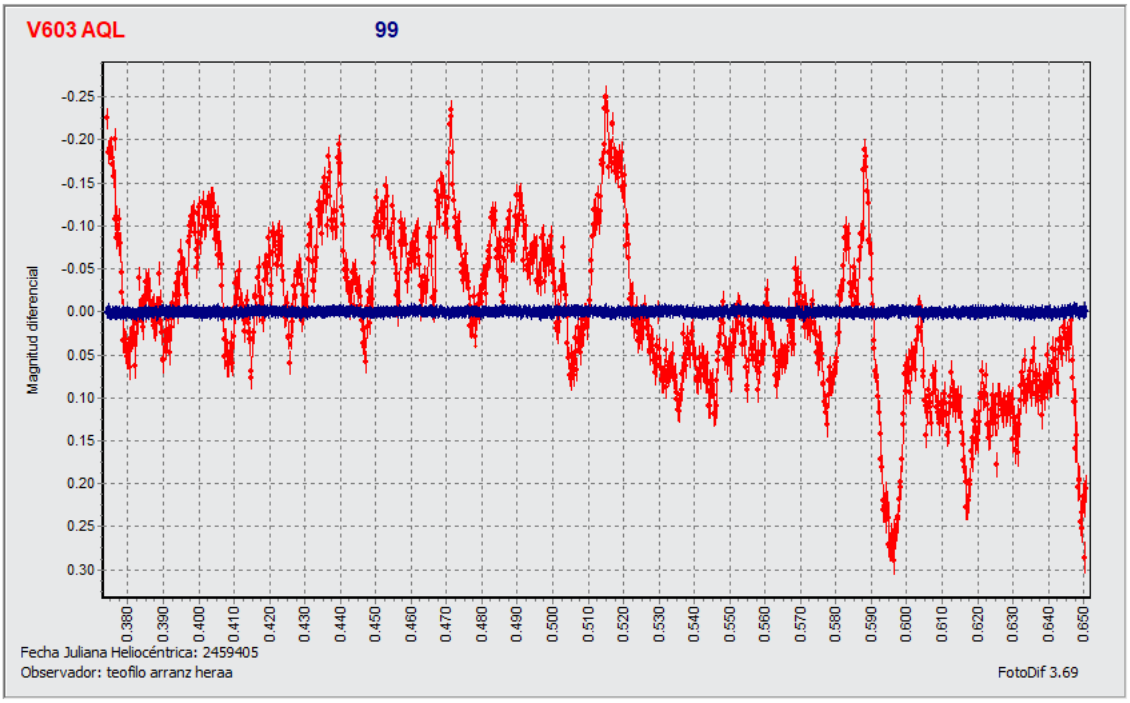

No.	Frequency (c/d)	Time (mins)	Theta
1	33.63600	42.81	0.14
2	42.63080	33.78	0.12
3	59.82440	24.07	0.09
4	53.17780	27.08	0.09
5	14.41260	99.91	0.08
6	26.59140	54.15	0.05
7	70.37140	20.46	0.04
8	66.19240	21.75	0.03
9	92.85840	15.51	0.03
10	48.00380	30.00	0.03

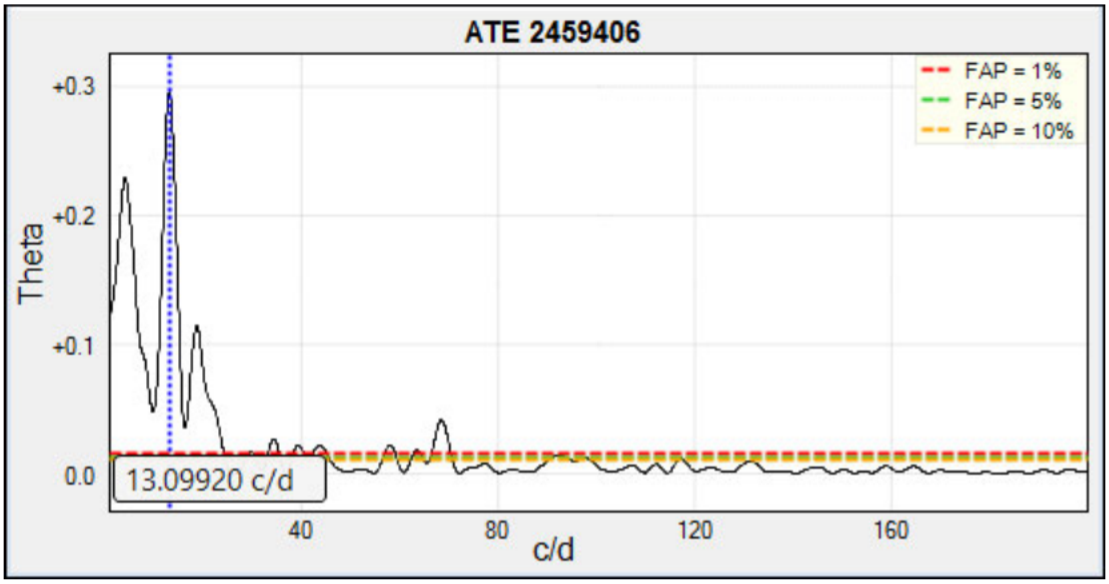

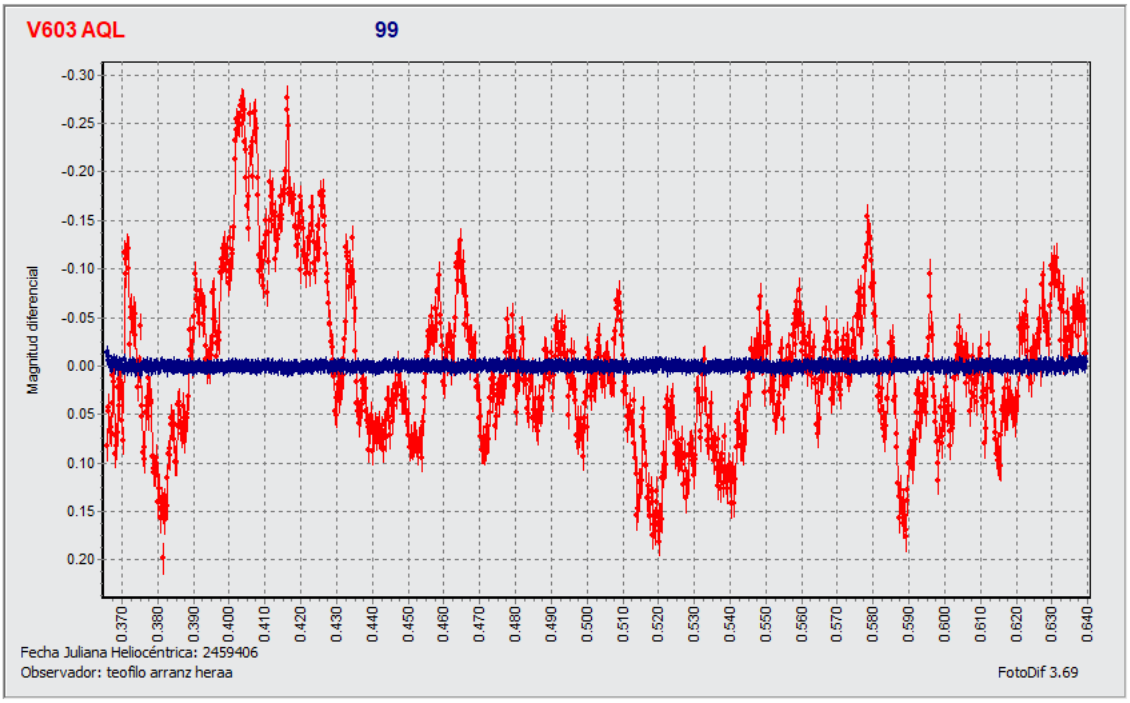

No.	Frequency (c/d)	Time (mins)	Theta
1	13.09920	109.93	0.30
2	4.14420	347.47	0.23
3	18.71100	76.96	0.11
4	68.50080	21.02	0.04
5	34.35240	41.92	0.03
6	39.32740	36.62	0.02
7	57.99360	24.83	0.02
8	43.74520	32.92	0.02
9	63.44620	22.70	0.02
10	29.73560	48.43	0.02

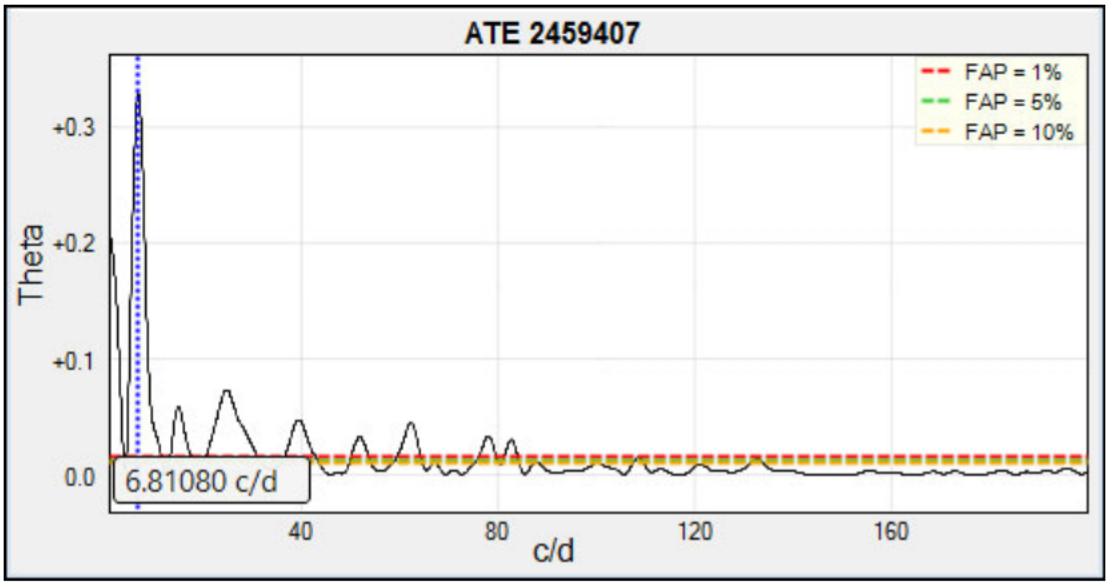

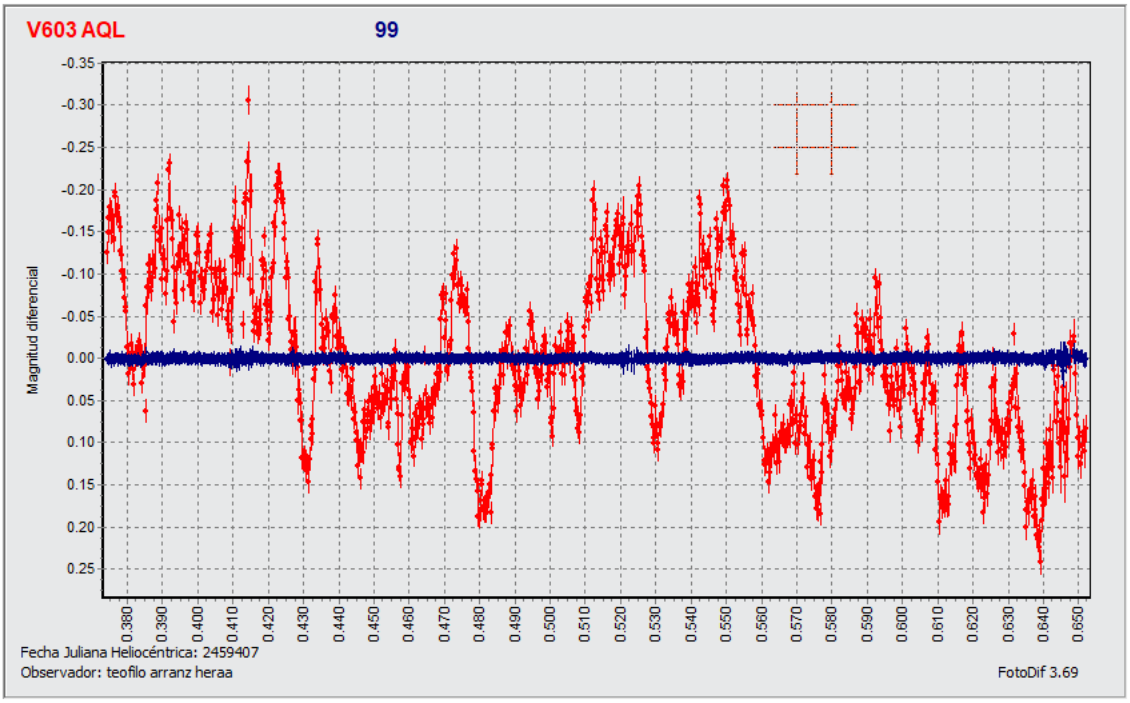

No.	Frequency (c/d)	Time (mins)	Theta
1	6.81080	211.43 (P_{NSH})	0.33
2	1.000000	1440	0.21
3	24.80040	58.06	0.07
4	14.96980	96.19	0.06
5	39.44680	36.50	0.05
6	62.29200	23.12	0.04
7	78.05280	18.45	0.03
8	51.82460	27.79	0.03
9	82.70940	17.41	0.03
10	108.53960	13.27	0.02

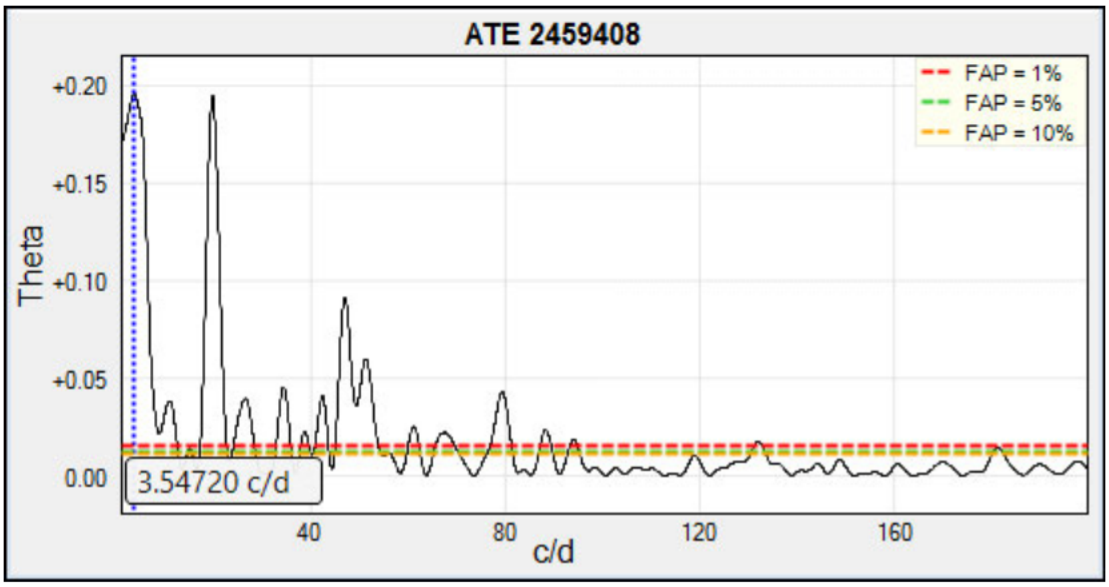

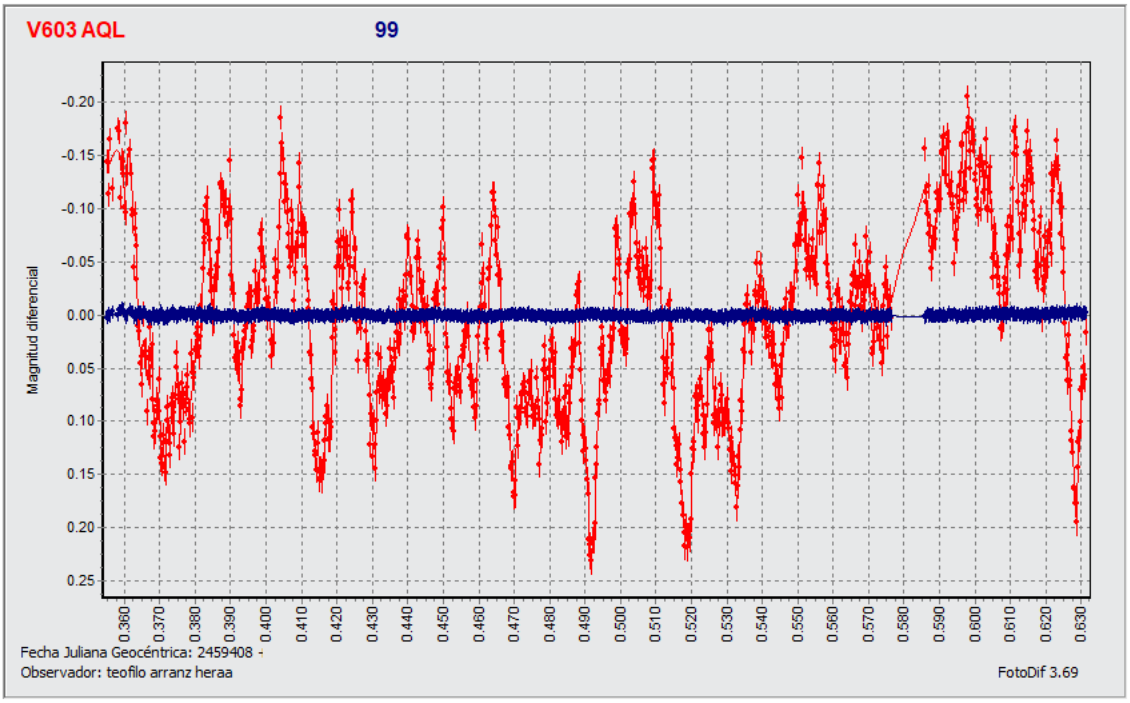

No.	Frequency (c/d)	Time (mins)	Theta
1	3.54720	405.95	0.20
2	19.70600	73.07	0.19
3	46.96900	30.66	0.09
4	51.26740	28.09	0.06
5	34.35240	41.92	0.05
6	79.32640	18.15	0.04
7	42.31240	34.03	0.04
8	26.47200	54.40	0.04
9	10.87040	132.47	0.04
10	61.13780	23.55	0.03

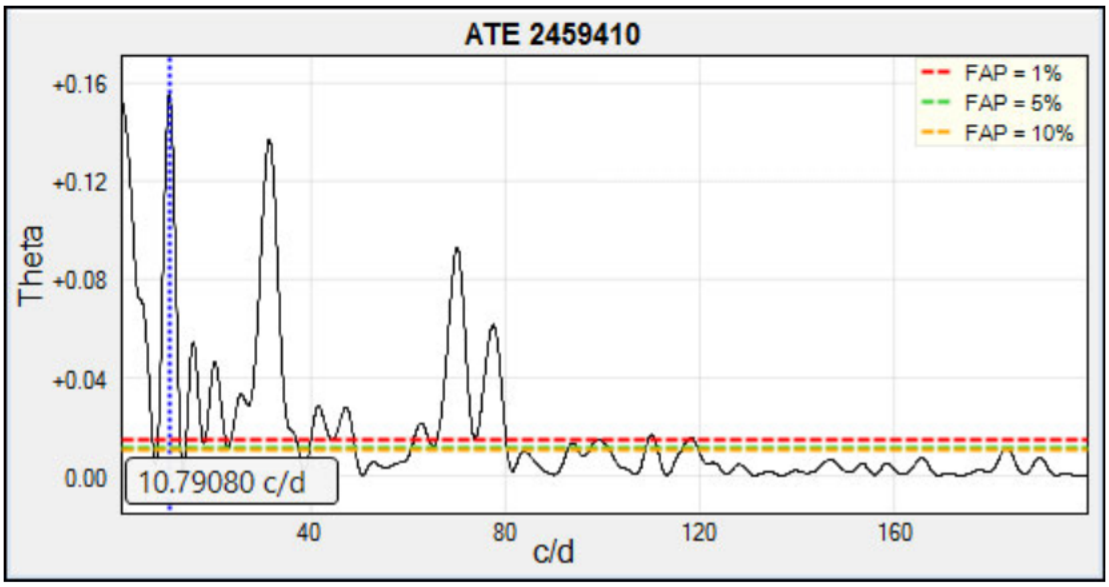

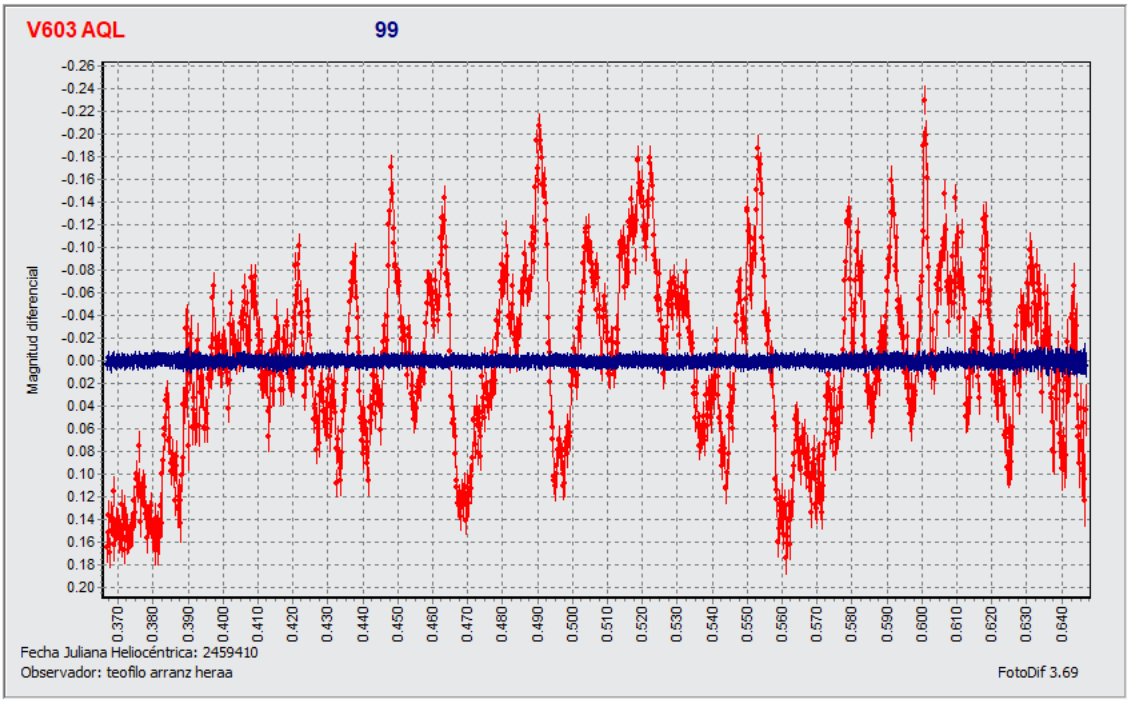

No.	Frequency (c/d)	Time (mins)	Theta
1	10.79080	133.45	0.16
2	1.000000	1440	0.15
3	31.40720	45.85	0.14
4	70.05300	20.56	0.09
5	4.90040	293.85	0.07
6	77.49560	18.58	0.06
7	15.72600	91.57	0.05
8	20.18360	71.35	0.05
9	25.63620	56.17	0.03
10	41.51640	34.69	0.03

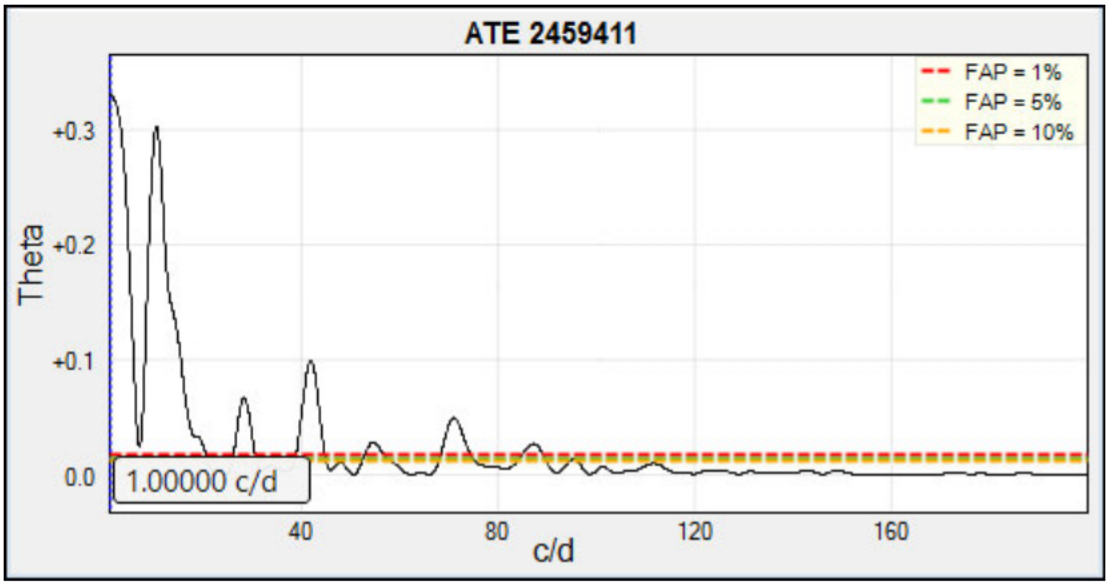

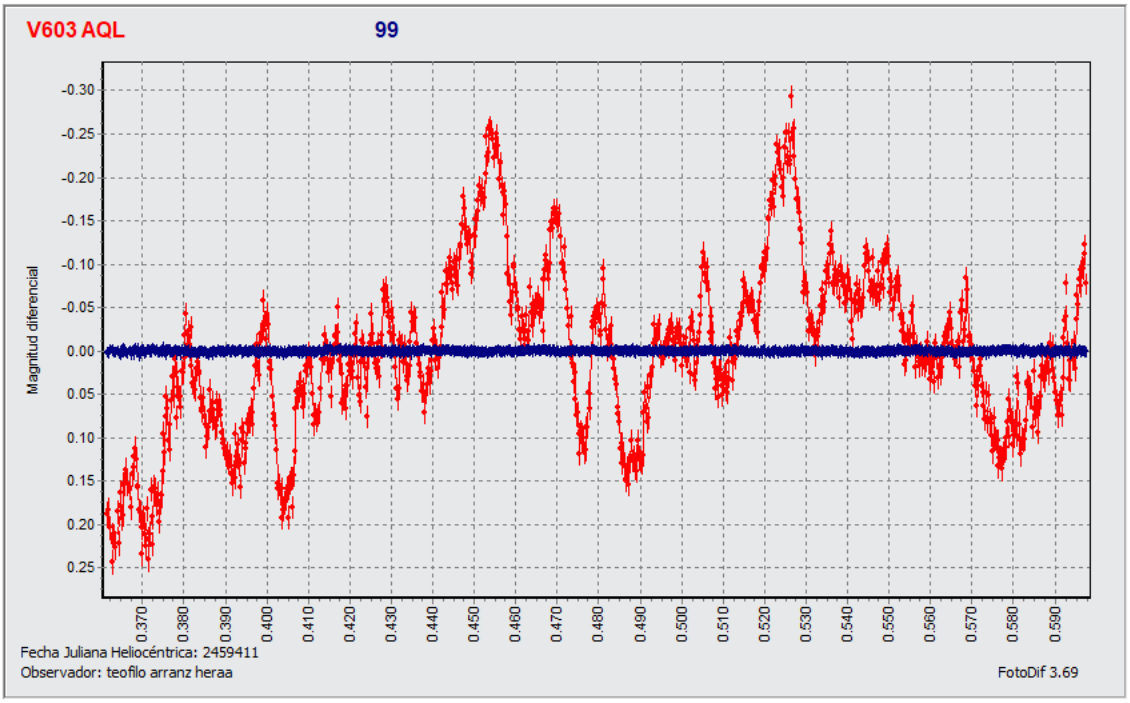

No.	Frequency (c/d)	Time (mins)	Theta
1	1	1440	0.33
2	10.47240	137.50	0.30
3	41.91440	34.36	0.10
4	28.30280	50.88	0.07
5	71.00820	20.28	0.05
6	54.53100	26.41	0.03
7	87.24660	16.50	0.03
8	95.36580	15.10	0.01
9	47.84460	30.10	0.01
10	111.56440	12.91	0.01

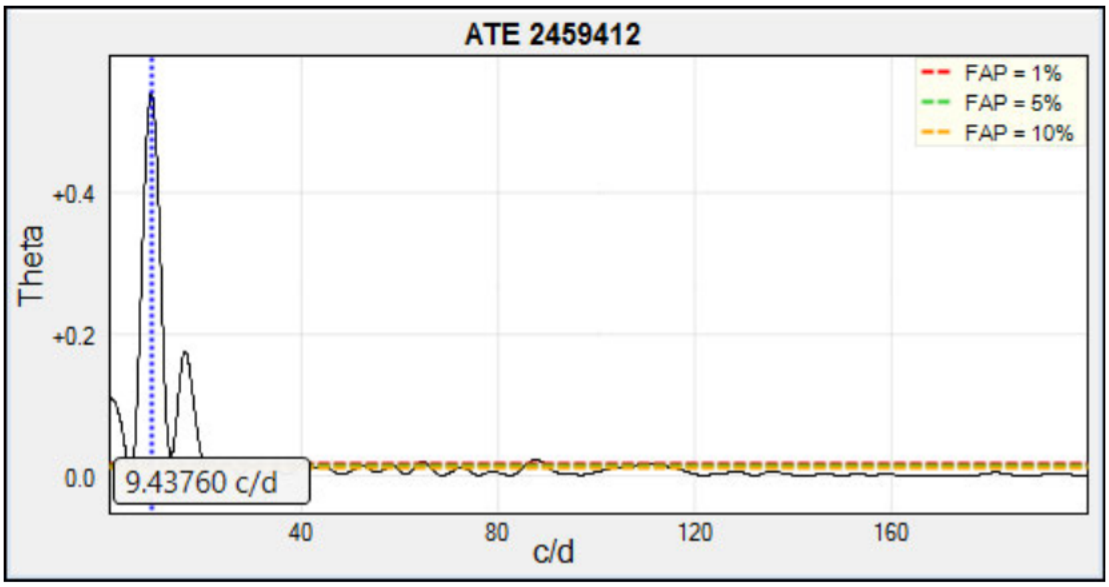

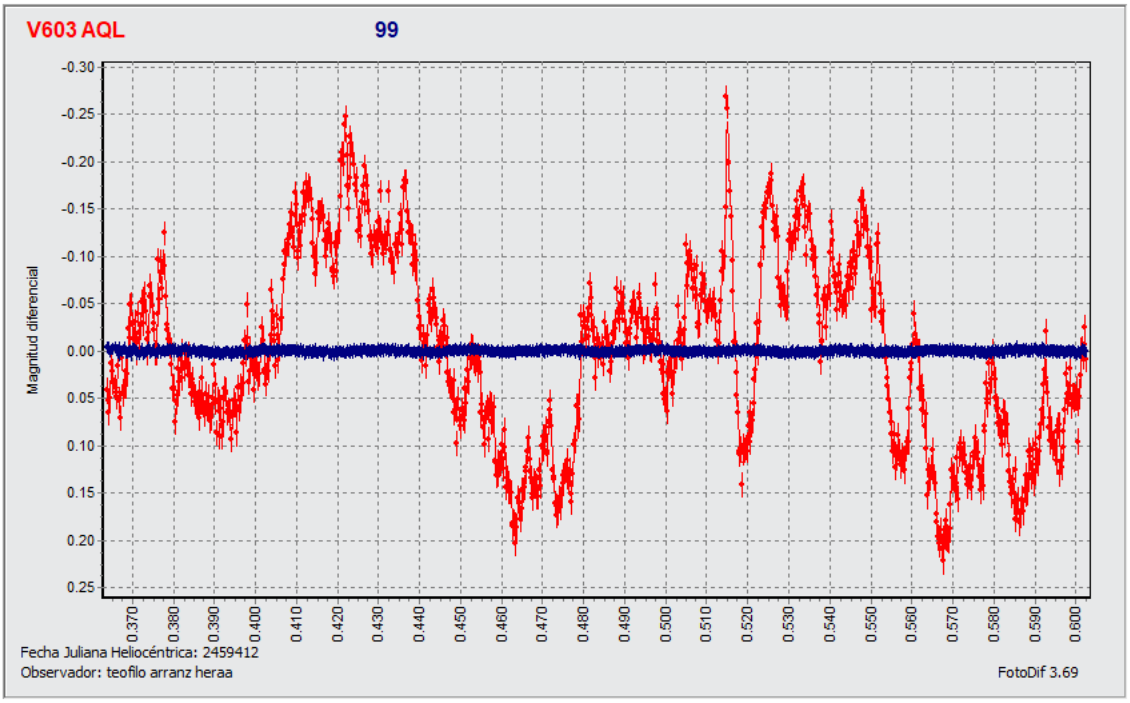

No.	Frequency (c/d)	Time (mins)	Theta
1	9.43760	152.58	0.54
2	16.28320	88.43	0.18
3	1	1440	0.11
4	87.68440	16.42	0.02
5	64.64020	22.28	0.02
6	109.97240	13.09	0.02
7	40.16320	35.85	0.02
8	24.80040	58.06	0.02
9	58.39160	24.66	0.01
10	30.09380	47.85	0.01

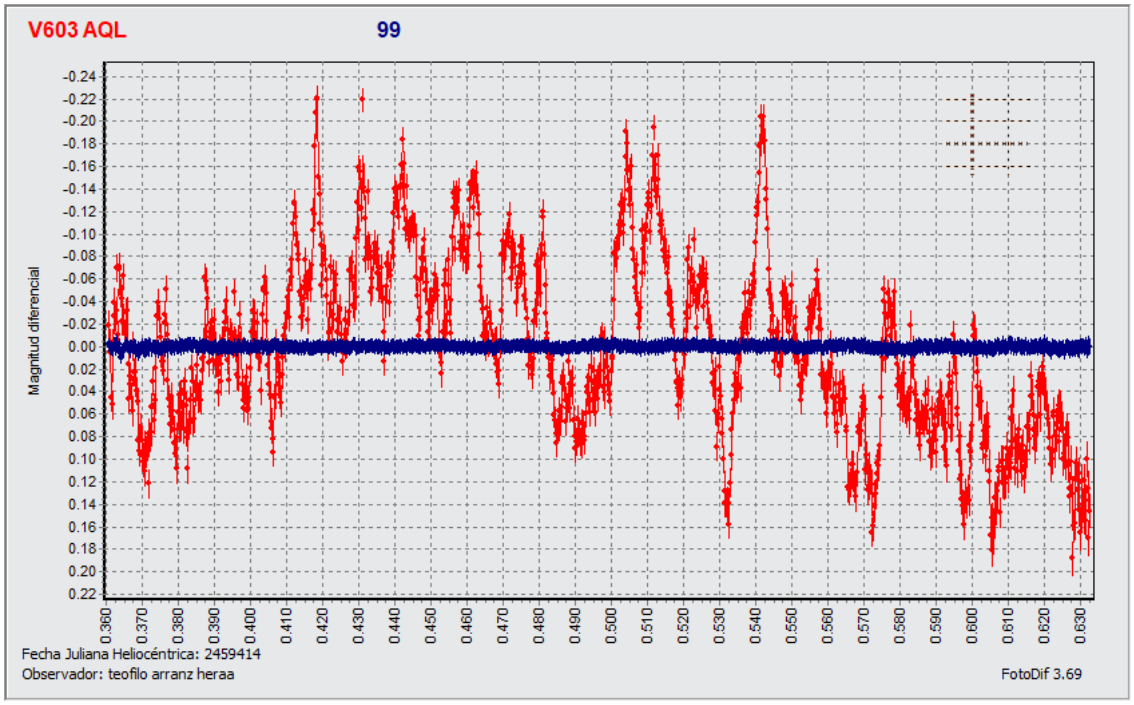
V603 AQL
99
Magnitud diferencial
Fecha Juliana Heliocéntrica: 2459414
Observador: teofilo arranz heraa
FotoDif 3.69

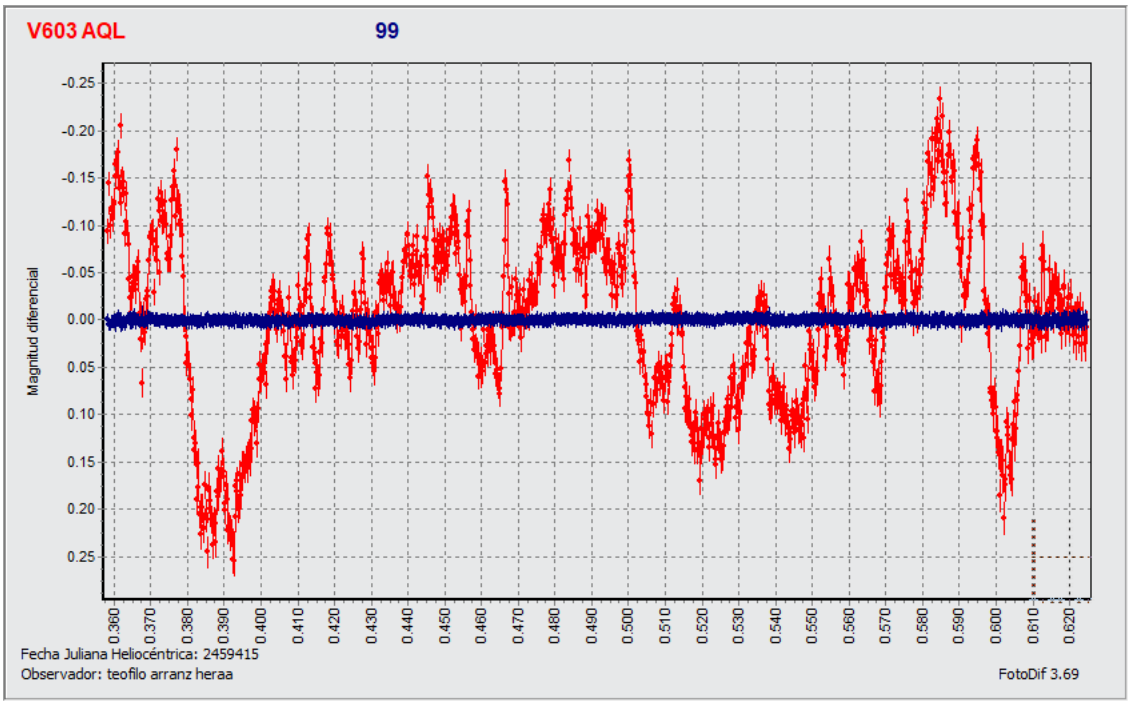
V603 AQL
99
Magnitud diferencial
Fecha Juliana Heliocéntrica: 2459415
Observador: teofilo arranz heraa
FotoDif 3.69

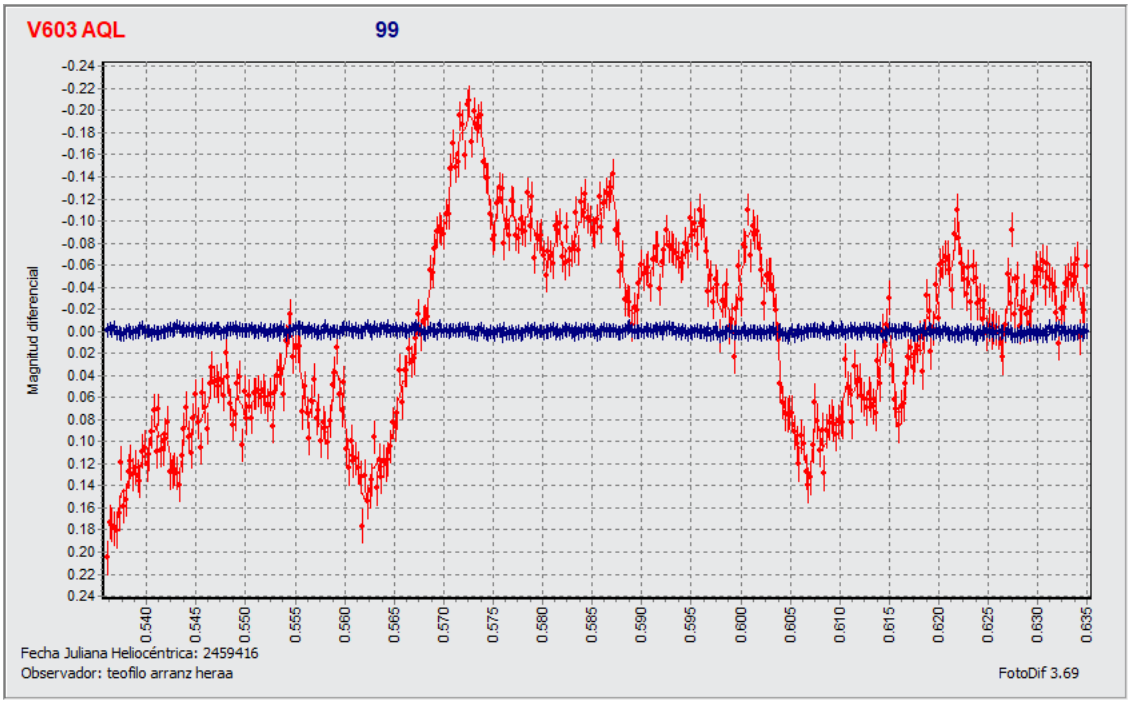
V603 AQL
99
Magnitud diferencial
Fecha Juliana Heliocéntrica: 2459416
Observador: teofilo arranz heraa
FotoDif 3.69

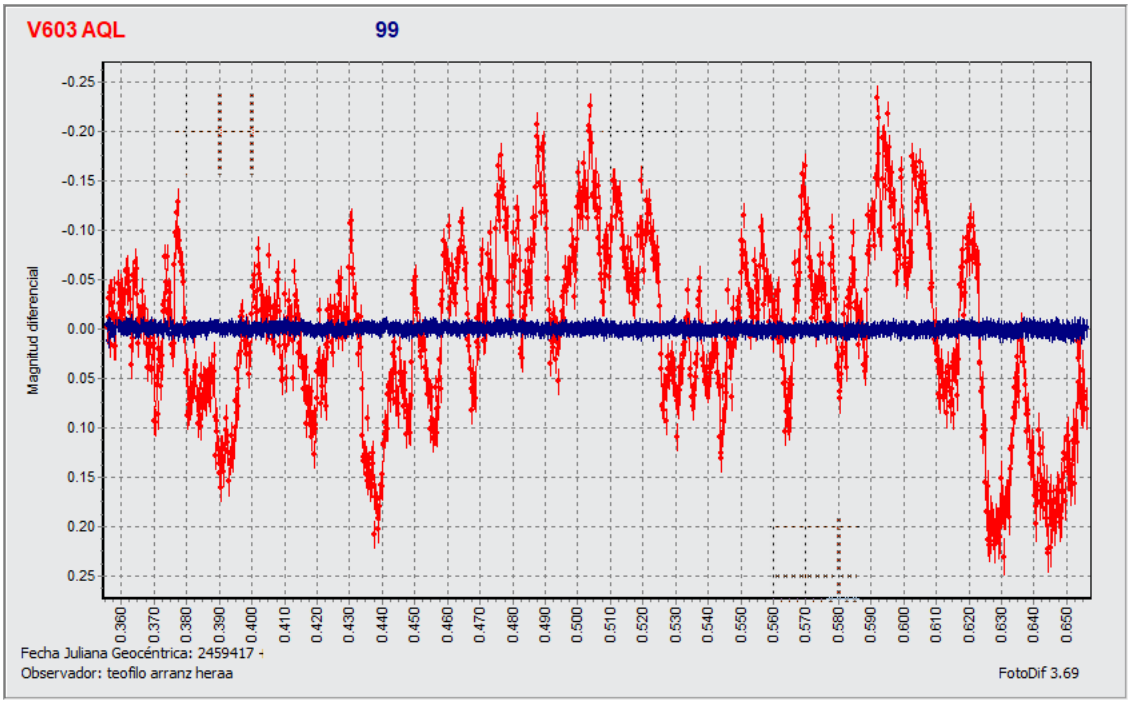
V603 AQL
99
Magnitud diferencial
Fecha Juliana Geocéntrica: 2459417 -
Observador: teofilo arranz heraa
FotoDif 3.69

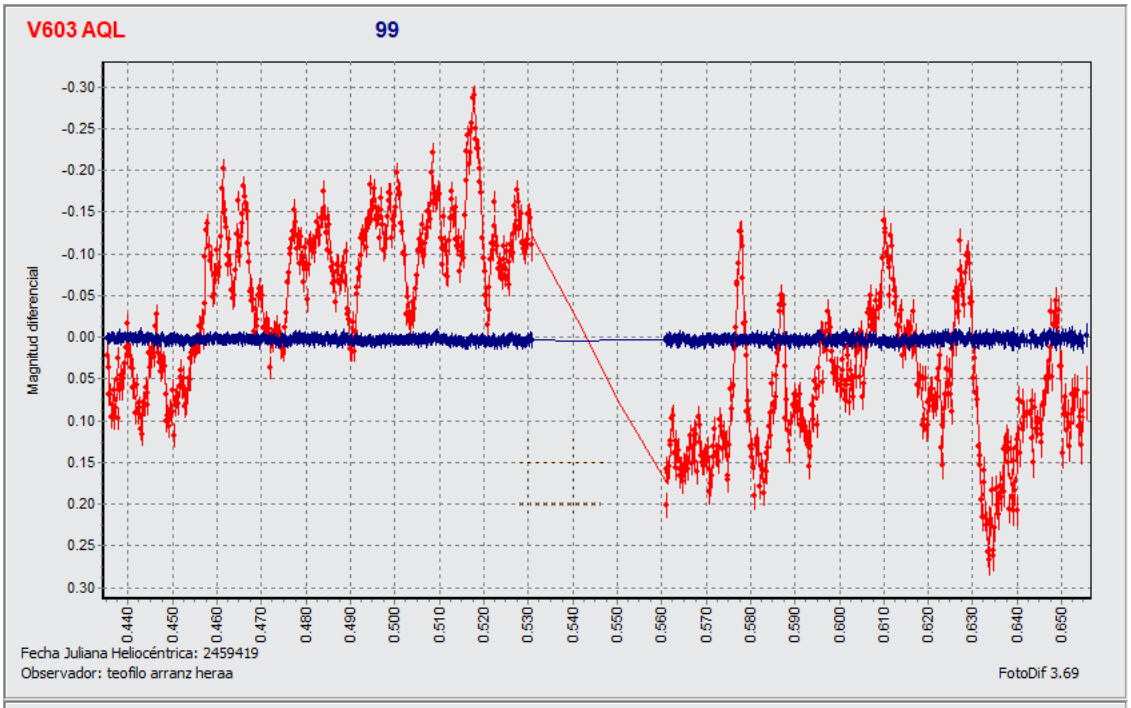
V603 AQL
99
Magnitud diferencial
-0.30
-0.25
-0.20
-0.15
-0.10
-0.05
0.00
0.05
0.10
0.15
0.20
0.25
0.30
0.440
0.450
0.460
0.470
0.480
0.490
0.500
0.510
0.520
0.530
0.540
0.550
0.560
0.570
0.580
0.590
0.600
0.610
0.620
0.630
0.640
0.650
Fecha Juliana Heliocéntrica: 2459419
Observador: teofilo arranz heraa
FotoDif 3.69

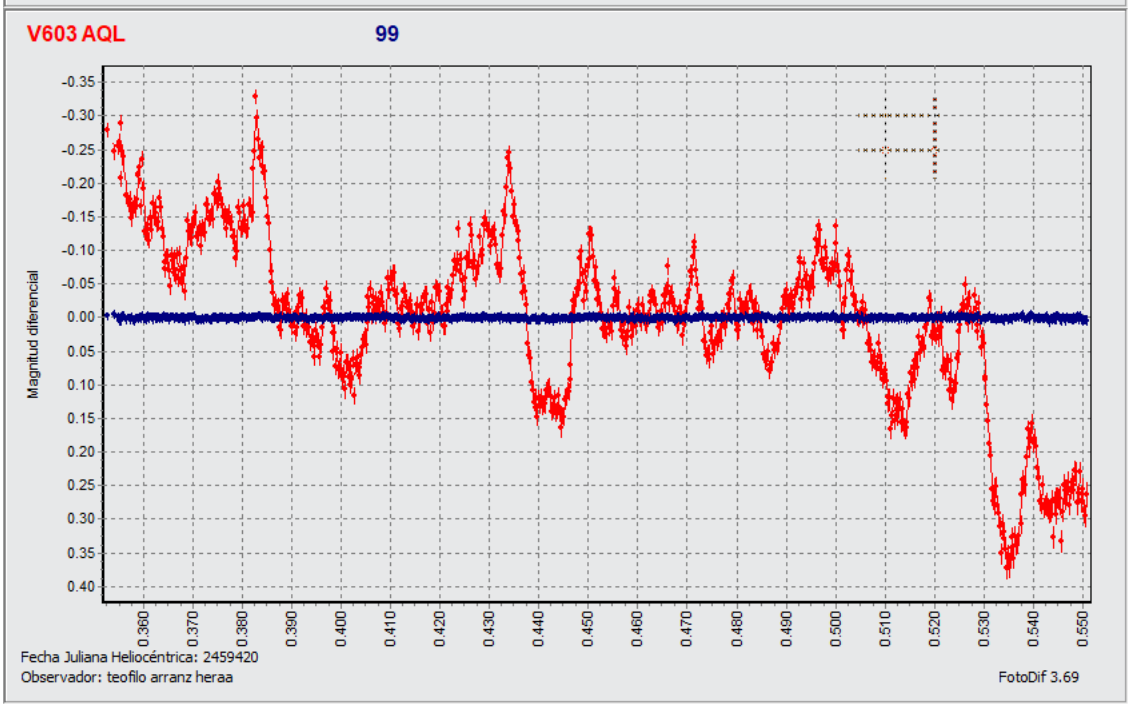
V603 AQL
99
Magnitud diferencial
-0.35
-0.30
-0.25
-0.20
-0.15
-0.10
-0.05
0.00
0.05
0.10
0.15
0.20
0.25
0.30
0.35
0.40
0.360
0.370
0.380
0.390
0.400
0.410
0.420
0.430
0.440
0.450
0.460
0.470
0.480
0.490
0.500
0.510
0.520
0.530
0.540
0.550
Fecha Juliana Heliocéntrica: 2459420
Observador: teofilo arranz heraa
FotoDif 3.69

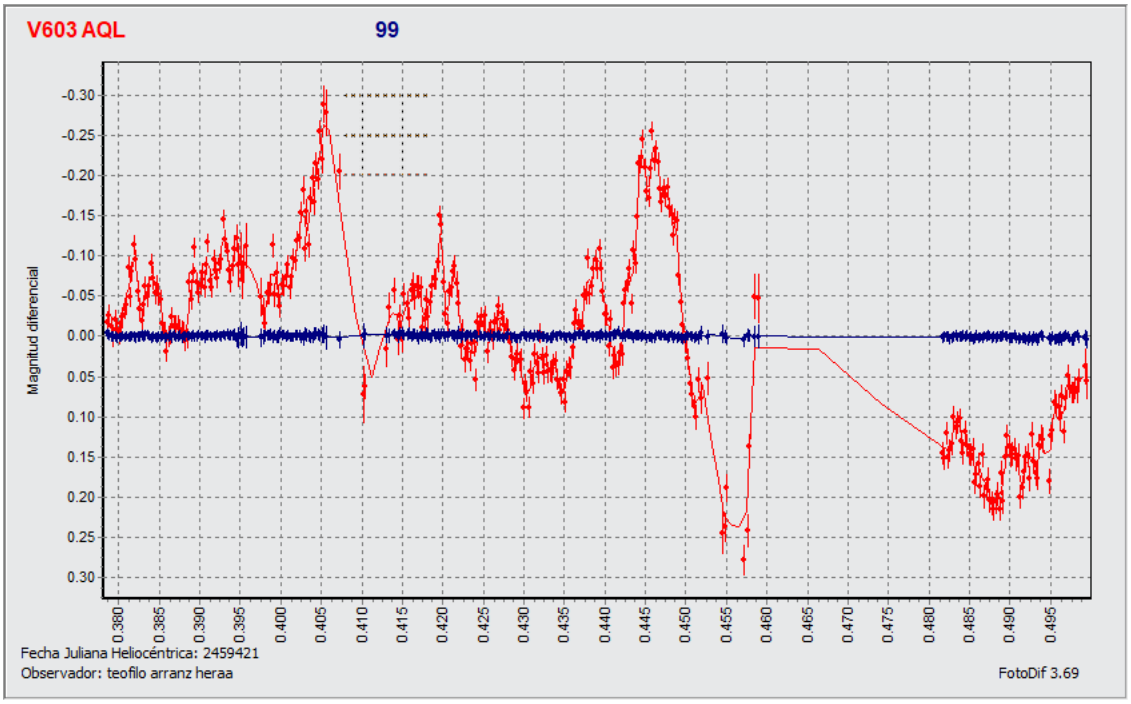
V603 AQL
99
Magnitud diferencial
Fecha Juliana Heliocéntrica: 2459421
Observador: teofilo arranz heraa
FotoDif 3.69

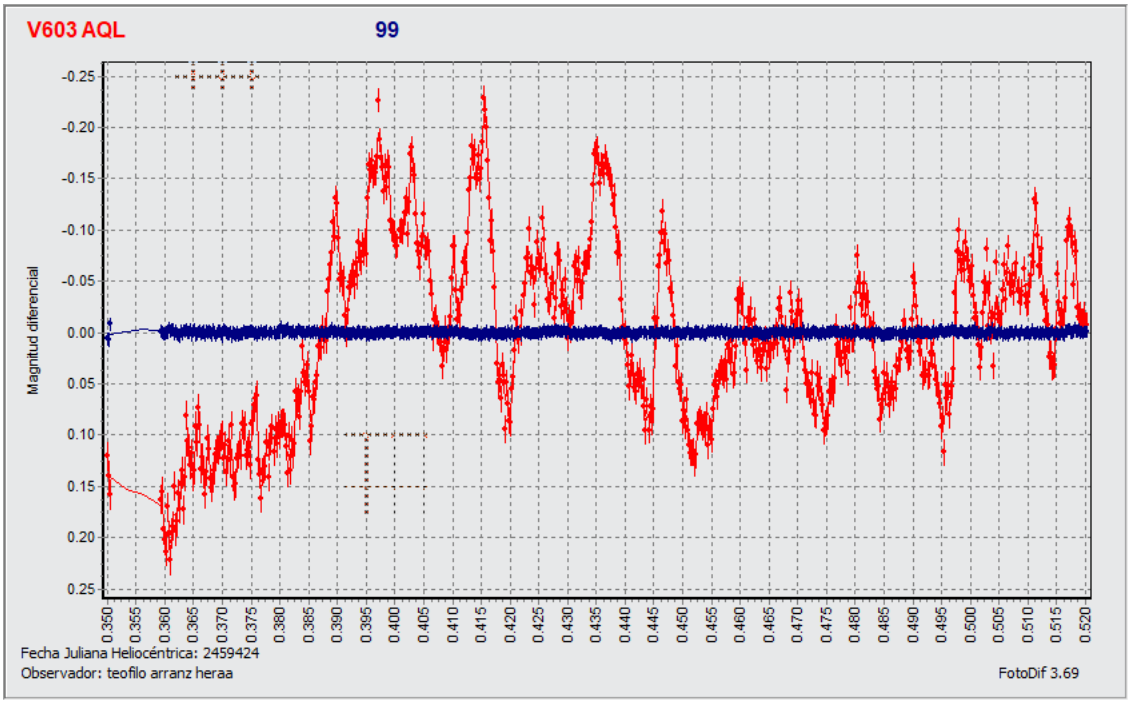
V603 AQL
99
Magnitud diferencial
Fecha Juliana Heliocéntrica: 2459424
Observador: teofilo arranz heraa
FotoDif 3.69